# Microfluidic Enabling Technologies for Measurement of the Selective Permeability of the Mucus Barrier



by

LEON DALIANG LI

B.S. Electrical Engineering, University of Pittsburgh, Pittsburgh, PA (2006)
S.M. Electrical Engineering and Computer Science (2009)

Submitted to the Division of Health Sciences and Technology
in partial fulfillment of the requirements for the degree of

Doctor of Philosophy in Electrical and Medical Engineering

At the

MASSACHUSETTS INSTITUTE OF TECHNOLOGY

February 2013



Signature of Author: _____
Harvard-MIT Division of Health Sciences and Technology
February 2013

Certified by: _____
Professor Jongyoon Han, PhD
Associate Professor of Electrical Engineering and Biological Engineering
Thesis Supervisor

Accepted by: _____
Emery Brown, MD, PhD
Director, Harvard-MIT Division of Health Sciences and Technology
Professor of Computational Neuroscience and Health Sciences and Technology

# Microfluidic Enabling Technologies for Measurement of the Selective Permeability of the Mucus Barrier

by

LEON DALIANG LI

Submitted to the Division of Health Sciences and Technology
in partial fulfillment of the requirements for the degree of
Doctor of Philosophy in Electrical and Medical Engineering

## Abstract

Mucus is a biological hydrogel which lines the wet (non-keratinized) epithelia of the body. Mucus provides a gateway between the cells of the epithelium and the outside world, and is postulated to provide a selective filtering function which is critical to physiological functioning and has been implicated in diseases. Currently, much of the mechanisms and criteria of this selective filtering function is not well understood.

In this thesis, we contribute novel microfluidic devices to characterize the selective permeability properties of the mucus barrier. Microfluidics provides the engineering ability to create channels with precise geometries, fluid flow capability, and allow chemical concentration gradients. Our devices mimic the physiological environment of the mucosa and enable improved measurements of the mucus layer selective permeability.

The first microfluidic device mimics the acid barrier function of the stomach mucus layer. This device reproduces on-chip the secretion of mucus by the gastric mucosa into an acidic stomach lumen. We use this device to demonstrate that the secretion of mucins, the glycoprotein structural component of mucus, contributes significantly to the acid barrier function by continuously binding $H^+$.

The second microfluidic device probes the permeability of the mucus barrier to nanoscale peptides, as a model for drug molecules and *in vivo* signaling molecules. The device enabled the creation of a mucus layer next to a flowing aqueous layer, mimicking the *in vivo* mucus layer and lumen of the gastrointestinal, respiratory, and female reproductive tracts. Peptides added to the aqueous flow diffused across the mucus barrier interface into the mucus layer. This device demonstrated that the mucus barrier provides selective permeability to nanoscale peptides based on electrostatic interactions, and suggest novel surface functionalization strategies for drug carriers to improve mucosal drug delivery.

Taken together, this thesis provides new microfluidic tools to probe the selective permeability function of the mucus barrier. Using the microfluidic tools, we show new mechanistic understanding of this barrier.

Thesis supervisor: Prof. Jongyoon Han
Title: Associate Professor of Electrical Engineering and Biological Engineering

## Acknowledgements

I am thankful to Prof. Jongyoon Han for his excellent mentorship during my Masters and PhD work. Prof. Han has provided me with insightful advice and helped me through difficult times. Prof. Han allowed me to explore the research arena and make fruitful mistakes, and then guided me into productive directions at the right times. I am glad to have worked with Prof. Han.

A big thanks to Prof. Katharina Ribbeck who inspired me to work on the mucus barrier selective permeability problem. Prof. Ribbeck has provided me on many occasions with great advice, and has mentored me in designing research projects and producing good academic writing. Prof. Ribbeck is an excellent professor and scientist to work with.

I am indebted to Prof. Alan Grodzinsky for informative and helpful discussions. As thesis committee chair, Prof. Grodzinsky provided fresh perspective on our research projects. His penetrating knowledge and wisdom has greatly improved this thesis and my PhD experience.

I would like to thank the support and guidance of the members of Prof. Han's lab who I had the pleasure of interacting with, including (in no particular order) Dr. Han Wei Hou, Dr. Aniruddh Sarkar, Dr. Lihfang Cheow, Prof. Yong-Ak Song, Dr. Rohat Melik, Dr. Hiong Yap Gan, Prof. Sung Jae Kim, Prof. Chia-Hung Chen, Prof. Zirui Li, Prof. Masumi Yamada, Prof. Jeong Hoon Lee, Dr. Reto Schoch, Dr. Hansen Bow, Dr. Pan Mao, Dr. Philip Dextras, Prof. Jianping Fu, Dr. Ying-Chih Wang, Rhokyun Kwak, Sha Huang, Lidan Wu, Ragheb El Khaja, and Vincent Liu. In Professor Ribbeck's lab, I wish to thank the help and support of Dr. Nicole Billings, Dr. Thomas Crouzier, Dr. Irena Jevtov, Julia Co, Nicole Kavanaugh, Andrew Rajczewski, Wesley Chen, Prof. Oliver Lieleg, Dr. Marina Caldara, and Alexander Chaim.

I especially wish to thank Prof. Oliver Lieleg for working with me and providing guidance on the acid barrier of the stomach project, Dr. Thomas Crouzier for providing advice and materials for the peptide mucus barrier project, Dr. Aniruddh Sarkar for working with me on microfluidic valve devices, and Prof. Jeong Hoon Lee for training me during my first Masters project in Prof. Han's lab. I also wish to thank MIT undergraduate researchers Sae Jang and Laura Dunphy for working with me on several projects.

Financial support for my thesis work was provided by the National Science Foundation Graduate Research Fellowships Program (GRFP), funding support from an MIT Electrical Engineering teaching assistant appointment, the Harvard-MIT Health Sciences and Technology (HST) fellowship program, fellowship funding provided by Thanassis and Marina Martinos to HST, and funding from the Singapore National Research Foundation under its Singapore MIT Alliance for Research and Technology (SMART) program.

Lastly, I wish to thank my friends and family for providing essential support and believing in me during my graduate school experience.

# Table of Contents

# List of Figures

# List of Tables

# Chapter 1

# Introduction

Mucus is a biological hydrogel which lines the wet (non-keratinized) epithelia of the body, including the respiratory tract, gastrointestinal tract, female reproductive tract, and the surface of the eye. The functions of the mucus barrier include protecting the underlying cells against pathogens and environmental toxins, preventing the acidic digestive juices in the stomach from damaging the stomach wall, and controlling the passage of sperm in the cervix.

Mucus is believed to be a selectively permeable barrier which permits the passage of beneficial cells and molecules while rejecting harmful ones. However, at this time, much of the criteria and mechanisms for this selective permeability function is not known. Understanding the selective filtration criteria and mechanisms would be highly meaningful, both in terms of gaining fundamental scientific knowledge of this important transport gateway, and for the development of new methods to deliver drugs through the barrier.

Mucus function is challenging to study for several reasons. First, mucin glycoproteins, the dominant structural component of mucus, are large and complex molecules containing a variety of surface structures and biochemistries. Second, as a heterogeneous and amorphous material, the *in vivo* mucus layers are difficult to stain and fix in histological preparations, complicating *in vivo* studies. Third, the mucus layers are mostly contiguous with the outside environment of the body and often colonized by bacteria, creating diverse microenvironments whose properties vary greatly from sample to sample. Such variations create practical challenges for the *in vitro* characterization of mucus.

This thesis aims to develop new tools to characterize mucus function in ways not previously feasible. Using these newly developed tools, we characterized the barrier function of native mucins, the structural glycoproteins purified from native mucus, and provide new insights into the selective permeability function.

The organization of this thesis is as follows. Chapter 1 reviews the physiology and physiological function of the mucus barrier. Chapter 2 reviews the existing technologies for study of mucus barrier properties. Chapter 3 presents our microfluidic device to measure the acid barrier function of mucus components.

Chapter 4 presents our microfluidic device to measure the charge selective permeability of the mucus layer to nanometer length peptides.

## 1.1 Physiology of the mucus barriers

The mucus layers of the body follow a common layout. The basolateral side faces or touches the epithelial cells, while the apical side is open to the lumen of the organ tract. (Fig. 1-1) This layout enables the mucus barrier to intercept foreign particles and molecules entering into the body before they reach the underlying tissues.

In the airways, mucus is secreted by goblet cells in the epithelium [1] and by sero-mucous glands of the submucosa. [2] The airway mucus layer rests on a watery fluid known as the periciliary layer, and reaches a thickness of up to ~50 µm. [3] Cilia on the apical side of the epithelium layer connect through the periciliary layer to the basolateral side of the mucus layer. The mucus layer traps particles and pathogens entering the lungs during each respiratory cycle. The continuous beating of the cilia in a wave like motion continuously transports mucus and trapped pathogens axially away from the deeper portions of the lung at a rate of ~40 µm/s in a process known as mucociliary clearance. [4]


**Fig. 1-1**: Physiology of the respiratory and gastrointestinal mucus layers.

In the gastrointestinal system, the mucus barrier is divided into two layers. The inner layer is a tightly adhering layer, consisting of mostly mucins bound to the apical cell membranes of the epithelium. [5, 6] This inner mucus layer is also mostly free of bacteria. The outer, more loosely adhering layer is directly exposed to the gastrointestinal lumen, and is extensively colonized by bacteria in the intestines. [7] Digestive enzyme action and fluid shearing due to peristalsis continuously remove mucus from the gastrointestinal mucus layer surface, but mucus is replenished from the epithelial side by both continuous and on-demand secretion mechanisms. [6, 8] This mucus layer protects the underlying cells from bacteria in the gastrointestinal tract, and also protects the stomach wall from auto-digestion by the acidic digestive juices in the gastric lumen.

In the female reproductive tract, the cervical and vaginal canals are protected by cervical mucus. Cervical mucus is predominantly secreted by epithelial cells in ~100 crypt-like structures lining the sides of the cervical canal. [9] Ciliated cells lining the cervical epithelium move the mucus towards the vaginal canal and out of the body. [9] Under normal circumstances, cervical mucus completely covers the opening to the uterus. Cervical mucus functions as a key gateway that controls sperm passage during the menstrual cycle.

## 1.2 Composition of the mucus barrier

Mucus is a hydrogel which contains more than 90% water. The mucin content of the mucus barrier varies with anatomical location. Airway mucus contains 1-2% mucins, [1] while gastrointestinal mucus

contains ~5% mucins. [10] Other mucus components include associated proteins/lipids, cellular debris and DNA from bacteria and sloughed off epithelial cells, and small ions.

Mucins are high molecular weight ($10^6$-$10^7$ Da), heavily glycosylated proteins. The simplified structure of a mucin molecule is shown in Fig. 1-2. Mucin mRNA is translated into a linear 100-250 kDa polypeptide known as apomucin. [11] Approximately one-third of the apomucin are tandem repeats containing serine and threonine residues, from which *O*-linked oligosaccharides are attached. The oligosaccharides may be linear or branched and project radially from the apomucin core. [12] This mucin molecule geometry is often described as a "bottle-brush" structure, where the apomucin core is analogous to the core of the brush and the glycans resemble the bristles.

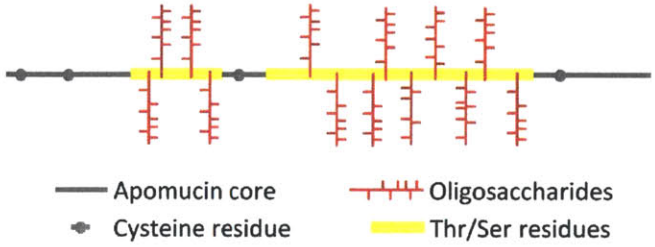


**Fig. 1-2**: Schematic of a mucin molecule.

The major types of mucins are shown in Table 1-1. The types are distinguished by different genes encoding the apomucin protein core, distributed over several chromosomes. [13] Mucins can be divided into three subtypes, including secreted gel forming, secreted non-gel forming (monomeric), and cell surface bound mucins. Gel forming mucins make up the bulk of the mucus layers of the body, and are distinguished by cysteine rich regions on the ends of the mucin molecule needed for disulfide bond formation during gelation. [14] Other forces, such as hydrogen bonding among the mucin glycans, also contribute to gel formation. [15]

Cell surface mucins contain transmemberane domains which anchor them to the plasma membrane. They are present on all apical surfaces of epithelial cells and likely work in concert with the secreted mucus layer to provide permeability control. Some cell surface mucins also contain intracellular domains which mediate downstream signaling. [16, 17]

**Table 1-1** Type and tissue distribution of mucins. Table adapted from [13]. Reproduced with permission. © 2008 Nature Publishing Group.

| Mucin | Distribution |
|---|---|
| ***Secreted gel forming*** | |
| **MUC2** | Small intestine, colon, respiratory tract, eye, middle ear epithelium |
| **MUC5AC** | Respiratory tract, stomach, cervix, eye, middle ear epithelium |
| **MUC5B** | Respiratory tract, salivary glands, cervix, gallbladder, seminal fluid, middle ear epithelium |
| **MUC6** | Stomach, duodenum, gallbladder, pancreas, seminal fluid, cervix, middle ear epithelium |
| **MUC19** | Sublingual gland, submandibular gland, respiratory tract, eye, middle ear epithelium |
| ***Secreted non-gel forming (monomeric)*** | |
| **MUC7** | Salivary glands, respiratory tract, middle ear epithelium |
| ***Cell surface*** | |
| **MUC1** | Stomach, breast, gallbladder, cervix, pancreas, respiratory tract, duodenum, colon, kidney, eye, B cells, T cells, dendritic cells, middle ear epithelium |
| **MUC3A/B** | Small intestine, colon, gall bladder, duodenum, middle ear epithelium |
| **MUC4** | Respiratory tract, colon, stomach, cervix, eye, middle ear epithelium |
| **MUC12** | Colon, small intestine, stomach, pancreas, lung, kidney, prostate, uterus |
| **MUC13** | Colon, small intestine, trachea, kidney, appendix, stomach, middle ear epithelium |
| **MUC15** | spleen, thymus, prostate, testis, ovary, small intestine, colon, peripheral blood leukocyte, bone marrow, lymph node, tonsil, breast, fetal liver, lungs, middle ear epithelium |
| **MUC16** | Peritoneal mesothelium, reproductive tract, respiratory tract, eye, middle ear epithelium |
| **MUC17** | Small intestine, colon, duodenum, stomach, middle ear epithelium |
| **MUC20** | Kidney, placenta, colon, lung, prostate, liver, middle ear epithelium |

The pH of the mucus layers varies with anatomical location. (Table 1-2) The stomach lumen is the most acidic region of the body, capable of reaching an $H^+$ concentration of greater than 100 mM. [18] This high $H^+$ concentration is needed for proper functioning of digestive enzymes and is maintained by $H^+$ secretion from parietal cells inside the gastric mucosa. The mucus layer of the stomach forms an $H^+$ concentration gradient from pH 6-7 near the epithelial cells to pH 1-3 near the gastric lumen. [19, 20] The $H^+$ barrier function of gastric mucus is discussed further in Section 1.3.3. The vaginal canal is also acidic and can reach a maximum $H^+$ concentration of ~1 mM. However, unlike in the stomach, vaginal acidity is primarily maintained by secretion of lactic acid by commensal bacteria. [21] Intestinal mucus pH varies from pH 5-7. Due to its proximity to the stomach, the pH of the duodenum varies during gastric emptying as acidic stomach contents flow into the small intestines, which may temporarily reduce pH to below 4. [22]

**Table 1-2** pH of the mucus barriers of the human body.

| Location | pH | Reference |
|---|---|---|
| Nose | 5 – 8 | [23] |
| Airway | 7 – 8 | [24] |
| Stomach | 1 – 3 (stomach lumen) | [18] |
| Intestines | 5 – 6 | [18, 25] |
| Female reproductive tract | 3.5 – 4.5 (Vagina)<br>6 – 7 (Cervix) | [26-28] |

Electrolyte content is another parameter which affects mucus barrier properties, as ionic strength affects the viscoelasticity [29] and aggregation [30] of mucins. In addition, many antimicrobial molecules that function by charge interaction is rendered less effective by altered ionic strength. [31] The ionic

content of mucus varies with anatomical location. In the stomach, gastric lumen $Na^+$ concentration is inversely proportional to the $H^+$ concentration, while the $K^+$ concentration is directly proportional to the $H^+$ concentration. [32] Cervical-vaginal mucus ionic strength is currently controversial. In one animal study, vaginal electrical resistance (presumably a measure of mucus electrical resistance) varied from ~30Ω to ~ 55Ω throughout the menstrual cycle, corresponding to an ionic strength change of ~80%. [33] The "fern test," which measures salt-dependent crystallization patterns of cervical mucus, [34] also finds that the cervical mucus ion content varies with the menstrual cycle. [35] Direct ion measurements of cervical mucus or vaginal fluid, however, show contradictory results. One study found significant variation as a function of the menstrual cycle, [36] while another did not. [37] Finally, respiratory mucus ion content also varies among different studies. Several studies showed an increase in the ionic strength of mucus sample from cystic fibrosis patients, [38, 39] but others showed equal ionic strengths. [40] At this time, it is clear that ionic content plays an important role in mucus layer function, but the specific changes which alter mucus function or lead to diseases are not well understood.

## 1.3 Physiological functions of the mucus barrier

### 1.3.1 Immune function

The mucus barrier is part of the innate immune system and a first line of defense against infection. Several mechanisms help to prevent infection. First, native mucins exhibit broad antiviral capability. In Lieleg *et al.*, native mucins at a concentration of 0.25% to 1% (w/v) added on top of a layer of cells *in vitro* were protective against infection by human papilloma virus type 16, Merkel cell polyoma-virus, and a strain of influenza virus. [41] Using single particle tracking of fluorescently labeled virus like particles, Lieleg *et al.* showed that such antiviral ability is related to the reduced diffusion mobility of the viruses in the presence of mucins. In a different study, mercaptoethanol (a reducing agent affecting gelation of mucins through disulfide bond disruption) and neuraminidase decreased the anti-viral capabilities of mucin, suggesting that the mucin structure and glycan content is important for anti-viral function. [42]

Mucins are also protective against bacteria. Muc 1 -/- mice, which are deficient in the cell surface Muc1, were much more susceptible to infection by *Campylobacter jejuni* than wild type mice. Systemic infection by *Campylobacter jejuni* through the gastrointestinal mucus barrier and epithelium are much more prevalent in Muc1 -/- mice than in wild type mice. [43] The inability of Muc1 -/- mice to prevent *C. jejuni* infection is due to loss of Muc1 from the gastrointestinal tract epithelium rather than by depletion of Muc1 from circulating leucocytes since pharmacological depletion of leucocytes in wild type mice did not significantly affect infection. [43] Muc 1 -/- mice are also more susceptible to *Helicobacter pylori* infection. [44] However, primary murine gastric epithelial cells expressing Muc1 bound fewer *H. pylori* than non-muc1-expressing cells. [44] These results led to the conclusion that cell surface mucins may serve as a detachable decoy which bind to pathogens and restrict their entry into the cell. [13] Such similar protective mechanism may also be present for cell surface mucins of the eye, as RNAi depletion of surface mucins from human corneal epithelial cells led to greater binding of *Staphylococcus aureus* bacteria. [45]

Unexpectedly, cell surface mucins may also perform the opposite function, which is to promote infection. This finding is supported by experiments showing that *Pseudomonas aeroginosa* lung infection is more easily cleared and with less inflammation by Muc1 -/- mice than wild type mice. [46] It appears that binding of Muc1 to the flagella of *P. aeroginosa* reduced NF-kB mediated innate immune response activation in the epithelium, thereby possibly aiding infection. [46-48] *H. pylori* has been shown to bind to mucin glycans through at least four adhesins, allowing *H. pylori* to bind differently based on mucin type, anatomical location, pH, and status of gastritis. [49] It is thought that such different binding modes

to mucins may play different roles for *H. pylori* during infection. These findings suggest that mucin binding in some circumstances may be hijacked by pathogens to promote infection.

Finally, mucin aids immune function by binding and sequestering antimicrobial molecules and antibodies. For example, muc5b secreted by submandibular and sublingual glands contain specific binding sites for antifungal histatin molecules. [50] In another example, IgA secreted into the mucus layer interact with a soluble peptide based "secretory component" to bind to the mucus layer. [51] It is important to note that antimicrobial proteins as histatin and antibodies do not have to be freely soluble to be effective. Charge interaction between histatin and the cell surface of *Candida albicans* permeablizes the *C. albicans* cell to damage it, suggesting that mucin bound forms of antimicrobial peptides such as histatin may contain active antimicrobial function. [52] The antimicrobial molecule binding ability of mucins may enable the mucus barrier to accumulate such antimicrobial molecules, thereby increasing immune system effectiveness.

## 1.3.2 Control of sperm transport by cervical mucus

During sexual intercourse, sperm enter the anterior vaginal canal and a small number travel through cervical mucus into the uterine cavity. [26] Estrogen levels during the ovulatory cycle affect the hydration of cervical mucus. [53, 54] Such changes in mucus hydrogen are correlated to the permeability of sperm. [53, 55] Indeed, intercourse during maximal mucus hydration in women is associated with higher incidence of pregnancy, consistent with cervical mucus as a permeability gateway controlling sperm uptake. [56]

Cervical mucus is thought to prevent the passage of morphologically abnormal sperm, thus providing a mechanism to favor the fittest sperm to reach the oocyte. [57, 58] The mechanism of selection is partially related to increased hydrodynamic resistance to abnormally shaped sperm heads. [58]

Neutrophils migrate easily through human cervical mucus. [59] Cervical mucus also provides a medium for IgG's and IgA's, and complement proteins. [60] These antibodies increase in concentration several days before ovulation. [61] Thus, cervical mucus may work together with immune cells and antibodies to control the permeability of the mucus barrier.

Cervical mucus composition not only varies as a function of the menstrual cycle, but also varies spatially within the genital tract. Histochemical studies demonstrate that mucus within mucosal folds in the cervix is less viscoelastic and express more negatively charges than mucus within the central cervical canal. [62] Animal studies also show that the mucosal folds contain fewer leucocytes than the central canal and appear to more readily retain sperm. [63] These studies led to the hypothesis that cervical mucus inside the mucosal folds and crevices may be the primary path for sperm to reach the uterine cavity, or conversely, may serve as a sequestration and storage compartment for mucus. [64, 65]

Another function of cervical mucus may be to direct movement of sperm. Sperm in cervical mucus swim in a straighter line than inside other media. [66] In addition, sperm align along the fibers of cervical mucus. [67, 68] Thus, it is speculated that sperm may be able to travel along the mucin fiber bundles through the cervical mucus layer.

### *1.3.2.1 Cervical mucus related infertility*

The cervical mucus function test, an *in vitro* diagnostic test to assay the ability of sperm to penetrate cervical mucus, shows that poor sperm penetration is correlated with fewer pregnancy rates. [69, 70] Such poor penetration is independent of the normal fluctuations in mucus permeability during the menstrual cycle, suggesting that cervical mucus dysfunction is an underlying factor for infertility.

One mechanism for poor sperm penetrability is the presence of anti-sperm antibodies. [71] Anti-sperm antibodies may be found both in cervical mucus and semen, demonstrating they may be produced by both males and females. [72, 73] One study showed that 15% ($n$ = 153) of women with infertility tested positive for anti-sperm antibodies in cervical mucus. [73] Such antibodies do not directly harm sperm, but immobilize them inside cervical mucus, leading to "shaking" of sperm in place rather than free movement of sperm. [74, 75] It was discovered that the Fc region of anti-sperm antibodies bind to cervical mucus, while the Fab region binds to sperm, thus allowing anti-sperm antibodies to cross link sperm to mucus. [76]

### 1.3.3 Acid barrier function of the mucus layer

In the stomach, a 50-500 μm thick mucus layer protects the gastric epithelium and mucosa against the acidic environment of the stomach lumen. Measurements in animals and humans have indicated a stable pH gradient across the gastric mucus layer of pH 5-7 at the epithelial tissue surface and pH 1-3 in the lumen. (Fig. 1-3) [19, 20] Since the digestion capabilities of gastric juice were discovered two centuries ago, two mysteries of the pH gradient regulation have remained unsolved. First, how does the mucus layer prevent diffusion of $H^+$ from the gastric lumen to the gastric epithelial cells? Second, how does $H^+$ secreted by parietal cells deep within the gastric pits become transported to the lumen through the more neutral pH zone at the epithelial surface?

Several theories seek to explain the acid barrier function of the stomach. The dominant theory, the bicarbonate pH neutralization theory, holds that bicarbonate continuously secreted by the gastric epithelium reacts with $H^+$ diffusing from the gastric lumen to the epithelium to form $CO_2$, thereby neutralizing acid diffusing toward the gastric wall. [77] Bicarbonate secretion is demonstrated by the presence of bicarbonate in the gastric juice. [78] It is also indirectly shown by a reduction in acid barrier function when carbonic anhydrase, the enzyme partially responsible for forming bicarbonate in the epithelium, is pharmacologically inhibited. [79-81] Bicarbonate secretion alone, however, appears quantitatively insufficient to account for the full barrier function. [82]

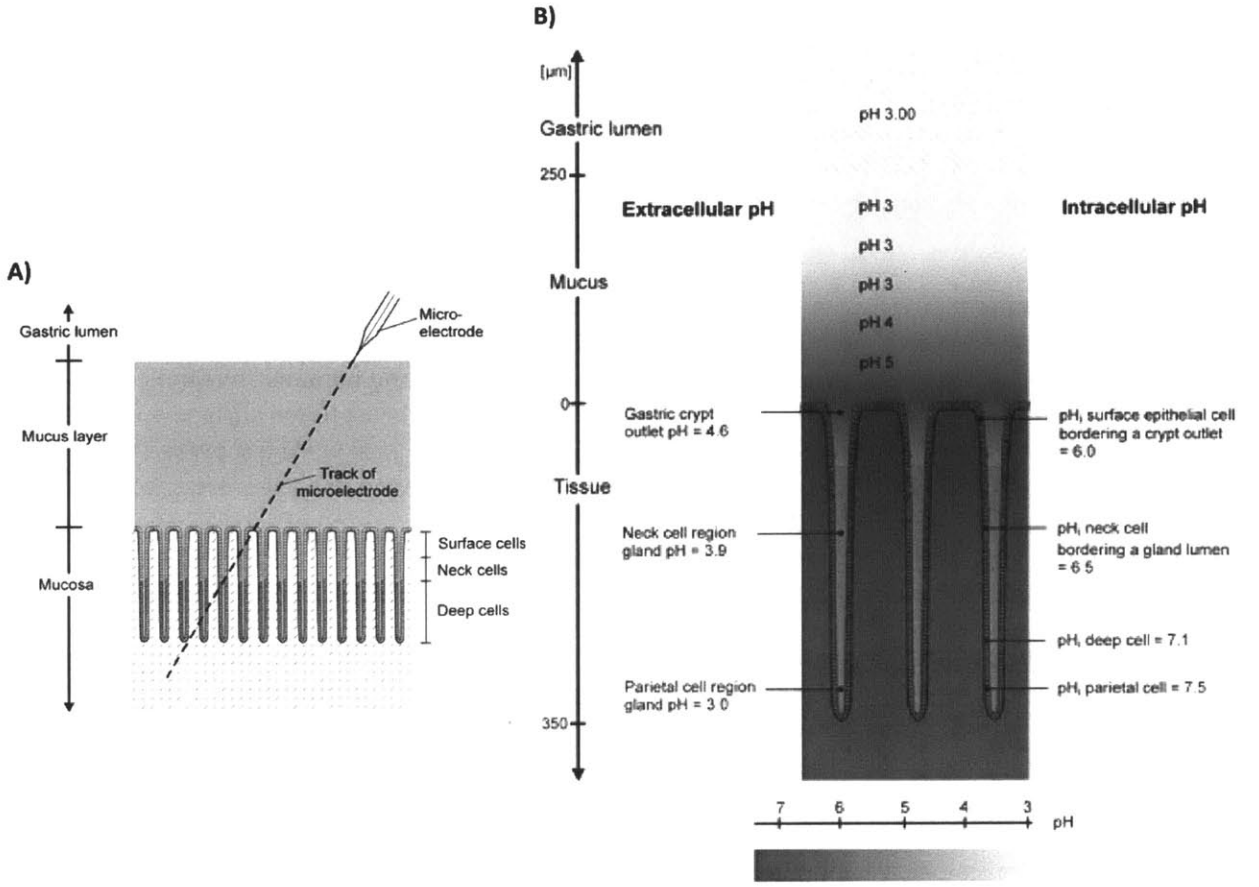


**Fig. 1-3**: pH gradient of the gastric mucus layer and mucosa. A) Scheme to measure the pH gradient of the gastric mucus layer. A pH microelectrode is gradually advanced into the mucus layer and mucosa, allowing the pH of the mucus layer, gastric pits, and the epithelial cell intracellular pH to be measured. B) pH gradient of the gastric mucus layer and mucosa, demonstrating that the mucus layer separates the acidic environment of the gastric lumen from the more neutral pH of the epithelial layer surface. Figure adapted from [20]. Reproduction permission not required. © 2000 American Physiological Society.

Lipids within the mucus barrier are also hypothesized to slow the penetration of acid. [83]The lipid barrier hypothesis is proposed after water contact angle experiments showed that the surface of the *in vivo* mucus layer is hydrophobic. [84] Mucus with lipids chemically removed also showed less resistance to $H^+$ *in vitro* than modified mucus, further supporting that lipids within the mucus barrier hinders $H^+$. [85] It is hypothesized that a hydrophobic monolayer of lipids may exist within or on the surface of the mucus layer which repels acid in a similar manner as the cell membrane slows the penetration of charged ions. (Fig. 1-4C) [83] This hypothesis remains controversial however, because no demonstration of the hypothesized lipid layer has been visualized.

Related to the question of how the gastric mucus layer prevents the transport of acid from the lumen to the epithelium is the question of how the gastric lumen becomes acidic in the first place. Acid is produced by parietal cells deep within the gastric pits several hundred microns behind the gastric epithelium. [86] This suggests that $H^+$ must travel through a relatively pH neutral zone near the surface of the epithelium and up an $H^+$ concentration gradient before it can reach the lumen. Several hypotheses have been proposed to explain this apparent unidirectional transport of $H^+$.

The mucus buffering model (Fig. 1-4A) proposes that the $H^+$ transport from the gastric pit to the gastric lumen is based on the ability of mucus to buffer $H^+$. [87] In this model, $H^+$ ions secreted by parietal cells in the gastric pits would be bound to the freshly secreted mucus. $H^+$ bound mucus are then transported along with pepsinogen secreted by other cells towards the lumen by the continuous pressure of secretion. Upon arriving at the lumen, pepsinogen is activated to pepsin in the low pH environment. Pepsin digestion of the $H^+$ laden mucins would then releases the $H^+$ into the lumen to maintain the low lumen pH.

Another explanation proposed is the viscous fingering model. [88] (Fig. 1-4B) In this model, the behavior of $H^+$ mobility through the mucus gel is thought to be dependent on gel pH. When a less viscous fluid is injected into a more viscous one, a complex interface develops. The less viscous fluid penetrates the more viscous one in multiple narrow streams rather than displacing the more viscous fluid in bulk. [89] In the mucus gel, since mucus viscoelasticity is pH dependent, this "viscous fingering" phenomenon occurs if HCl is injected into a gel at pH 5 and higher. If the mucus pH is 4 or less, however, the injected HCl does not enter the gel, but instead leaks out and travels around it. These results suggest that $H^+$ back diffusion from the lumen to the epithelium would not occur since the lumen pH of less than 4 would cause the mucus gel to resist $H^+$ penetration. The authors claimed that secreted acid from the epithelium can forms viscous fingers and penetrate the mucus gel from the parietal cells on the epithelial side. However, although the formation of viscous fingers is clearly shown to be dependent on the gel pH, it is unclear how the mucus gel would allow the formation of viscous fingers to transport acid from the epithelium side to the lumen side but not similarly allow viscous fingers to form and transport acid in reverse.

**A)**

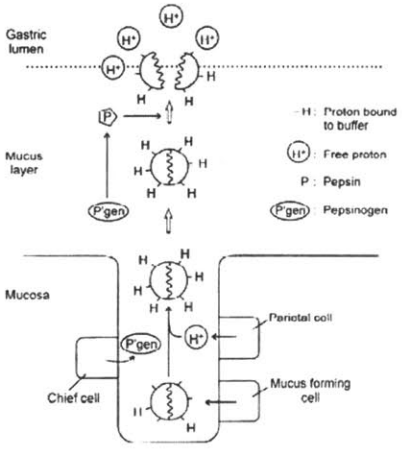


**B)**

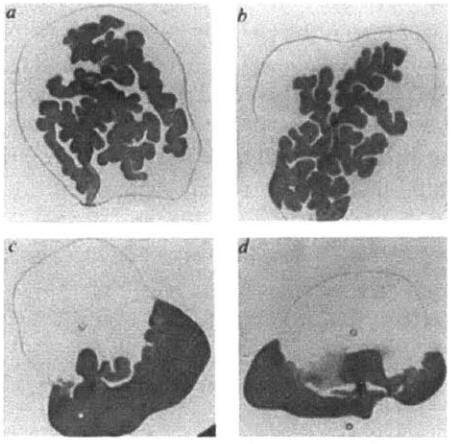

C)

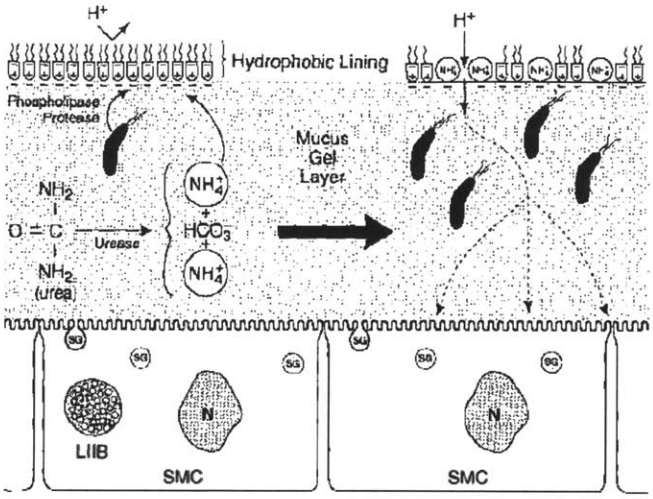


**Fig. 1-4**: Proposed mechanisms in the literature for the $H^+$ barrier function and unidirectional $H^+$ transport.

A) Mucus $H^+$ carrier model. $H^+$ secreted by parietal cell in the mucosa binds to freshly secreted mucus. Upon migration to the lumen, digestive enzymes including pepsin degrade the mucus. Degraded mucus then releases $H^+$ and lowers the lumen pH. Adapted from [87]. Reproduction permission not required. © 1997 American Physiological Society.

B) Viscous fingering model. HCl solution injected into partially purified gastric mucus gel at pH 7 (a), 5 (b), 4 (c), and 2 (d). HCl solution forms "viscous fingers" which penetrate the mucus gel at pH 5 and higher but does not enter the gel at pH 4 and less. This model seeks to explain the observed unidirectional transport of $H^+$ through the mucus layer from the parietal cells to the gastric lumen but not in reverse. Adapted from [88]. Reproduced with permission. © 1992 Nature Publishing Group.

C) Lipid layer model. Approximately 10-40% of native mucus is composed of lipids. A surface lipid layer composed of positively charged fatty acids provides an acid resistant hydrophobic coating. A mechanism for *H. pylori* mediated mucus layer damage and peptic ulceration is also proposed, where urease secreted by the bacteria generates ammonia and disrupts the surface lipid layer, leading to acid damage of the epithelium. Adapted from [83]. Reproduced with permission. © 1995 American Physiological Society.

At this current time, no single or combination of these mucus barrier components has been shown to be quantitatively sufficient to account for the entire acid barrier function of the stomach or can fully explain the unidirectional acid transport from the parietal cells to the gastric lumen.

## 1.3.4 Control of macromolecule and particle permeability

Particles such as bacteria and viruses routinely contact the mucus layers of the body. The transport of macromolecules such as signaling molecules, toxins secreted by bacteria, and drug molecules across the mucus layer is also important physiologically. Two models describe the selective permeability of the mucus layer to macromolecules and particles.

### *1.3.4.1 Size exclusion model of mucus permeability*

One model to describe the permeability of the mucus barrier to macromolecules is the size exclusion model. Based on this model, macromolecules or particles larger than the ~100 nm pore size of mucus [90] would be hindered, whereas smaller molecules would diffuse freely. Olmsted *et al.* [90] and Saltzman *et al.* [91] tested the diffusivity of native proteins and antibodies using fluorescence recovery after photobleaching (FRAP) for mid cycle cervical mucus, finding that the majority of such native

macromolecules were not hindered by mucus. In contrast, the HSV virus, where is larger than mucus pores, were hindered by mucus. [90] (Fig. 1-5) Olmsted *et al.* adapted a gel filtration mathematical model to describe the size exclusion of macromolecules and particles, given by

$$\frac{D_m}{D_o} = exp\{(-\pi/4)[(r_s + r_f)/(r_m + r_f)]\} \tag{1.1}$$

where $D_m$ is the diffusivity of the particle in mucus, $D_o$ is the diffusivity in water, $r_s$ is the particle hydrodynamic radius, $r_f$ is the mucin fiber radius, and $r_g$ is the radius of the mucus network spacing.

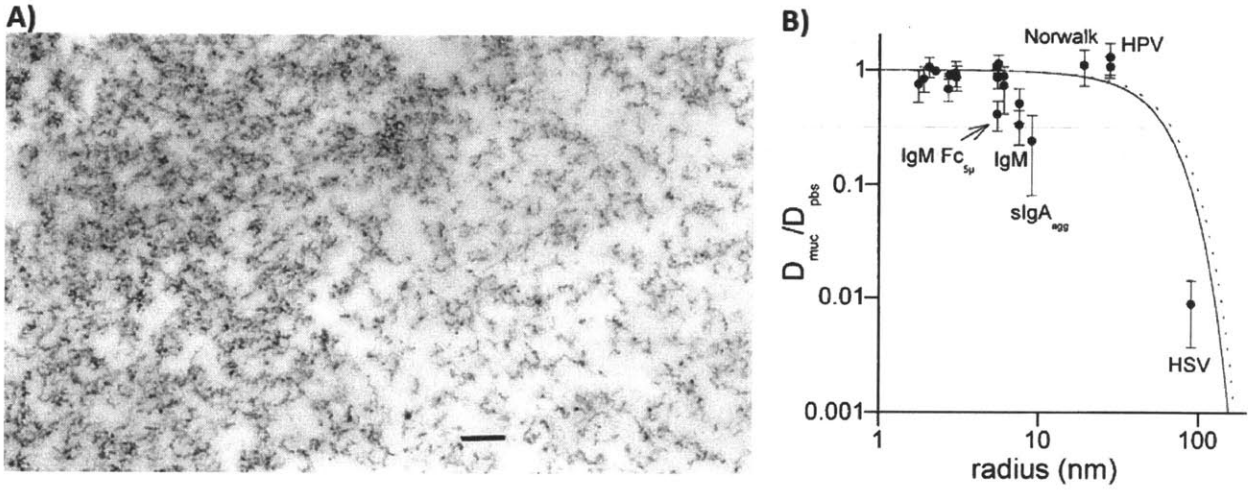


**Fig. 1-5**: Size exclusion model of mucus permeability to macromolecules and particles. A) Transmission EM of human mid-cycle cervical mucus. Scale bar is 200 nm. The interfiber diameters range from ~10 to ~100 nm, while the mucin fiber diameters are ~10 nm. B) Normalized diffusivity of native proteins, antibodies, and the Norwalk, HPV, and HSV virus particles inside mid-cycle cervical mucus. The solid and dotted lines represent the size exclusion model of mucus permeability as described by equation (1.1). In the size exclusion model, proteins and particles larger than the pore size of mucus would be hindered. Figure adapted from [90]. Reproduced with permission. © 2001 Elsevier.

### *1.3.4.2 Interaction filtration model of the mucus barrier*

The size exclusion model of mucus permeability cannot fully explain the permeability barrier of the mucus layer. In Fig. 1-5, the size exclusion model correctly predicted that most small proteins diffused unhindered through cervical mucus, but did not predict the reduced diffusivity of several antibodies.

Recently, the interaction filtration model of mucus permeability was developed. This model is based on the diffusivity of functionalized artificial microspheres. Lai *et al.* showed that polystyrene microspheres functionalized with poly-ethylene-glycol (PEG) diffused much faster inside cervical mucus than carboxyl terminated microspheres. [92, 93] Indeed, larger PEG functionalized (500 nm) microspheres diffused several orders of magnitude faster than smaller (100 nm) unfunctionalized microspheres, suggesting that interaction based filtering can be much more powerful than size exclusion. [92]

Charge selective transport may be an interaction filtration mechanism. Lieleg *et al.* [94] probed the permeability of purified mucins using 1 μm diameter microspheres functionalized with amine groups, carboxyl groups, or 750 Da PEG polymers. At all pH values probed, the amine and carboxyl microspheres were equally hindered by mucins, while PEG functionalized microspheres diffused much faster. Lieleg *et al.* interpreted the results as indicating that mucins contain positively and negatively charged groups

which bind to and hinder the amine and carboxyl microspheres, but would not bind to the neutrally charged and hydrophilic PEG polymers. [94] Another source of hindrance, however, is the hydrophobic polystyrene groups on the microsphere surface which may bind to mucins through lipophilic interactions. Amine and carboxyl groups are smaller than PEG polymers. Thus, the PEG coated microspheres may diffuse faster since PEG more effectively shields the polystyrene surface. A different charge selective criterion is found by Crater *et al.*, who showed that negatively charged 200 nm microspheres diffused 3 fold faster than positively charged 200 nm microspheres. [95] (Table 1-3) These results indicate that electrostatic interaction with mucins may be an interaction selective filtration mechanism, but hydrophobic interactions may also play a significant role.

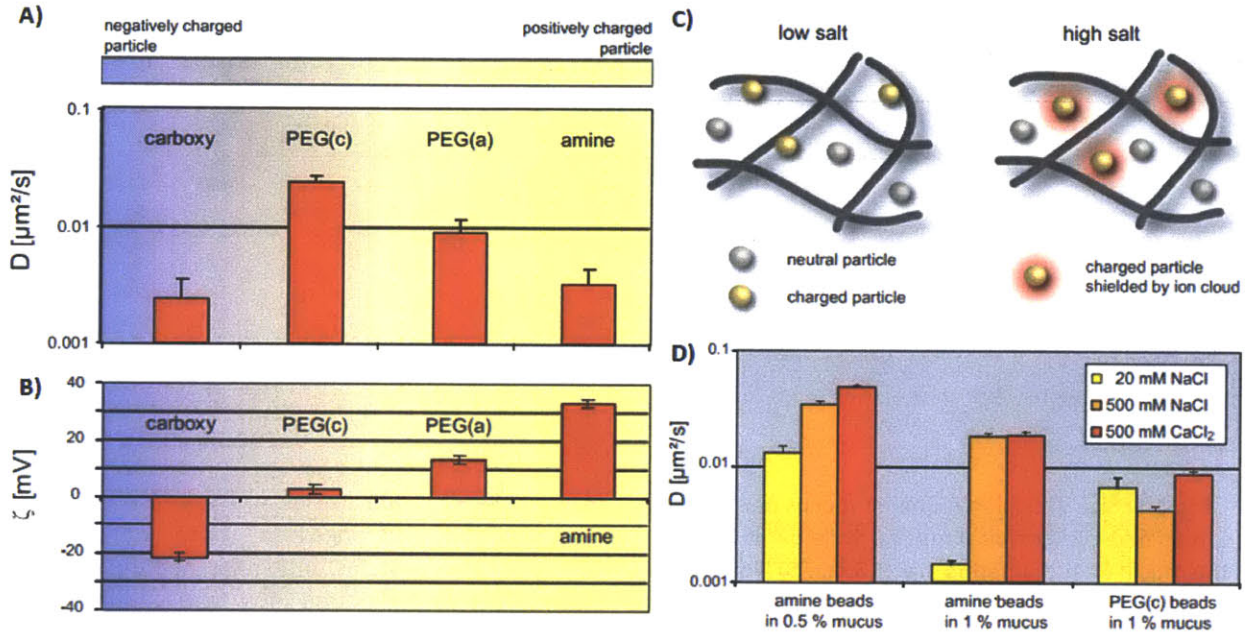


**Fig. 1-6**: Charge selective interaction filtering by mucins. A) Diffusivity of 1 μm polystyrene microspheres functionalized with different surface groups in 0.5% (w/v) mucins at physiological pH and 20 mM NaCl ionic strength. PEG(c) and PEG(a) microspheres were created by PEG functionalization of amine terminated and carboxyl terminated microspheres, respectively. The presented findings demonstrate that charged microspheres are more hindered than PEG functionalized microspheres. B) ζ-potential of each microspheres surface type. C) Schematic of the effect of ionic strength on mucin-microspheres interactions. D) Effect of ionic strength on the diffusivity of amine and PEG particles. These findings suggest that electrostatic interactions underlie the charge selective permeability of purified mucins. Figure adapted from [94]. Reproduced with permission. © 2010 Elsevier.

Charge selective filtration of functionalized particles has also been investigated in native mucus *in vitro*. As in the experiments in purified mucins, it is also unclear whether positively charged or negatively charged microspheres diffused faster. Polystyrene microspheres with diameters 100, 200, and 500 nm used to probe the permeability of human cystic fibrosis sputum showed that amine coated microspheres diffused ~3 folds faster than carboxyl ones. [96] These results contradicted findings by Crater *et al.* that carboxyl and sulfated coated microspheres diffused at 1.3x to 2x the speed of the amine coated microspheres in intestinal mucus. [95] The discrepancy may result from different charge density on the particles used by the two studies, as evidenced in Table 1-3, where the difference in surface charge between the amine and carboxyl particles used by Dawson *et al.* were much smaller than the difference in the surface charge between the amine and carboxyl particles used by Crater *et al.*

**Table 1-3** Comparison of ζ-potential (surface charge density) of 200 nm functionalized polystyrene particles and ratios of their ensemble average diffusion coefficients in mucus ($D_m$) and in water ($D_w$).

| Study | Mucus Source | Particle surface | ζ potential at physiological pH (mV) | $D_m/D_w$ |
|---|---|---|---|---|
| **Dawson *et al.* [96]** | CF sputum | Amine | -4.6 | 0.003998 |
| **Dawson *et al.* [96]** | CF sputum | Carboxyl | -19.1 | 0.001333 |
| **Crater *et al.* [95]** | Intestinal | Amine | 6.9 | 0.025 |
| **Crater *et al.* [95]** | Intestinal | Carboxyl | -36.6 | 0.032 |
| **Crater *et al.* [95]** | Intestinal | Sulfate | -55 | 0.049 |
| **Crater *et al.* [95]** | Purified mucin | Amine | 6.9 | 0.021 |
| **Crater *et al.* [95]** | Purified mucin | Carboxyl | -36.6 | 0.086 |
| **Crater *et al.* [95]** | Purified mucin | Sulfate | -55 | 0.091 |

## 1.4 Mucus as a barrier for drug delivery

Orally taken drugs destined for systemic circulation must pass through the gastrointestinal mucus barrier, and inhaled drugs must pass through airway mucus. *In vivo* experiments indicate that mucolytics drugs, or compounds which disrupt gel structure of the mucus layer, tend to increase absorption of drugs across the mucus layer. For example, antibiotic transport from the bloodstream into respiratory secretion improved when bromhexine, a mucus fluidizing agent, is administered. [97] Treatment of chronic bronchitis patients with erythromycin attached with N-acetylcystein, a reducing agent which can disrupt the disulfide bonds of mucins, also led to improved patient outcomes than erythromycin alone. [98] N-acetyl-cysteine co-administered with Dextrans into the gastrointestinal tract of rats increased Dextran absorption into the blood stream, [99] and N-acetyl-acetylcystine co-administered with inhaled gene carriers resulted in improved gene expression in the epithelium. [100] Such experiments suggest that the mucus layer hinders drug permeability across the mucosa. One challenge in interpreting *in vivo* experiment results, however, is that mucolytics often alter other physiological parameters other than mucus structural integrity. For examples, bromhexine can alter mucus secretion rates, [101] and N-acetyl-cysteine can alter the pH of the mucus layer.

Mucus permeability to drug molecules has also been measured *in vitro*. Niibuchi *et al.* determined through equilibrium dialysis and gel filtration that binding occurred between intestinal mucins and 13 β-lactam and 3 aminoglycoside antibiotics. Such binding decreased as a function of ionic strength, suggesting that charge selective mechanisms mediate binding to mucins. [102] Bhat *et al.* measured the permeability of a purified mucin barrier against the diffusion of five drugs which spanned a range of aqueous solubilities and ionization states, finding that all five drugs were similarly hindered by mucins. [103] Bataillon studied the binding of positively charged antibiotic amikacin to CF sputum samples, finding that the degree of binding depends on the quantity of DNA and the presence of acidic mucins, consistent with electrostatic binding between amikacin and negatively charged DNA and acidic mucins. [104] Diffusion of radiolabeled EDTA and DTPA through purified mucins from chronic bronchitis patients was assayed by capillary desorption method, finding that these molecules bind strongly to mucins and are unlikely to penetrate through the mucus barrier of physiological thickness over a period of several hours. [105] Tetracycline binding to intestinal mucins was assessed using equilibrium dialysis, showing that tetracycline binding to mucins is consistent with electrostatic and hydrophobic interaction processes. [106] Overall, these *in vitro* studies confirmed that mucus hinders the passage of many small molecule and macromolecule drugs.

Currently, two types of dosage forms are under development to improve the delivery of drugs through the mucus layer. These are mucoadhesive and mucoinert dosage forms.

### 1.4.1 Mucoadhesive dosage forms

The transit speed of drugs through the gastrointestinal tract significantly affects the time available for orally ingested drugs to diffuse across the mucus layer and absorb into systemic circulation. For example, targeting and maintaining a drug dosage form to the duodenum, as is optimal for absorption of common drugs including furosemide [107] and riboflavin, [108] is difficult because the transit time through the duodenum is only several minutes long. [109, 110] Mucoadhesive dosage forms have been developed to prolong this residence time, thus prolonging the time duration available for drug absorption. [111] Mucoadhesives formulations may also enable closer contract of the drug dosage form to the mucus layer, which would increase drug transport flux.

Mucoadhesive materials primarily bind to mucus through nonspecific binding interactions. Cross-linked acrylic acid based microspheres were found to adhere to the gastrointestinal mucosa in *ex vivo*

experiments. [112] Carboxylvinyl based microspheres are another type of mucoadhesive delivery system found to adhere to the stomach wall, and have demonstrated the improved delivery of amoxicillin to the gastric mucosa for *H. pylori* treatment. [113] Presumably, both the acrylic acid based and carboxylvinyl microspheres adhere to the stomach wall via mucus interaction rather than cell interaction, since they are several hundred microns in diameter and therefore too large to pass through the mucus barrier to bind to the underlying epithelium. [112, 113] Chitosan has been extensively studied as mucoadhesive drug encapsulating material, and have been shown to improve drug and gene delivery. [114] Examples of chitosan based drug encapsulating nanoparticles include chitosan-insulin nanoparticles [115], chitosan nanoparticles encapsulating lipophilic drugs such as cyclosporine A, [116] and chitosan layer functionalized liposomes containing the peptide drug calcitonin. [117] Chitosan is positively charged, and therefore likely adheres to the negatively charged mucins in the mucus barrier. However, since free chitosan administered into the GI tract also improves absorption of drugs, [118] it is possible that chitosan binding alters the structural integrity of the mucus barrier, as has been demonstrated for the binding of small particles to mucus. [119] Chitosan also improves drug delivery by increasing the permeability of the epithelium cell layer, which is a mucus-independent pathway to improve drug adsorption. [120]

Other synthetic polymers used for non-specific mucoadhesion include cellulose, poly-hydroxyethyl-methylacrylate, poly-ethylene-glycol, poly-vinyl-pyrrolidone, and poly-vinyl-alcohol. Natural polymers include alginate, xanthan gum, and gelatin. [121] It is currently unclear by what molecular mechanisms the most such nonspecific mucoadhesives polymers function. The possible types of bonds between mucus and mucoadhesive molecules include ionic bonds between positively charged polymers and sialic acids, hydrogen bonds, van der Waals interactions, and hydrophobic interactions. [121] Theories using combinations of these forces to describe mucoadhesion include the electronic theory, adsorption theory, diffusion theory, wetting theory, fracture theory, mechanical theory. Detailed discussions of the theories which underlie mucoadhesion may be found in Smart. [122]

A "second generation" of mucoadhesives is currently development. Second generation refers to the ability for the mucoadhesive to specifically target receptors inside the mucus barrier or on the epithelial cell surface. This second generation includes thiolated polymers which selectively bind to the cysteine rich regions of mucins, [123] and lectins which bind to specific glycans on mucins or the cell surface. [124]

### 1.4.2 Mucoinert dosage forms

Mucoinert dosage forms are designed for the opposite behavior as mucoadhesives. They seek to reduce binding interactions with mucins, thus resulting in rapid penetration through the mucus layer. We have already reviewed the use of PEG coating to improve the diffusion mobility of polystyrene microspheres inside native cervical mucus . (See Section 1.3.4.2) PEG coating can also improve the diffusion speed of poly(lactic-co-glycolic acid) and polysebacic acid microspheres inside cervical mucus [125], polystyrene microspheres in CF sputum, [126] and polystyrene microspheres in purified mucins. [94] Faster diffusion inside mucus enables the drug encapsulated microspheres to penetrate closer to the epithelial tissue rather than be stuck to the surface of the mucus layer, as is the tendency for mucoadhesives. Such PEG coated nanoparticles improved delivery of antiviral drugs *in vivo* through cervical mucus to the vaginal epithelium. [127]

The mechanism causing PEG coated particles to diffuse much faster than non-PEG particles are controversial. Wang *et al.* compared the diffusivity of 200 nm carboxyl terminated polystyrene particles functionalized with 2 kDa PEG vs. 10 kDa PEG, shown in Fig. 1-7A. The results showed that 2 kDa PEG converted mucoadhesive particle behavior into mucoinert behavior, whereas 10 kDa PEG did not. One

possibility is that longer PEG chains create greater physical entanglements with mucus, thus causing hindrance. [128] The density of surface coverage also plays a role in PEG coating effectiveness. (Fig. 1-7B)

**A)**

| PEG MW [kDa] | Diameter [nm] | ζ-potential [mW] | PEG Coverage [%] | $D_m/D_w$ |
|---|---|---|---|---|
| None | 217 ± 5 | -59 ± 4 | n/a | 0.00042 |
| 2 | 231 ± 6 | -2 ± 4 | 69 ± 1 | 0.15 |
| 10 | 229 ± 3 | -1 ± 3 | 65 ± 1 | 0.00015 |
| 2 | 224 ± 6 | -10 ± 3 | 42 ± 3 | 0.00022 |

**Table: Characterization of carboxyl terminated and PEG modified polystyrene particles and ratios of their ensemble average diffusion coefficients in mucus ($D_m$) and in water ($D_w$).**

**B)**

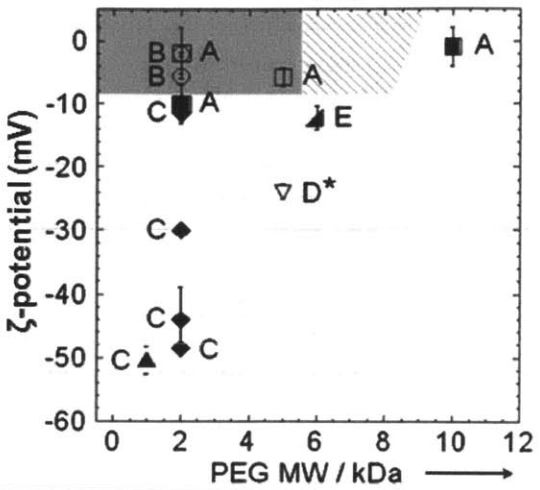


**Fig. 1-7**: Effect of PEG coating on hindrance of particles by mucus. Left: Table comparing effectiveness of PEG coating on improving diffusivity of 200 nm carboxyl terminated polystyrene particles. Coating of 2 kDa PEG at a high coverage drastically improves diffusivity, whereas coating of 10 kDa PEG or coating of 2 kDa at lower coverage does not improve diffusivity significantly. Right: Phase diagram comparing effectiveness of PEG coating on improving diffusivity. Open symbols indicate PEG coating increased diffusivity relative to control, while closed symbols indicate increased mucoadhesive behavior. The shaded and hatched areas represent the PEG molecular weight and ζ-potentials corresponding to mucoinert diffusion as postulated by Wang *et al.* [128] Figure adapted from [128]. Reproduced with permission. © 2008 John Wiley and Sons.

## 1.5 Challenges and unanswered scientific questions

We have reviewed the selective permeability function of the mucus barrier as it relates to its ability to regulate acid transport, protect against pathogens, and regulate drug transport. Many important scientific questions regarding the selective permeability of the mucus layers remain unanswered. These questions include: what are the molecular criterions which determine whether molecules, particles, or viruses can transit through the mucus layers, accumulate within the mucus layer, or does not enter the mucus layer? Understanding such criterions may improve understanding of mucosal diseases, as well as improve the design of drugs or drug carriers with targeted mucus layer interaction and penetration characteristics. Another important question is how the selectively permeability may change in response to altered mucus layer composition such as altered ionic content, pH, and mucin concentration. As we discussed in this chapter, such mucus layer composition changes can occur with disease processes in the mucus layers.

For the acid barrier function, the current literature has shown that bicarbonate pH neutralization, the lipid barrier, and mucus buffering are mechanisms which contribute to the $H^+$ barrier function. Unanswered scientific questions include: What is the relative importance of each of these three barrier components? Are the components quantitatively sufficient to account for the entire barrier? And by what biophysical mechanisms do the lipids and mucins protect the barrier against acid?

# Chapter 2

# Current *in vitro* technologies to characterize mucus permeability function

This chapter presents current technologies most often used to study the permeability of the mucus barrier *in vitro*. An overview of the design and operating concepts of each technology is presented, along with advantages and disadvantages of each technique for the study of mucus permeability.

## 2.1 Diffusion chambers

The diffusion chamber consists of two continuously stirred chambers separated by a compartment where a semi-permeable material to be tested is placed. (Fig. 2-1) The two chambers are usually filled to the same level so that convection does not occur. The diffusing species being tested is placed in one chamber, where it diffuses down the gradient into the other chamber. The steady state flux is used to calculate the effective diffusivity of the diffusing species.

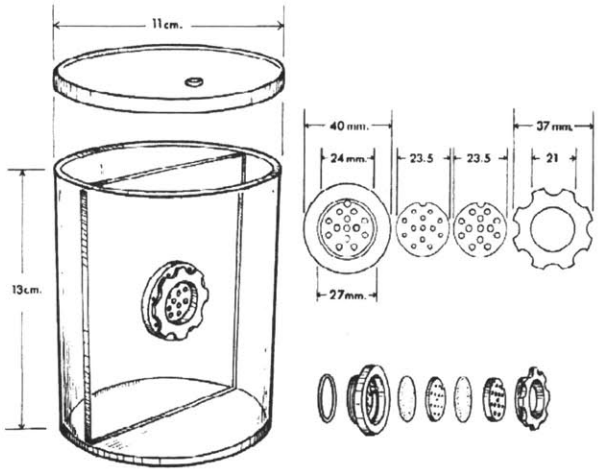


**Fig. 2-1**: Schematic of a typical diffusion chamber used to assay mucus barrier function. The mucus sample is loaded into the center chamber, and small molecules placed on one side of the chamber diffuse through the mucus samples into the other. The effective diffusivity of the diffusing molecule is calculated using the measured flux from one side of the chamber to the other according to (2.3). Figure adapted from [129]. Reproduction permission not required. © 1981 American Physiological Society.

At steady state, the concentration profile of the diffusing species in the diffusion chamber can be described by the diffusion equation and boundary conditions, given by

$$\begin{cases} 0 = \frac{Dd^2c}{dx^2} \\ c(x=0) = c_0 \\ c(x=L) = 0 \end{cases} \tag{2.1}$$

where $D$ is the effective diffusion coefficient, $c$ is the concentration of the diffusing species, $L$ is the length of the mucus chamber, and $c_0$ is the concentration of the diffusing species in the donor chamber. Note that $D$ is the effective diffusivity, which includes all sources of diffusion hindrance including steric hindrance, binding interactions with mucus, Donnan exclusion effects, and etc. The solution to eqn (2.1) is linear and given by

$$c(x) = c_0\left(1 - \frac{x}{L}\right) \tag{2.2}$$

The diffusion flux from one side of the chamber to the other (in units of mol/s) is calculated from eqn (2.2) based on Fick's first law of diffusion, arriving at

$$f = DA\frac{c_0}{L} \tag{2.3}$$

where $A$ has units of $m^2$ and is the effective cross sectional area of the mucus compartment. $f$ is an experimentally accessible parameter and is measured by monitoring the concentration of the diffusing species in the receiver chamber, allowing eqn (2.3) to be used to solve for $D$.

In general, the diffusion chamber is widely used because it is conceptually easy to set up and the data analysis is straightforward. This technique can be used for any species where an analytical method is available to measure the species concentration in the receiver chamber. This is an advantage to techniques such as multiple particle tracking or FRAP where fluorescence labeling of the species must be feasible.

The diffusion chamber also has a number of disadvantages. First, the amount of time mucus can be maintained in the center compartment without substantial loss through the membranes is limited. In effect, this sets an upper limit on the size of the diffusing species which can be tested, since species which are too large would not diffuse through the mucus barrier or reach steady state flux before the mucus sample diffuses away. Another disadvantage is that the diffusion chamber gives a single diffusivity value which takes into the account the average hindrance provided by the mucus, and heterogeneities in the mucus sample are difficult to study. Lastly, relatively large sample volumes must be used for the diffusion chamber, limiting the number of experiments which may be practically carried out, particularly using well purified samples which are usually limited in quantity.

In general, the diffusion chamber experiments cannot distinguish between slowed diffusion due to steric hindrance of the mucus network *vs.* slowed diffusion due to binding interactions. An exception to this rule occurs when a competitive binding species is available, and the material under test can withstand a long experiment. One example is the use of fluorescently labeled species to measure the steady state flux, and then add a non-fluorescent version of the diffusing species to the donor chamber. If binding is a mechanism for the diffusion hindrance, then the non-fluorescent version of the species would compete with the fluorescent version for binding sites, leading to a measurable increase in the steady state flux of the fluorescent species. [130, 131]

## 2.2 Multiple Particle tracking

Multiple particle tracking (MPT) is a technique used to measure the biochemical and mechanical properties of mucus by tracking the diffusion characteristics of particles as probes within the mucus sample. In the active approach to MPT, the force or deformation is actively applied such as by atomic force microscope [132] or optical tweezers. In the passive approach, Brownian motion drives the random movement of the particles. By using particles which have known size and surface properties, the diffusion response of the particles can be used to deduce the viscoelastic property of the mucus as well as binding interactions between the particles and the mucus. (Fig. 2-2)

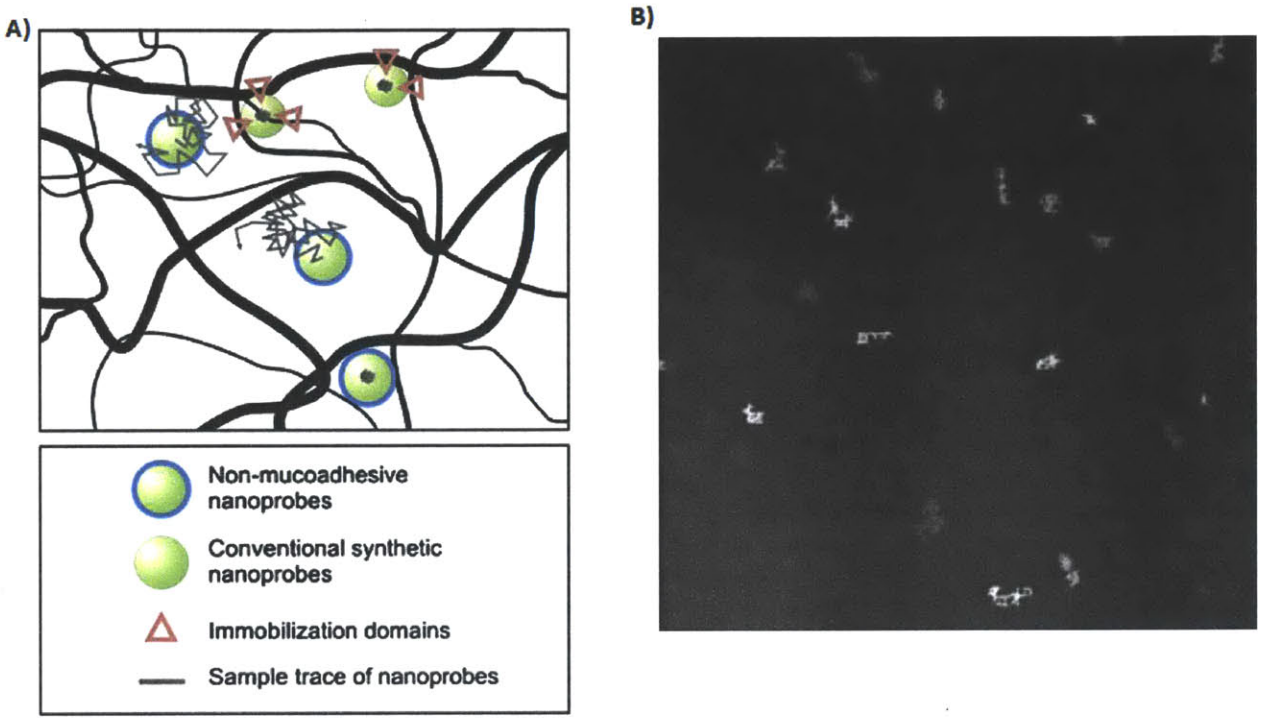


**Fig. 2-2**: Multiple particle tracking technique characterizes interactions of particles with the mucus barrier microenvironment. A) Mucoadhesive particles interact more strongly with mucins than mucoinert particles, and thus mucoadhesive particles diffuse more slowly. Figure adapted from [133]. Reproduced with permission. © 2009 Elsevier. B) Typical trajectory of microparticles obtained by fluorescence microscopy. Figure adapted from [95]. Reproduced with permission. © 2009 Elsevier.

Mucus is primarily studied using the passive approach of MPT. Fluorescently labeled particles are first mixed with a mucus sample. The sample is then mounted on a fluorescence microscope to track the trajectory of the particles as a function of time. The mean squared displacement of a particle diffusing for time interval $\Delta t$ is given by

$$msd(\Delta t) = \frac{1}{N}\sum_{i=1}^{N}[\boldsymbol{r}(t+\Delta t) - \boldsymbol{r}(t)]^2 \tag{2.4}$$

where $N$ is the number of particles and $\mathbf{r}(t) = (x(t), y(t))$ is their two dimensional trajectories. The diffusion coefficient of the particles is then calculated by eqn (2.5).

$$msd(\Delta t) = 4D\Delta t \tag{2.5}$$

For mucus, the primary purpose for MPT is to probe the permeability of the mucus barrier as a function of the surface properties of transiting particles, by comparing *D* of the microspheres of the same size but functionalized with different surface properties. [94-96, 134]

The key advantage of MPT is that the measurements are resolved for individual particles. This ability allows MPT to probe heterogeneous geometric constraints or binding sites distributions within mucus samples. The need to resolve individual particles is also a disadvantage. Almost all studies of mucus permeability using MPT used particles 100 nm or larger. This is on the same order of magnitude as the mucus pore size. [90] Thus, the particles would be expected to interact with the geometric constraints of the mucus network. The selective permeability mechanisms elucidated using the particles and MPT, therefore, may not apply to smaller particles and molecules, as smaller molecules would not be geometrically hindered. Another disadvantage is that MPT tracks the diffusion of particles already fully mixed with mucus. In contrast, *in vivo* transport of molecules into the mucus layer must come from outside the mucus layer interface. Thus, transport effects arising from transport across the mucus layer interface such as partitioning [135] cannot be determined.

## 2.3 Fluorescence recovery after photobleaching (FRAP)

First developed by Axelrod *et al.* in the 1970's [136], fluorescence recovery after photobleaching (FRAP) uses an intense burst from a high powered laser to photobleach a section of the fluorescent molecules inside a biological sample. During the "recovery" phase, fluorescent molecules outside of the zone of photobleaching diffuse into the photobleached area over time. For a circular light beam and assuming two dimensional diffusion, the diffusivity *D* of the fluorescent molecule inside the biological sample is given by

$$D = \frac{0.88w^2}{4t_{1/2}}, \tag{2.6}$$

where *w* is the laser beam radius, and $t_{1/2}$ is the time needed to complete 50% of the recovery. [136] Moreover, any fluorescent molecules irreversibly bound to mucus (the immobile fraction) are photobleached, but remain bound after photobleaching. Therefore, the difference in fluorescence intensity before photobleaching and fully recovered intensity after photobleaching is calculated as the concentration of bound molecules.

The primary benefit of FRAP over other techniques is that intracellular diffusion processes can be assessed. Fig. 2-3 shows the use of FRAP to characterize the mobility of mucin-GFP inside goblet cells. FRAP has been the primary technique used to assay the size selective permeability control of mucus. (See Section 1.3.4.1, Size exclusion model of mucus permeability) One drawback of FRAP is that like multiple particle tracking, fluorescent probes are mixed together with the mucus sample before the start of the experiment, and therefore transport processes across an mucus interface as it occurs *in vivo* has not been measured.

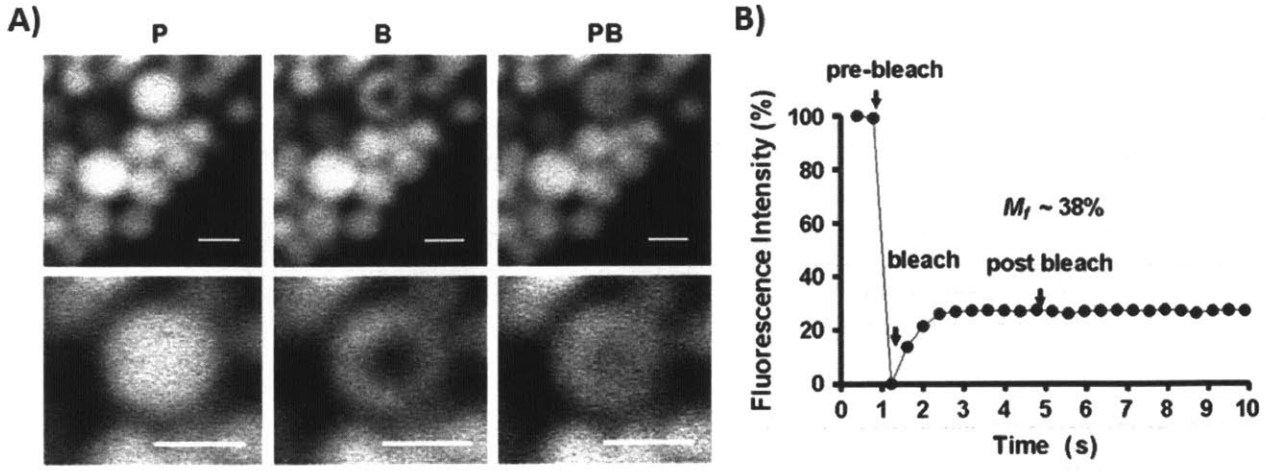


**Fig. 2-3**: FRAP study of mucin-GFP diffusion inside goblet cells. A) Fluorescent micrographs showing photobleaching and fluorescence recovery of mucin containing vesicles in goblet cells. B) Fluorescence as a function of time during the FRAP experiment. The diffusivity of mucin-GFP molecules can be calculated using this fluorescence curve based on eqn (2.6), and the fraction of immobile mucins can be calculated by subtracting the post-bleach equilibrium fluorescence from the pre-bleach fluorescence. Figure adapted from [137]. Reproduced with permission. © 2007 American Thoracic Society.

In summary, we reviewed three technologies used most often to characterize the selective permeability of the mucus barrier. Each technology contains a number of advantages and disadvantages. An ideal technology to characterize mucus layer permeability would contain several features. First, it would enable the study of how molecules and particles transport from outside to inside the mucus layer, rather than purely measure the diffusion speed within the mucus layer as is the case with particle tracking and FRAP. Transport into a mucus barrier consists of two processes. First, a molecule must transport across the mucus layer interface, and then it must translocate inside the mucus layer. The forces which may hinder or aid particle transport may be different for the two processes. For examples, an interfacial electric field may form across the mucin layer interface due to the presence of fixed charge on the mucin molecules. [131] Another desirable feature of the assay would be to reproduce the continuously replenished nature of the mucin barrier as it occurs *in vivo*, which may provide fresh binding sites for the diffusing particles and molecules and thus alter transport behavior. A final desirable feature is to measure the concentration profile of molecules and particles as they transport into the mucus barrier, rather than the indirect measurement of diffusion flux measured using the diffusion chamber. Obtaining the concentration profile may lead to better understanding of the interactions between the molecules/particles with mucins and how such interactions affect transport. In the following chapters, we present two microfluidic designs which contain these desirable features.

# Chapter 3

# Microfluidic *in vitro* system for quantitative study of the stomach mucin acid barrier

Note: significant portions of this chapter appear in the following publication: Leon Li, Oliver Lieleg, Sae Jang, Katharina Ribbeck and Jongyoon Han, "A microfluidic in vitro system for the quantitative study of the stomach mucus barrier function," *Lab on a chip*, 2012, **12**, p4071-4079.

Section 3.2.3, Preparation of apomucin by deglycosylation of purified mucin is written by Dr. Thomas Crouzier of the MIT Laboratory for Hydrogel Filters in Biology. Dr. Crouzier also performed the apomucin preparation process as described in the Section 3.4.6.

## 3.1 Introduction

As described in Section 1.3.3, the mucus layer of the stomach protects the gastric epithelium from the acidic digestive juices in the gastric lumen. The currently hypothesized mechanisms underlying this acid barrier of the stomach include bicarbonate neutralization, lipid barrier, and mucus $H^+$ buffering. However, many unanswered questions remain. Our current inability to fully understand the acid barrier of the stomach mucus layer is partly due to the lack of suitable *in vitro* tools to measure $H^+$ transport through mucus. Most *in vitro* studies of acid interaction with mucus use the macroscale diffusion chamber, where the acid diffusion is measured through a static layer of mucus sandwiched between two membranes. (see Section 2.1) While seemingly straightforward as a method, the diffusion chamber contains several drawbacks. First, it requires relatively large sample volumes, precluding the practical use of low-volume native samples or purified native mucins. Second, it is a static device where the mucus cannot be continuously replaced, as is the case *in vivo* due to continuous secretion. Third, it is difficult to measure $H^+$ concentration profiles inside the mucus layer because the device is not easily accessible to live microscopy.

In this work, we present a novel microfluidic system (Fig. 3-1B) that aims to overcome the major limitations of the macroscale diffusion chamber. This device produces a continuous stream of mucus, which flows against incoming acid. A fluorescent pH reporter inside the sample tracks the $H^+$ penetration into the mucin layer, enabling the study of the $H^+$ permeability as a function of time, mucin concentration, and secretion rate. This system requires smaller sample volumes than the macroscale diffusion chamber, and moreover, can be connected to live fluorescence microscopy for the visualization of acid concentration gradients within the mucin barrier.

With this system, we characterize the contribution of purified native mucins to the mucus acid barrier. Native mucins obtained from pig gastric mucus according to the technique of Gong *et al.* [138] are well suited for such study, and have proven valuable for the investigation of mucin gelation properties, [29] *Helicobacter pylori* orientation in the mucus layer, [139], the relationship between particle charge and diffusion through mucin gels, [94] and the antiviral capabilities of mucin. [41] Our results demonstrate that mucins can directly sequester $H^+$ and thereby hinder their diffusion. We estimate the magnitude of the *in vivo* barrier arising from $H^+$ to mucin binding and find that mucin secretion may be equally potent in neutralizing $H^+$ diffusion flux as bicarbonate secretion. Our work demonstrates that the microfluidic system is a suitable *in vitro* model to characterize the barrier of mucus components.

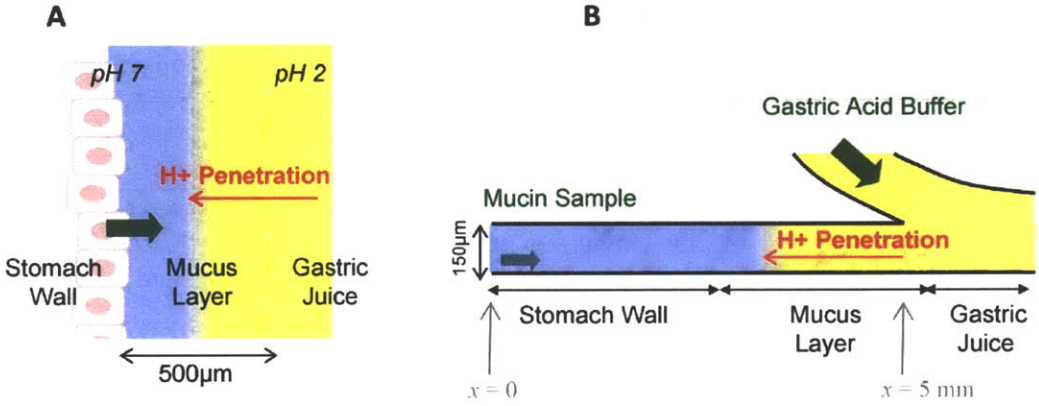


**Fig. 3-1**: Microfluidic device to mimic gastric mucus barrier function. A) Gastric mucus protects the stomach wall from damage from the strongly acidic (pH 1-3) gastric juice. The biophysical mechanism of the mucus $H^+$ barrier is to date unknown. B) Microfluidic *in vitro* model to mimic the *in vivo* gastric mucus acid barrier, reflecting continuous mucin secretion and an $H^+$ concentration gradient. Using this in vitro model, we study $H^+$ penetration into the mucus layer as a function of physiologically relevant parameters.

## 3.2 Methods

### 3.2.1 Mucin purification

Native gastric mucins are purified from scrapings of pig stomachs based on the method of Gong *et al.*, [138] except that the cesium chloride density gradient centrifugation step is omitted. The method is described in details as follows:

1. The stomachs of 20-40 slaughtered pigs are rinsed with tap water to remove partially digested stomach contents. The mucus layer is then carefully scraped to remove and collect the mucus.
2. The scrapings are diluted to a volume of ~4L using a solution containing 200 mM NaCl and 0.04% (0.04 g per 100 mL) $NaN_3$. $NaN_3$ is used as a preservative. The mixture is adjusted to pH 7.4 using NaOH.
3. The following protease inhibitors were added to the mixture. This prevents natural enzymes in the scraped mucus from digesting the mucins
    a. 5 mM Benzamidine
    b. 1 mM dibromoacetophenone
    c. 1 mM phenylmethylsulfonylfluoride
    d. 5 mM EDTA pH 7
4. The mixture is stirred gently overnight at 4 C to solubilize the mucus

5. The mixture is centrifuged at 7000 rpm for 30 minutes at 4°C, and the supernatant is collected. This removes large debris pieces scrapped off with the mucus.
6. The collected supernatant is ultracentrifuged at 30,000 rpm at 4°C for 1.5 hours, and the supernatant is collected. This further removes debris and large aggregates.
7. The collected supernatant is fed by gravity through into a PD-10 column (GE Healthcare, Pittsburgh, PA) and the flow through is collected. The PD-10 column consists of cross linked dextran beads and is usually used as a size exclusion column with an exclusion limit of 5000 Da. However, in this case, we completely saturate the column, thus using the matrix of the column for size filtration, where large debris is trapped in the pores while mucins and smaller proteins flow through the matrix. This step removes any debris not removed by the ultracentrifugation or dislodged from the ultracentrifugation pellet during supernatant collection.
8. The collected supernatant is pumped into a Sepharose 4B-Cl size exclusion column (exclusion limit 2 MDa), and then eluted using 200 mM NaCl solution at a flow rate of 60 ml/h.
9. Fractions of 9 mL each are collected from the Sepharose 4B-Cl column. A periodic acid-Shiff stain assay is performed on a 50 µL of sample from each fraction. The positive fractions indicate the presence of high molecular weight glycoprotein. These fractions are pooled together.
10. The pooled sample is at an ionic strength of 200 mM NaCl (the ionic strength of the Sepharose column elution buffer). We dilute this with DI water in a 1:9 ratio to achieve an ionic strength of 20 mM NaCl.
11. The diluted samples are transferred into an ultrafiltration cell (Series 8000 stirred cell, EMD Millipore, Billerica, MA) with Amicon XM300 membrane (300,000 Da molecular weight cut off). This is used to concentration ~1 L of sample into ~ 50 mL.
12. The concentrated samples are divided into 1.5 mL aliquots, flash frozen in liquid nitrogen, and then lyophilized. This results in lyophilized native purified mucins. The mucins are stored at -80°C until needed for reconstitution.

### 3.2.2 Mucin reconstitution and sample preparation

For microfluidic experiments, the lyophilized mucins were reconstituted at concentrations from 0 to 1% (w/v) in 2 mM and 20 mM HEPES (4-(2-hydroxyethyl)-1-piperazineethanesulfonic acid) buffer, containing 20 mM NaCl, 0.0007% (w/v) of 500 nm polystyrene microspheres (Polysciences Inc., Warrington, PA) and 1.13 µM of the pH sensitive fluorescent dye Oregon Green (Invitrogen Inc., Carlsbad, CA). Oregon Green is not expected to interfere with the mucin barrier function as it is used at relatively low concentrations, and similarly, microspheres added at a similar concentration as used here to native mucus do not alter mucus permeability. [119] At 20 mM, HEPES does not affect the pH dependent viscoelasticity of mucin as measured by rheometry, [94] suggesting that this buffer component does not interfere with the molecular organization of mucins. *In vivo*, the secreted gastric juice is a complex mixture of electrolytes including $H^+$, $Na^+$, $K^+$, and $Cl^-$, [140] and digestive enzymes. The concentrations of these ions, especially $Na^+$, change with the acid secretion rate of the stomach. [32] We approximate the gastric juice in our system using the HEPES buffer solutions titrated to pH 2.0, so that the contribution of mucins to the barrier can be studied without interference by other components.

### 3.2.3 Preparation of apomucin by deglycosylation of purified mucin

The mucin was deglycosylated following a previously published protocol [141] consisting in the combination of an acidic treatment using trifluoromethanesulfonic acid (TFMS) followed by the oxidation and beta-elimination of the residual sugars. Briefly, 5 mg of dry purified mucins, cooled on ice, was mixed with 375 µL of an ice-cold solution of TFMS containing 10 % (v/v) anisole. The solution was gently stirred on ice for 2 hours and then neutralized by the addition of a solution containing 3 parts pyridine, 1 part methanol and 1 part deionized water. Any precipitate was further dissolved using

deionized water. The solution was dialyzed against water using a 20 KDa MWCO membrane for 2 days. NaCl was then added to the mucin solution to reach 0.33 M and acetic acid added to reach 0.1 M, and the pH was adjusted to 4.5 with NaOH. Then, the oxidation step was started by adding an ice-cold 200 mM $NaIO_4$ solution to a final concentration of 100 mM $NaIO_4$ and allowing the solution to stand in the dark at 4 ºC for 5 hours. The unreacted periodate was destroyed by adding a ½ volume of 400 mM $Na_2S_2O_3$, 100 mM NaI, 100 mM $NaHCO_3$ solution. The elimination was initiated by adding 1 M NaOH to pH 10.5 and letting it stand for 1 h at 4 ºC. The solution was then dialyzed overnight at 4 ºC against a 5 mM $NaHCO_3$ buffer, with the pH adjusted to pH 10.5 with NaOH and further dialyzed against ultrapure water for 2 days. The resulting deglycosylated mucin solution was then concentrated before being dissolved in the same HEPES buffer as described above for mucin.

### 3.2.4 Microfluidic device fabrication

Polydimethylsiloxane (PDMS) was used to fabricate the microfluidic chip following an established PDMS microfluidics method. [142] First, the microchannel features were defined using positive AZ4620 photoresist on a 6-inch silicon wafer, where the channel areas are exposed. Deep reactive ion etching was used to etch 150 µm deep channels, followed by oxygen plasma treatment to remove photoresist residues from the wafer. The finished wafer was treated with a perfluorinated trichlorosilane (T2492-kg, United Chemical Technologies, Bristol, PA) in a desiccator jar for at least four hours to prevent irreversible PDMS bonding to the wafer. Liquid PDMS prepolymer mixed in 10:1 ratio with curing agent (Dow Corning Sylgard 184 Silicone Elastomer Kit) was poured onto the silicon master to a height of approximately 1cm. The polymer was cured at 120°C for 15 minutes, then the cured PDMS layer was peeled off the wafer. This PDMS layer has channel features that are obtruding from the surface and will serve as the master for subsequent PDMS molding as a negative replica. The trichlorosilane and PDMS curing was repeated on this master to obtain the PDMS patterned channels. To avoid the necessity of repeating the two PDMS casting processes each time a device is made, a durable plastic mould of the PDMS patterned channels was made according to the methods of Desai *et al.* [143] and used to mold subsequent PDMS patterned channels. Finally, 350 µm diameter access holes for tubings were punched using a Harris Uni-core™ 0.5 mm biopsy punch (Ted pella Inc., Redding, CA). and the PDMS was exposed to oxygen plasma and bonded to a glass slide to complete the device.

## 3.3 Experimental setup and device operation

The mucin sample and acid buffer are loaded in separate 50 µL volume glass syringe (Model 1705, Hamilton Company, Reno, NV). The samples are loaded carefully to ensure that loaded samples are free of gas bubbles. The bonded device is mounted on an inverted epifluorescence microscope (IX-71, Olympus American Inc., Central Valley, PA) with attached fluorescent camera (ORCA-ER camera, Hamamatsu Corp) and light source. Fluidic access into the mucin channel was provided via capillary tubing and syringe. Fused silica capillary tubing (TSP100375, Polymicro Technologies, Phoenix, AZ) with outer diameter 360 µm and inner diameter 100 µm are inserted into the punched assay holes in the completed device. The flexible PDMS self-seals around the capillary tubing, creating a water tight connection. This flexible tubing is connected to the syringe through a tubing union device (MicroTight® Union P-720, IDEX Corp., Oak Harbor, WA). The mucin and acid sample syringes are mounted on separate precision syringe pumps (PHD 2000, Harvard Apparatus Inc., Holliston, MA) to provide precise metering of flow into the device.

Using syringe pumps (Harvard Apparatus 2000, Harvard Apparatus Inc. Holliston, MA), the nearly neutral pH mucin sample is pumped in at the left side of the device with a controlled flow rate of 11.5 µm/s while the acid buffer of pH 2 is pumped in at a rate of 1 mm/s at the top. The pH 2 value of the acid

buffer is chosen as an intermediate value in the physiological gastric lumen pH range of 1-3. The pH inside the mucin channel is visualized by the pH sensitive dye Oregon Green.

### 3.3.1 Acid titration of mucins

The acid binding ability of mucins is studied using titration of purified mucins with HCl. For this purpose, purified mucin is reconstituted to a volume of 300 µL in deionized water at concentrations of 0.25%, 0.5%, and 1% (w/v). The pH is measured using a micro pH electrode (MI-413, Microelectrodes Inc., Bedford, NH) and recorded as a function of the volume of HCl (10 mM and 100 mM stock solutions) added. At each titration step, the mucin solution is carefully mixed for 1 minute using a pipette tip. The quantity of $H^+$ bound to mucin is then calculated by subtracting the free quantity of $H^+$ (determined from the measured pH) from the total quantity of $H^+$ added.

### 3.3.2 Mass transport theory inside the microfluidic device

To study the effect of $H^+$-mucin interaction on the diffusion of $H^+$ a numerical model of the mass transport inside the device is constructed. The derivation of the model is based on work by Nussbaum *et al.* [144] The species relevant to $H^+$ binding that are included in the model, are the concentration of mucin, $H^+$, and HEPES. We assume that all three species are mobile and are carried by convection. The output of the model is the computed pH profile inside the device.

The microfluidic device is modelled as a 1D system with 5 mm length, equal to the mucin channel length (Fig. 1B). Mucin is pumped in at $x = 0$, and the acid/mucin mixing point is located at $x = 5$ mm.

Mucin is modelled as a collection of two species with distinct pKa values, based on the biochemical makeup of mucin as shown in Table 1. The pKa values of mucin $H^+$ binding sites may be classified into two groups: the NeuAc (neuraminic acid) and sulfate groups are between pKa ~2 and ~2.5, while the Glu (glutamic acid) and Asp (aspartic acid) residues are both pKa ~4. Therefore, we model mucin as two species with $pK_{a\_mucin\_1} = 2.25$ representing NeuAc and sulfates, and $pK_{a\_mucin\_2} = 4$ representing Glu and Asp. Similarly, HEPES also contains two $H^+$ binding sites, which are modelled as $pK_{a\_HEPES\_1} = 3$ and $pK_{a\_HEPES\_2} = 7.55$.

**Table 3-1** Residues and chemical groups on mucin capable of binding $H^+$.

| Chemical Group | pKA | Quantity (mM) for 1% mucin | Reference |
|---|---|---|---|
| Aspartic acid (Asp) | 3.9 | 0.7 | [145] |
| Glutamic acid (Glu) | 4.1 | 1.0 | [145] |
| Neuraminic acid (NeuAc) | 2.0-2.6 | 0.3 | [141, 146] |
| Sulfates | 2.0-2.5 | 3.0 | [146] |

The $H^+$ binding sites of mucin are negatively charged when they are in the ionized form. The presence of these negative charges may change the $H^+$ concentration inside the gel by Donnan equilibrium which may in turn affect the $H^+$ penetration distance. We estimate the effect of Donnan partitioning by considering the electroneutrality condition both inside and outside the mucin gel, given by eqn (3.1).

$$\bar{c}_+ = \bar{c}_- + p, c_+ = c_- = c_o \tag{3.1}$$

The terms $c_+$, $c_-$ represent the positive ($Na^+$ and $H^+$) and negative ion concentrations ($Cl^-$) outside of the mucin gel, respectively. The over bar terms $\bar{c}_+$ and $\bar{c}_-$ represent the same quantities inside the mucin gel. The term $p$ represents the concentration of negative charge on mucin, and $c_o$ is the ionic strength

outside of the gel. Combining the equations and rearranging the terms of eqn (3.1) gives eqn (3.2) below, which describes the fractional rise of positive ions inside the gel as a result of Donnan partitioning.

$$\frac{\bar{c}_+}{c_o} = \frac{p}{2c_o} + \sqrt{\frac{p^2}{(2c_o)^2} + 1} \tag{3.2}$$

Given the above approximations, the mass transport of $H^+$, HEPES, and mucin in the system can be described by a set of convection, diffusion, and reaction equations, which, written as the steady state balance ($\partial/\partial t = 0$) becomes:

$$v\frac{\partial[H^+]}{\partial x} = D_{H+}\frac{\partial^2[H^+]}{\partial x^2} - k_{on\_B1}[H^+][B_1] + k_{off\_B1}[H_{B1}] - k_{on\_B2}[H^+][B_2] + k_{off\_B2}[H_{B2}] - k_{on\_M1}[H^+][M_1] + k_{off\_M1}[H_{M1}] - k_{on\_M2}[H^+][M_2] + k_{off\_M2}[H_{M2}] \tag{3.3}$$

$$v\frac{\partial[B_1]}{\partial x} = D_B\frac{\partial^2[B_1]}{\partial x^2} - k_{on\_B1}[H^+][B_1] + k_{off\_B1}[H_{B1}] \tag{3.4}$$

$$v\frac{\partial[H_{B1}]}{\partial x} = D_{HB}\frac{\partial^2[H_{B1}]}{\partial x^2} + k_{on\_B1}[H^+][B_1] - k_{off\_B1}[H_{B1}] \tag{3.5}$$

$$v\frac{\partial[B_2]}{\partial x} = D_B\frac{\partial^2[B_2]}{\partial x^2} - k_{on\_B2}[H^+][B_2] + k_{off\_B2}[H_{B2}] \tag{3.6}$$

$$v\frac{\partial[H_{B2}]}{\partial x} = D_{HB}\frac{\partial^2[H_{B2}]}{\partial x^2} + k_{on\_B2}[H^+][B_2] - k_{off\_B2}[H_{B2}] \tag{3.7}$$

$$v\frac{\partial[M_1]}{\partial x} = D_M\frac{\partial^2[M_1]}{\partial x^2} - k_{on\_M1}[H^+][M_1] + k_{off\_M1}[H_{M1}] \tag{3.8}$$

$$v\frac{\partial[H_{M1}]}{\partial x} = D_{HM}\frac{\partial^2[H_{M1}]}{\partial x^2} + k_{on\_M1}[H^+][M_1] - k_{off\_M1}[H_{M1}] \tag{3.9}$$

$$v\frac{\partial[M_2]}{\partial x} = D_M\frac{\partial^2[M_2]}{\partial x^2} - k_{on\_M2}[H^+][M_2] + k_{off\_M2}[H_{M2}] \tag{3.10}$$

$$v\frac{\partial[H_{M2}]}{\partial x} = D_{HM}\frac{\partial^2[H_{M2}]}{\partial x^2} + k_{on\_M2}[H^+][M_2] - k_{off\_M2}[H_{M2}] \tag{3.11}$$

The terms $v$, $k_{on}$, and $k_{off}$ are the flow velocity, forward $H^+$ reaction rate, and reverse $H^+$ reaction rate, respectively. The terms $[B_1]$ and $[H_{B1}]$ represent the free and $H^+$-bound HEPES buffer molecules for the pKa 3 titratable group of HEPES, respectively, while $[B_2]$ and $[HB_2]$ represent the free and $H^+$-bound HEPES buffer molecules for the pKa 7.55 titratable group of HEPES, respectively. The terms $[M_1]$ and $[H_{M1}]$ represent the free and $H^+$ bound mucin NeuAc and sulfate groups at pKa 2.25, while $[M_2]$ and $[H_{M2}]$ representing the free and $H^+$ bound mucin Asp and Glu residues at pKa 4. $D_B$ and $D_{HB}$ represent the HEPES diffusivity, both equal to $5\times10^{-10}$ $m^2/s$. [147] $D_M$ and $D_{HM}$ represent the diffusivity of protonated and deprotonated mucin, which are assumed to be ~0 for simplicity. $D_{H+}$ represents the diffusivity of $H^+$ in mucin gel, which we assume to be the $H^+$ diffusivity in infinitely dilute electrolyte equal to $9.31\times10^{-9}$ $m^2/s$. We further assume fast reaction kinetics, where the reaction between $H^+$ to mucin and $H^+$ to HEPES is always at equilibrium even if mass transport is not.

Rigorously speaking, both HEPES and mucin should each be modelled as a single molecule with two titratable groups, but we model each as two separate species which may independently protonate or

deprotonate. This approximation has the potential to introduce inaccuracies because diffusion may cause the two species of HEPES to separate in the model, which would not occur in the microfluidic experiments. The inaccuracy would not apply to mucin because $D_M$ and $D_{HM}$ are ~ 0. The magnitude of inaccuracy for HEPES may be estimated considering the shape of the $H^+$ concentration profile in the microfluidic experiments. As shown in Fig. 3-2A (see Results Section 3.4.1 Continuously replenished mucin layer hinders $H^+$ diffusion *in vitro*), the pH of the mucin flow only changes in the acid penetration zone. Outside of the acid penetration zone, the two species of HEPES will not separate, because the uniform pH ensures zero diffusive flux for HEPES. We therefore need only to estimate the error arising from the diffusion of the two HEPES species within the acid penetration zone. Based on a maximum acid penetration distance of ~ 2 mm for the 0% mucin experiment, $D_B$ and $D_{HB}$ as given above, and a flow speed of 11.5 um/s in the channel, the maximum distance the two HEPES species may separate by diffusion would be ~ 420 μm, which is ~ 20% of the 2 mm acid penetration for 0% mucin. The maximum HEPES separation for higher mucin concentrations are of similar magnitude. Thus, the modelling approximation to separate the two pKa values for HEPES will not significantly affect the model accuracy.

Under these circumstances, we may simplify the mass transport equations by adding together eqn (3.3), (3.5), (3.7), (3.9) and (3.11) to arrive at eqn (3.12); then add eqn (3.4) to (3.5), eqn (3.6) to (3.7), eqn (3.8) to (3.9), and eqn (3.10) to eqn (3.11) to arrive at eqn (3.13), (3.14), (3.15), and (3.16) respectively.

$$D_{H+}\frac{\partial^2[H^+]}{\partial x^2} + D_{H_B}\left(\frac{\partial^2[H_{B1}]}{\partial x^2} + \frac{\partial^2[H_{B2}]}{\partial x^2}\right) + D_{H_M}\left(\frac{\partial^2[H_{M1}]}{\partial x^2} + \frac{\partial^2[H_{M2}]}{\partial x^2}\right) = v\left(\frac{\partial[H^+]}{\partial x} + \frac{\partial[H_{B1}]}{\partial x} + \frac{\partial[H_{B2}]}{\partial x} + \frac{\partial[H_{M1}]}{\partial x} + \frac{\partial[H_{M2}]}{\partial x}\right), \tag{3.12}$$

$$D_B\frac{\partial^2[B_1]}{\partial x^2} + D_{H_B}\frac{\partial^2[H_{B1}]}{\partial x^2} = v\frac{\partial[B_1]}{\partial x} + v\frac{\partial[H_{B1}]}{\partial x}, \tag{3.13}$$

$$D_B\frac{\partial^2[B_2]}{\partial x^2} + D_{H_B}\frac{\partial^2[H_{B2}]}{\partial x^2} = v\frac{\partial[B_2]}{\partial x} + v\frac{\partial[H_{B2}]}{\partial x}, \tag{3.14}$$

$$D_M\frac{\partial^2[M_1]}{\partial x^2} + D_{H_M}\frac{\partial^2[H_{M1}]}{\partial x^2} = v\frac{\partial[M_1]}{\partial x} + v\frac{\partial[H_{M1}]}{\partial x}. \tag{3.15}$$

$$D_M\frac{\partial^2[M_1]}{\partial x^2} + D_{H_M}\frac{\partial^2[H_{M1}]}{\partial x^2} = v\frac{\partial[M_1]}{\partial x} + v\frac{\partial[H_{M1}]}{\partial x}. \tag{3.16}$$

Four additional governing equations are given by the pKa values of HEPES and mucin as

$$K_{a\_HEPES\_1} = \frac{[B_1][H^+]}{[H_{B1}]},\ K_{a\_HEPES\_2} = \frac{[B_2][H^+]}{[H_{B2}]}$$
$$K_{a\_mucin\_1} = \frac{[M_1][H^+]}{[H_{M1}]}, K_{a\_mucin\_2} = \frac{[M_2][H^+]}{[H_{M2}]} \tag{3.17}$$

At $x$ = 5 mm, the boundary conditions for $[H^+]$ is given by eqn (3.18), based on the pH of the acid flow (pH = 2).

$$[H^+]_{x=5mm} = 10\ mM \tag{3.18}$$

At $x$ = 0 mm, the boundary condition for $[H^+]$ is set by the measured pH of the mucin sample before they are introduced into the microfluidic device, given by eqn (3.19).

$$\begin{aligned} [H^+]|_{1\%\ mucin,x=0mm} &= 10^{-5.9}\ \mathrm{M} \\ [H^+]|_{0.5\%\ mucin,x=0mm} &= 10^{-6.1}\ \mathrm{M} \\ [H^+]|_{0.25\%\ mucin,x=0mm} &= 10^{-6.4}\ \mathrm{M} \\ [H^+]|_{0\%\ mucin,x=0mm} &= 10^{-6.7}\ \mathrm{M} \end{aligned} \tag{3.19}$$

Boundary conditions for HEPES and mucin molecules are set by the pH dependent degree of dissociation given by eqn (3.20) to eqn (3.27) at both $x$ = 0 mm and $x$ = 5 mm, where $B_0$ = 2 mM is the total HEPES concentration, $M_{01}$ is the sum of Asp and Glu residue quantities in Table 1 (1.7 mM for 1% mucin, scaled linearly for other mucin concentrations), and $M_{02}$ is the sum of NeuAc and sulfate group quantities in Table 3-1 (3.3 mM for 1% mucin, scaled linearly for other mucin concentrations).

$$[B_1]_{x=0mm,x=5mm} = \frac{B_0}{[H^+]/K_{a\_HEPES\_1} + 1} \tag{3.20}$$

$$[H_{B1}]_{x=0mm,x=5mm} = \frac{B_0}{K_{a\_HEPES\_1}/[H^+] + 1} \tag{3.21}$$

$$[B_2]_{x=0mm,x=5mm} = \frac{B_0}{[H^+]/K_{a\_HEPES\_2} + 1} \tag{3.22}$$

$$[H_{B2}]_{x=0mm,x=5mm} = \frac{B_0}{K_{a\_HEPES\_2}/[H^+] + 1} \tag{3.23}$$

$$[M_1]_{x=0mm,x=5mm} = \frac{M_{01}}{[H^+]/K_{a\_mucin\_1} + 1} \tag{3.24}$$

$$[H_{M1}]_{x=0mm,x=5mm} = \frac{M_{01}}{K_{a\_mucin\_1}/[H^+] + 1} \tag{3.25}$$

$$[M_2]_{x=0mm,x=5mm} = \frac{M_{02}}{[H^+]/K_{a\_mucin\_2} + 1} \tag{3.26}$$

$$[H_{M2}]_{x=0mm,x=5mm} = \frac{M_{02}}{K_{a\_mucin\_2}/[H^+] + 1} \tag{3.27}$$

The system described by eqn (3.12) through (3.17) with boundary conditions described by eqn (3.18) to (3.27) is solved for the pH profile ($-\log_{10}[H^+]$) using Comsol 4 (Comsol Inc., Burlington, MA).

# 3.4 Results

## 3.4.1 Continuously replenished mucin layer hinders $H^+$ diffusion *in vitro*

Fig. 3-2A shows the equilibrium $H^+$ penetration into a barrier of purified mucins, which are "secreted" at a flow speed of 11.5 μm/s. In the buffer channel, the acid stream (pH 2) flows much faster (~100×) than the mucin stream, so that the pH of the two streams after mixing is set by the acid pH. Acid diffuses from the buffer channel into the mucin channel, against the direction of mucin flow.

The false colour blue is derived from the Oregon Green dye, which has a pKa of 4.7 and therefore fluoresces at neutral pH, but becomes non-fluorescent at acidic conditions below pH 4.7. The mucin solution upstream of the acid penetration zone is at nearly neutral pH and accordingly, the dye has high uniform fluorescence. In contrast, the dye loses its fluorescence on mixing with the acid stream, indicating strongly acidic conditions. The $H^+$ penetration distance is measured as the distance between the location where the dye loses half its fluorescence (near pH 4.7) and the intersection of the two channels (Fig. 3-1B and Fig. 3-2B). Tracking of the fluorescent microspheres in the mucin flow indicate that the mucin flow is controlled and not adversely affected by mucin gel viscoelasticity.

Fig. 3-2B quantifies the $H^+$ penetration distance into the mucin barrier as a function of time, with data averaged from three separate mucin batches. The shape of each curve has the form of an exponential, where the $H^+$ penetration increases from 0 to a final equilibrium value. Our data reveal that the $H^+$ penetration distance decreases with increasing mucin concentration, demonstrating that mucins can indeed hinder the penetration of $H^+$ and thus provide an acid barrier inside the microfluidic system.

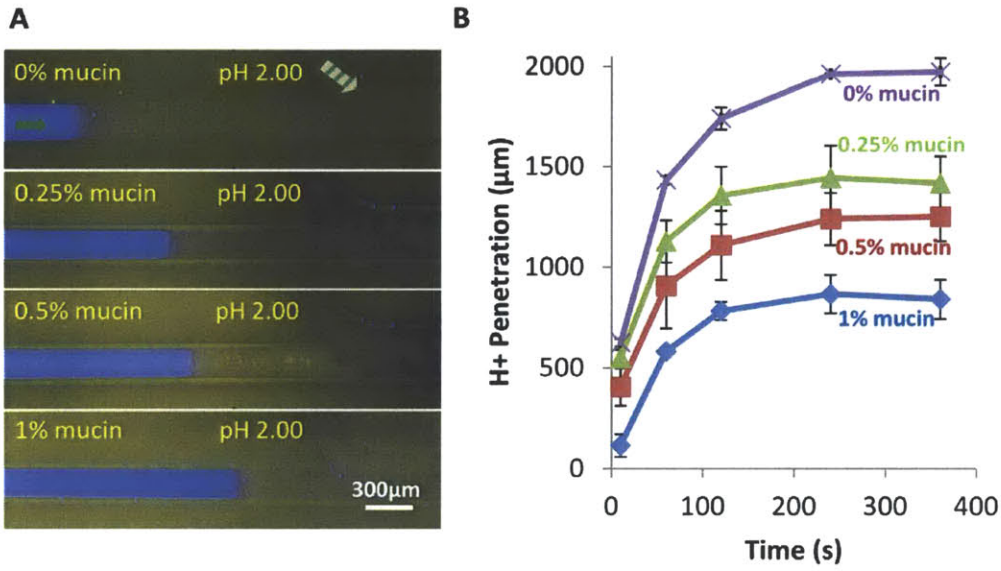


**Fig. 3-2**: A continuously replenished mucin layer hinders $H^+$ penetration. A) Fluorescent micrographs showing $H^+$ penetration into a solution of continuously secreted mucins inside a buffer of 2 mM Hepes and 20 mM NaCl at pH 7. Solid arrow: mucin flow. Hashed arrow: acid flow. Each micrograph has been scaled 0.5X horizontally. The scale bar represents the horizontal distance after scaling. B) Time response of $H^+$ penetration into the continuously secreted mucin layer. Increasing concentrations of mucin decreases $H^+$ penetration and demonstrates the acid barrier function contributed by mucin. The error bars represent a 95% confidence interval as obtained from measurements with three different mucin batches.

## 3.4.2 Mucins can bind $H^+$ in mM quantities

The observed $H^+$ barrier function could be brought about by direct binding of $H^+$ to the mucins, thereby removing free $H^+$ from solution and decreasing the diffusion flux of $H^+$ from the acid stream into the mucin layer. A reduced diffusion flux, in turn, would lead to a shorter $H^+$ penetration distance in the microfluidic experiments. To measure potential $H^+$ binding to the mucins we performed a titration experiment. We titrated solutions containing mucins at different concentrations (0.25% - 1%) from the

initial pH ~5-6 as measured after reconstitution in deionized water, down to pH ~1.7, covering the range of pH values used in the microfluidic experiments.

Fig. 3-3A shows the quantity of mucin-bound $H^+$ at each titration step. Within the tested pH range, we obtained the $H^+$ binding capacity of the mucins from the initial pH 5 down to an end point of pH ~1.7, but we did not reach a saturation of the proton binding sites on the mucins. Fig. 3-3B shows that the quantity of bound $H^+$ for mucins titrated to pH 2 scales linearly with the mucin concentration. For titration to pH 2, the $H^+$ binding capacity of mucin was 0.8 mM, 2.2 mM, and 4.5 mM for mucin concentrations of 0.25%, 0.5%, and 1%, respectively. These results demonstrate that, in the concentration regime studied here, the purified mucins provide $H^+$ binding sites in the mM range.

The measured quantity of $H^+$ binding to mucin is compared with the quantity of titratable chemical groups or residues published in the literature (Table 3-1). Based on the values in Table 3-1, the quantity of $H^+$ expected to bind to mucin at pH 2 is calculated to be 0.8mM, 1.9 mM, and 3.8 mM for 0.25%, 0.5%, and 1%, respectively. These values are similar to the ones measured from our titration, demonstrating that the quantity of $H^+$ binding to mucin is consistent with the biochemical composition of mucin. Unfortunately, Fig. 3-3A did not show any distinct pKa values, making it impossible to verify the pKa values of the mucin groups given in Table 3-1. One possible explanation is that mucin contains binding sites at a broad range of pKa values.

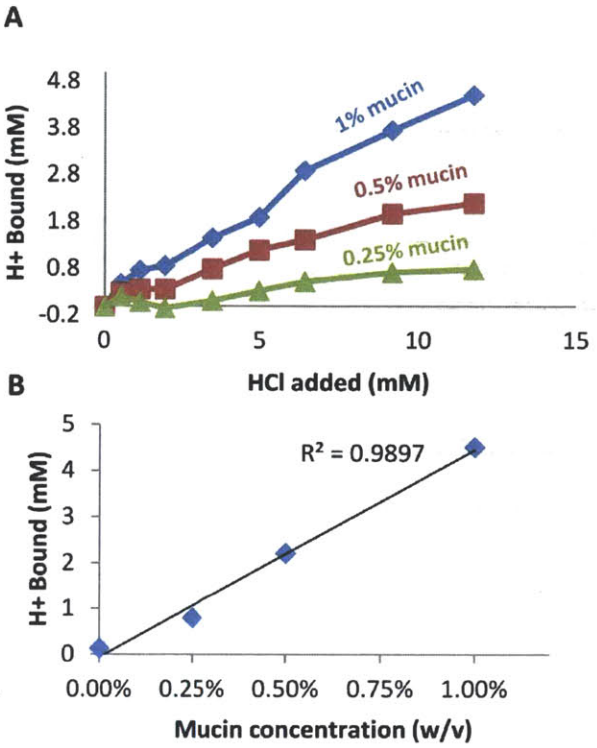


**Fig. 3-3**: Mucins bind $H^+$ in significant quantities. A) Titration of solutions containing native mucins with HCl, demonstrating the $H^+$ binding ability of gastric mucins. The amount of $H^+$ bound by mucin is dependent on the mucin concentration at each titration step. Measurement errors are on the order of the symbol size. B) Concentration of $H^+$ bound by purified mucin after titration from the initial pH ~5 (directly after reconstitution) to pH 2. The corresponding $H^+$ binding capacity is linearly proportional to mucin concentration.

### 3.4.3 $H^+$ hindrance inside a continuously replenished mucin layer occurs by mucin-$H^+$ binding

We construct a numerical mass transport model to verify that the mM $H^+$ binding ability of mucin explains the observed $H^+$ hindrance in Fig. 3-2. The derivation of the mass transport model is given in the Methods section, where transport equations for mucin, $H^+$, and HEPES are solved to calculate the pH profile inside the microfluidic device. Mucin is modelled as a collection of $H^+$ binding sites, whose $pK_a$ values and concentrations are based on the biochemical composition of mucin listed in Table 3-1.

Fig. 3-4A shows the computed pH profiles inside the microfluidic device calculated using the model. The pH profiles are similar in shape to the pH fluorescence profiles of the microfluidic device, consisting of a uniform pH zone starting at $x = 0$ followed by a drop in pH to pH 2 close to the mucin to acid mixing point at $x = 5$ mm. We calculate the $H^+$ penetration distance from the model pH profiles as the distance between $x = 5$ mm to the $x$ value where the pH is equal to 4.7, in accordance with the definition of $H^+$ penetration distance in the microfluidic experiments. As shown in Fig. 3-4B, the model predicted similar acid penetration distances as the experimental values measured from microfluidics, demonstrating that the binding of $H^+$ to mucin can explain the $H^+$ hindrance measured in the microfluidic experiments.

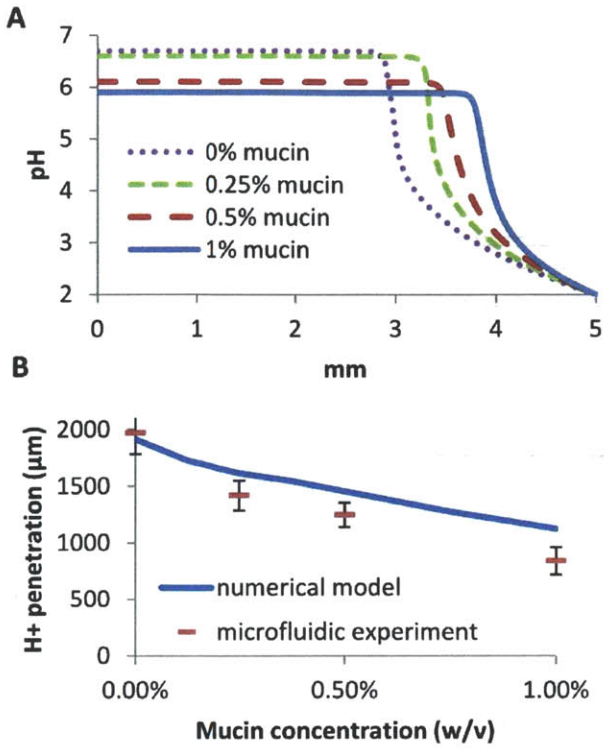


**Fig. 3-4**: Comparison of microfluidic $H^+$ penetration measurements with numerical modeling results. A) pH profiles inside the microfluidic device computed by the numerical mass transport model. The $H^+$ penetration distance is reduced by higher concentration of mucins (modeled as higher concentrations of $H^+$ binding sites). B) Comparison of the $H^+$ penetration distance calculated by the numerical model to the microfluidic experiment, showing direct binding of $H^+$ to mucin explains the $H^+$ hindrance effect during mucin secretion.

### 3.4.4 *In vivo*, mucin-$H^+$ binding contributes significantly to the acid barrier

We estimate the impact of $H^+$ binding by mucins under *in vivo* secretion conditions in the stomach. A linear extrapolation of the $H^+$ binding capacity shown in Fig. 3-3B to that of an *in vivo* mucin concentration of ~5 % (w/v) suggests a mucin associated $H^+$ binding site concentration of ~22.5 mM in the gastric mucus layer for intermediate acid conditions of pH 2. Given a maximum *in vivo* secretion rate of approximately 1 μm/minute as measured by Atuma *et al.*, [6] the equivalent $H^+$ binding site flux generated by the mucosa by means of secreting mucins would amount to 0.38 μmol/$m^2$/s. Alternatively, Schreiber *et al.* [87] measured a secretion rate of 3 μm/min at baseline, corresponding to a binding site flux of 1.13 μmol/$m^2$/s, and 7.5 μm/min under histamine stimulation, corresponding to a binding site flux of 2.81 μmol/$m^2$/s.

Currently, bicarbonate secretion to the mucus layer is thought to be the dominant mechanism of pH neutralization in the mucus layer. $H^+$ binding to mucin entails a removal of protons from the gastric juice. Therefore, this mechanism neutralizes pH, similar to $H^+$ neutralization by bicarbonate. The bicarbonate secretion rate of the gastric mucosa has been previously measured *in vivo*. Kauffman *et al.* [148] estimated a secretion flux of 1.4 μmol/$m^2$/s in dogs. Rees *et al.* [149] and Forssell [150] estimated a total bicarbonate secretion rate of 0.3 – 0.4 mmol/hr in humans, corresponding to a secretion flux of 0.83 – 1.11 μmol/$m^2$/s assuming an approximate mucus surface area in the human stomach of 0.1 $m^2$. [151] This range of values also agrees well with measurements from *in vitro* tissue cultures of the gastric

mucosa which estimated 0.28 – 1.4 μmol/m$^2$/s for amphibian and 0.83 – 2.7 μmol/m$^2$/s for mammalian preparations. [152]

Averaging over all these literature values, we arrive at an averaged estimated bicarbonate secretion rate of 1.1 μmol/m$^2$/s. In comparison, the mucin secretion estimated here would contribute a maximum of 35% of the $H^+$ binding barrier function provided by bicarbonate secretion alone as estimated using the secretion rate from Atuma *et al*, [6] but would be as high as 100% to 250% as estimated using the secretion rate estimated by Schreiber *et al*. [87]

### 3.4.5 Mucin $H^+$ hindrance effect is masked by higher concentration buffers

We have showed that mucin-$H^+$ binding decreases $H^+$ penetration into the mucin layer. To further confirm mucin-$H^+$ binding is the underlying mechanism, we measure the $H^+$ penetration distance for 0.5% (w/v) mucins in 20 mM HEPES, 20 mM NaCl buffer at pH 7. The 20 mM HEPES concentration is 10 times the concentration of HEPES buffer than used in the experiment in Fig. 3-2, and provides approximately 10 times the quantity of $H^+$ binding capacity provided by 0.5% mucins. With non-mucin buffers at such a high concentration, mucins should not a play a significant role in the penetration hindrance of $H^+$.

Fig. 3-5 compares the $H^+$ penetration distance inside the microfluidic device as a function of mucin concentration and acid flow pH at a mucin secretion rate of 23 μm/s. The findings indicate that when the HEPES concentration is an order of magnitude higher than the $H^+$ binding site concentration on mucins, the resulting $H^+$ penetration distance is not affected by 0.5% mucins. This result can be explained by the $H^+$ binding capacity of HEPES overwhelming the $H^+$ binding capacity of mucins. These findings provide further confirmation that $H^+$ binding to mucins is the mechanism of the observed hindrance of $H^+$ on-chip.

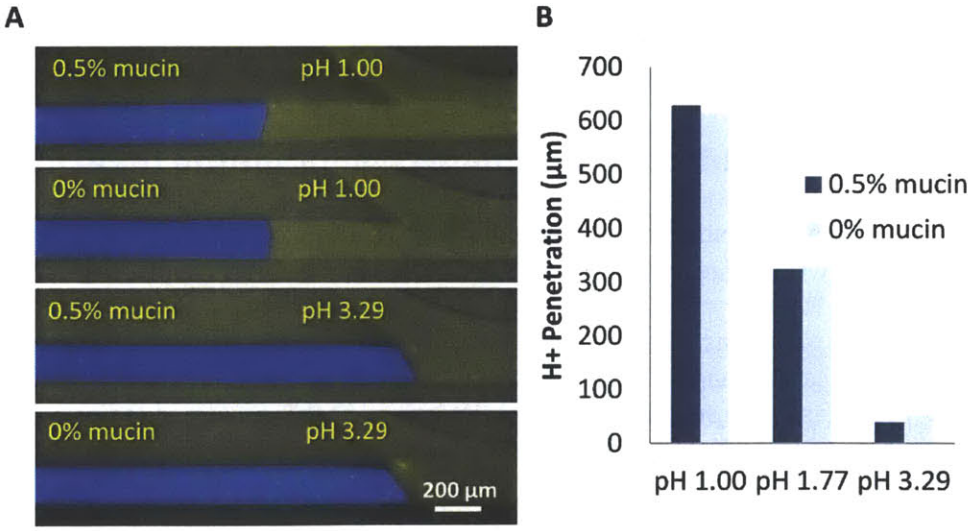


**Fig. 3-5**: Buffering by 20 mM HEPES overwhelms mucin $H^+$ binding sites. A) Fluorescence micrograph of $H^+$ penetration. B) $H^+$ penetration distance as a function of mucin concentration and acid flow pH. Unlike in Fig. 3-2, mucins do not affect the $H^+$ penetration distance as the $H^+$ binding capacity of 20 mM HEPES is much greater than the $H^+$ binding capacity of 0.5% (w/v) mucins.

### 3.4.6 Apomucins partially contribute to $H^+$ barrier function

Much of the $H^+$ binding sites on mucins are present on the glycans. Removing such glycans would be expected to reduce the $H^+$ barrier function of mucins. To test this hypothesis, we compared the $H^+$

barrier function of 0.5% (w/v) mucins with 0.5% (w/v) deglycosylated mucins (apomucins). Glycans consist of 60% to 80% of the mucin molecule by weight. In our experiment, 0.5% (w/v) mucins are equal in molarity to 2 mg/ml apomucins, assuming mucins contained 60% glycans. Fig. 3-6 shows that apomucins hindered $H^+$ penetration but to lesser degree than full scale mucin molecules. This finding is consistent with the finding that both mucin glycans and the apomucin core contain $H^+$ binding sites and contribute to $H^+$ hindrance.

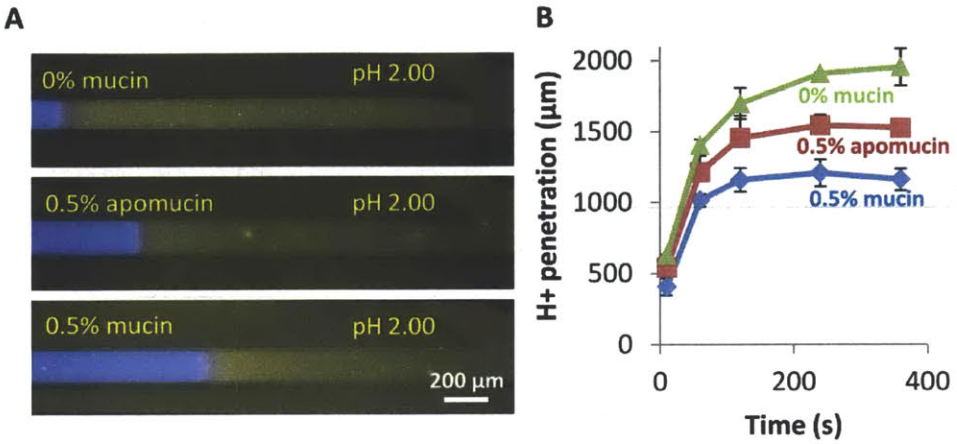


**Fig. 3-6**: Comparison of $H^+$ penetration into 0.5% mucins and 0.5% deglycosylated mucins (apomucin). A) Fluorescent micrographs of equilibrium $H^+$ penetration into a layer of continuously secreted 0.5% mucin and 0.5% apomucin. B) Time response of $H^+$ penetration into the continuously secreted mucin and apomucin layer, demonstrating that apomucins hinder $H^+$ but not as effectively as full length mucins.

## 3.5 Discussion

We have created an *in vitro* microfluidic system that replicates a dynamic mucin barrier, which is continuously replenished and counteracts the penetration of acid, as occurs in the stomach mucosa. Acid penetration on chip is monitored by live fluorescence microscopy, permitting the study of barrier efficiency as a function of physiologically relevant parameters such as mucin concentration, mucin secretion rate, and acid pH.

This system has several advantages over the macroscale diffusion chamber. For example, it allows tracking of transient processes such as acid penetration through a mucin layer by monitoring the concentration profile in the system as a function of time. Furthermore, the ability to visualize the inside of the microfluidic system allows for the simultaneous measurements of several components at once. Here we used microspheres to track the flow velocity inside the device, while visualizing the acid penetration in parallel. In future work, the device may be used to track the behaviour of other biologically relevant components in mucus, such as bacteria, or small molecules. Second, this system conducts measurements in dynamic flux conditions. This ability may be extended to the measurement of diffusion in other mucus systems which undergo dynamic replenishment, including the mucus in the respiratory tract, the female reproductive tract, or on the surface of the eye.

We employed the microfluidic system to measure the contribution of purified native mucin polymers in the protective capacity of the gastric mucus barrier. We find that isolated mucins can hinder $H^+$ diffusion, a result that had been shown with experiments based on the macroscale diffusion chamber and titration experiments. [87, 129, 153, 154] With a theoretical model we showed that the observed acid barrier function of mucins can be quantitatively explained by the direct sequestration of $H^+$ by the mucins.

One implication of this mechanism is that the *in vivo* barrier effect depends on the rate of mucin secretion, as the secretion rate determines the concentration of available $H^+$ binding sites. By taking into account the estimated *in vivo* mucin concentration and secretion rate, we calculated that the barrier function arising from $H^+$ to mucin binding is comparable to the barrier function provided by bicarbonate pH neutralization. This calculation provides only a rough approximation since we are limited by the lack of secretion rate measurements acquired in *in vivo* or *ex vivo* systems. Furthermore, the experimental data currently available indicate significant differences in secretory rates. [6, 87] Nevertheless, even a conservative estimation based on the available data suggests that mucin secretion at physiological rates may make a significant contribution to the barrier. Importantly, *in vivo* mucin secretion rates can vary depending on physiological conditions or external factors. For example, the mucus layer thickness *in vivo* and in *ex vivo* tissues increases on addition of exogenous molecules such as histamine, prostaglandins, and carbenoxolone by up to ~3 fold. [8, 87, 155] Stomach peristalsis and pepsin degradation may also alter the mucus secretion rate. Thus, mucus barrier properties may be altered by the body through modulating mucus secretion rates depending on physiological needs; it may also be amenable to pharmacological intervention, either by agents which alter the secretion rate, or by supplements of proton adsorbing mucin-mimics.

In its present form, our microfluidic model system has several limitations, which can be overcome by future development. For example, we are currently only able to stably reproduce flow speeds of 10 μm/s or above, which is fast compared to the *in vivo* mucus secretion speed of 1-7.5 μm/min. This limitation does not affect our conclusion since we can compensate for the difference in flow speed computationally (see Methods section). Nevertheless, lowering flow speeds by improving the microfluidic device design to more closely mimic the *in vivo* secretion speeds will greatly improve a future dissection of the mucus barrier function. Furthermore, the maximum mucin concentration that can be used in our device is 1% (w/v), as a higher viscoelasticity of mucin samples with concentrations greater than 1% (w/v) reduces the reproducibility of the mucin flow inside the device. Thus, we have been unable to study the behaviour of $H^+$ in gels of higher mucin concentrations. At *in vivo* mucin concentrations approaching 5% (w/v), additional effects such as Donnan exclusion effects [156] might kick in that hinder $H^+$ transport in addition to $H^+$ binding.

We envision this device useful for dissecting the contribution of other mucus components to the acid barrier, including mucin associated lipids and peptides. In addition, it may be suitable to test or develop therapeutic agents which improve or alter barrier function. [119, 157] Moreover, precious clinical mucus samples, for example from the gastrointestinal tract obtained by endoscopic biopsy, [158] can be analysed. Such comparative clinical studies will reveal potential differences of the mucus barrier function from individuals with different pathologies. Last, this device can be used to test the interaction of drugs with mucus. Any orally taken drug must pass through the gastrointestinal mucus layer before being absorbed by the body. Our microfluidic platform may be optimized to become a test platform for studying the penetration of drug molecules into the mucus layer.

# Chapter 4

# Microfluidic device to characterize penetration and uptake of peptides into a mucin barrier

Note: fluorescent labeling of mucins in this section is performed by Dr. Thomas Crouzier of the MIT Laboratory for Hydrogel Filters in Biology.

## 4.1 Introduction

As described in Section 1.1, mucus layers exhibit inherent spatial polarity. One side of the mucus barrier connects to the cells of the epithelium, while the other is open to the lumen of the body cavity. In some cases, proper physiological function requires that mucus prevent penetration of molecule or pathogen. For example, bacteria in the intestinal tract reside only in the outer portion of the mucus layer but cannot penetrate the inner layer. [159] In other cases, it is beneficial to maximize uptake of particles and molecules from the lumen, such as in the airways, where trapping of foreign particles and toxins by mucus acts as an absorptive filter to remove particles and pathogens from inhaled air which is travelling to the lungs. [160] This suggests that different physiological situations require different selectivity function of the mucus barrier. It is generally thought that mucins, the dominant structural component of mucus, play an important role in the selective permeability of the mucus barrier, but the criteria and mechanisms by which the mucin network alters permeability are largely unknown.

Resolving the question of which factors affect lead to penetration and uptake into the mucin network requires systematic *in vitro* analysis of molecular transport into the mucin barrier, so that barrier function from mucins can be tested independently from other mucus and mucosal barrier components. Currently, the permeability barrier of mucins are probed using the technique of multiple particle tracking, finding that the surface properties of particles and their interactions with mucins govern the diffusion mobilities of the particles. [94] However, the particles used are at least several hundred nanometers in diameter and thus too large to approximate the nanoscale signaling molecules and peptides which transit within and through the mucin barrier. The particles are also designed to exhibit uniform surface properties, which are quite different from native proteins or pathogens which contain heterogeneous surfaces. [161] Diffusion of native proteins have not been studied on mucins, but have been studied in native mucus. [90] Some differences in diffusivity, which cannot be explained by molecular size, has been found, presumably due to interactions with mucus components but without conclusive supporting evidences. Moreover, these studies did not address the critical issue of molecular uptake into the mucus barrier.

In this work, we systematically probe the selective permeability of a layer of purified mucins to nanoscale peptides as molecular probes. These ~2kDa, fluorescently labeled peptides express a combination of positive and negative charged residues with systematically varied arrangements. Using a microfluidic device based on the design of Li *et al.* [162], these peptides are carried to the surface of an *in vitro* mucin layer by a continuous flow, and are then transported into the mucin layer by diffusion and interactions with mucins. Fluorescent microscopy determines the concentration profiles of the peptides, from which penetration speeds and accumulation rates of the peptides are obtained. Our results show that the sequence and arrangement of charged residues on the peptides affect the ability of the peptides to penetrate or uptake into the mucin barrier.

## 4.2 Methods

### 4.2.1 Device design

The top-down schematic view the microfluidic device is based on [162] and shown in Fig. 4-1A. The device consists of a mucin channel (bottom), connected to a probe channel (top). As shown in Fig. 4-1A, a push-down style microfluidic valve is integrated into the mucin channel. [163] Mucin sample is flowed into the device, where it fills both the mucin and probe channels. The microfluidic valve shown at the bottom of the schematic is then closed, thus stopping the flow of mucins into the channel. Then, a buffer solution is flowed through the probe channel at the top portion of the schematic, flushing away mucins in its flow path. The geometry of the device and closed microfluidic valve in the mucin channel ensures that the buffer flow removes mucins a fixed distance into the mucin channel, leaving a fixed width of mucins which is not flushed out by the buffer flow. To perform permeability experiments, fluorescently labeled peptide probes would be flushed into the device. The peptides would then diffuse into the mucin layer. The concentration profiles inside the mucin layer and across the mucin interface can then be obtained by fluorescence microscopy, allowing the interactions of the peptides with the mucin layer and the penetration speed to be assessed as a function of time.

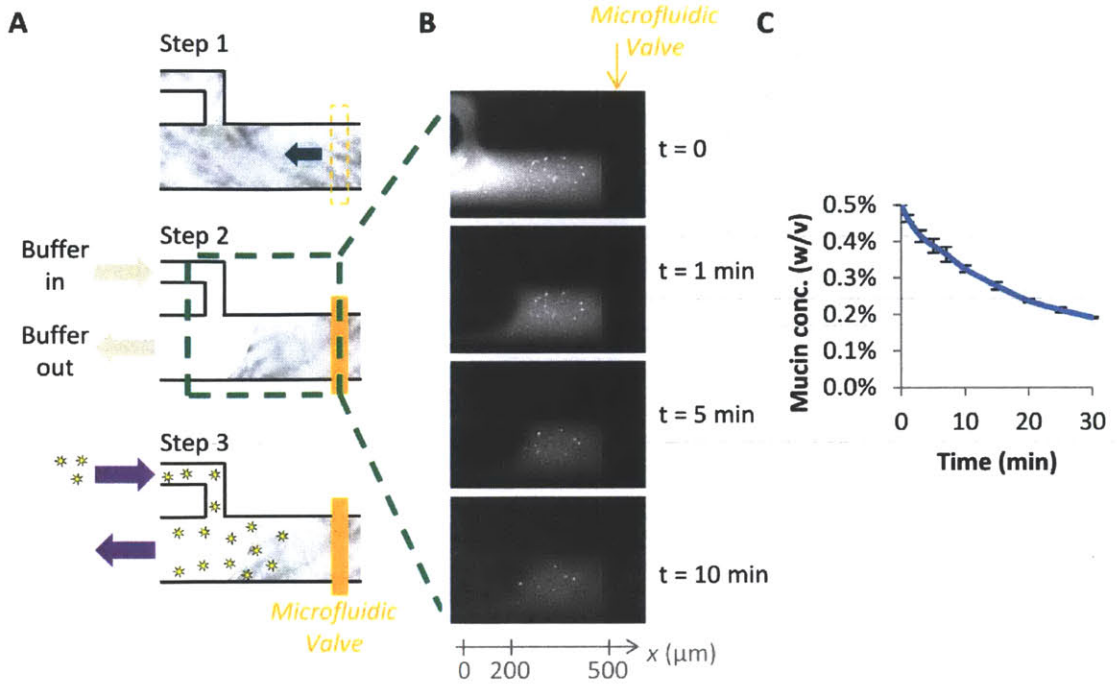


**Fig. 4-1**: Microfluidic scheme to measure the diffusion and interaction of peptide probes with a mucin layer. A) Schematic of mucin filling and device operation. Step 1: a solution contained 0.5% (w/v) purified mucins are pumped into the device. Step 2: The microfluidic valve at the base of the mucin channel closes, preventing further mucin flows. A flush buffer is flowed through top channel, flushing away excess mucins and creating a mucin layer of fixed width. Step 3: fluorescently labeled peptide probes are flowed into the device at the same speed as the flush buffer. The diffusion of peptides into the mucin layer, mimicking the in vivo transport of peptides into a mucus barrier, is measured as a function of time using fluorescence microscopy. B) Fluorescent micrographs demonstrating the stability of the mucin layer over time using fluorescently labeled mucins. C) The concentration of mucins in the mucin layer is reduced over time, due to loss of mucins as a result of fluid shearing at the mucin layer surface.

### 4.2.2 Microfluidic mold fabrication

Soft polymer microfluidic device fabrication techniques are used to fabricate the microfluidic devices. [163] For the flow channels wafer, the microchannel features were defined in AZ4620 positive photoresist coated onto a silicon wafer to a height of 30 μm. The wafer is then baked for 1 hour at 150°C, causing the photoresist to reflow, resulting in features with a rounded rather than rectangular profile. This rounded profile is needed for microfluidic valve activation. For the valves wafer, valve features were defined in SU8 negative photoresist coated onto a silicon wafer to a height of 20 μm. Both finished wafers were treated with a perfluorinated trichlorosilane (T2492-kg, United Chemical Technologies, Bristol, PA) in a desiccator jar for at least four hours to prevent irreversible RTV bonding to the wafer.

RTV prepolymer and curing agent (RTV615, Momentive Performance Materials Inc., Albany, NY) were mixed in a 1:5 (w/w) ratio, degassed for 1 hour inside a desiccator jar, and poured onto the flow channels wafer to a height of ~1 cm. Prepolymer and curing agent were mixed in a 1:20 (w/w) ratio, degassed for 1 hour, and spun onto the valves wafer at 1200 rpm for 60 seconds, resulting in an RTV thin layer of ~60 μm. The two wafers were baked on hotplates at 95°C for 45 minutes, after which the partially cured RTV structures was peeled from the flow channels wafer and aligned to the valve

features on the valves wafer. Proper alignment of the flow channel features with the valve features were made with the aid of a dissection microscope. The valves wafer with the aligned flow channel RTV structures was placed on a hotplate at 95°C for at least 24 hours, allowing the RTV flow channels and the RTV thin layer holding the valve features to fully cure into a monolithic structure. These structures were then peeled from the wafer and cut into individual devices. Finally, an access hole was punched using a 0.35mm biopsy punch (Harris Uni-core tip inner diameter 0.35mm, Ted Pella Inc., Redding, CA) for access to the mucin channel, access holes for fluid connections to the sample channels and valve channel are punched using a 1.5mm biopsy punch (Miltex disposable biopsy punch 1.5mm, Integra LifeSciences Corp., Plainsboro, NJ). Finally, and the RTV structure was bonded to a glass slide after treatment with oxygen plasma for 1 minute (Expanded Plasma Cleaner PDC-001, Harrick Plasma, Ithaca, NY) to complete the device.

### 4.2.3 Microfluidic device preparation and operation

The bonded device is filled and operated according to the following steps:

1. 5 μL of DI water is pipetted into the valve channel reservoir. Positive air pressure is applied at this reservoir, causing the DI water to completely displace the air inside the valve channel. This step prevents the air from the valve channel from crossing the thin valve membrane into the mucin and probe channels during device operation.
2. 2 μL of isopropyl alcohol is added into one of the probe reservoirs. The isopropyl alcohol wets all of the mucin and sample channels based on capillary action. Note that alcohol is used to wet the channels because they are hydrophobic and cannot be wetted by water. Bonding of RTV devices by using oxygen plasma normally renders the RTV surface hydrophilic. However, in this case, the mucin and probe channels are not exposed to oxygen plasma because they are protected by the valve membrane and remain hydrophobic even after the RTV superstructure is treated with oxygen plasma.
3. Any remaining isopropyl alcohol inside the probe reservoir is removed by pipette.
4. 3 μL of DI water is pipetted into each of the 8 probe channel reservoirs, and negative air pressure is applied at the mucin reservoir. This causes a flow in the device which replaces the isopropyl alcohol in all mucin and probe channels with DI water.
5. Any remaining DI water inside the 8 probe channel reservoirs is removed by pipette.
6. 2 μL of PLL-g-PEG at 1 mg/ml in DI water is added into each of 8 probe channel reservoirs, and negative air pressure is applied at the mucin reservoir. This replaces the DI water inside all mucin and probe channels with PLL-g-PEG solution, which will bind nonspecifically the channel walls. PLL-g-PEG forms a passivation layer which greatly reduces the absorption of proteins onto the channel walls during the experiment.
7. Any remaining PLL-g-PEG solution inside the 8 probe channel reservoirs is removed by pipette.
8. Pipette tips with 200 μL volume (USA Scientific, Ocala, FL) were modified by cutting the 2 mm from the tip using a razor blade and inserted into each of the 8 probe channel reservoirs to expand the volume of each reservoir.
9. 20 μL of DI water is added to each probe channel reservoir (with inserted 200 μL pipette tip), and negative pressure is applied at the mucin reservoir to replace PLL-g-PEG solution inside the channels with DI water.
10. A 0.5 x 0.5 cm square of black electrical tape is placed on the top side of the RTV structure, over the portion of the chip which will be imaged by the fluorescent microscope. The electrical tape prevents stray fluorescence inside the reservoirs from creating a large fluorescence background from interfering with the experiment.

11. The device is now mounted on an inverted epifluorescence microscope (IX-71, Olympus American Inc., Central Valley, PA) with attached fluorescent camera (ORCA-ER camera, Hamamatsu Corp) and light source (Excitation System, CoolLED Ltd, Andover, United Kingdom).
12. A 3 mL plastic syringe (BD™ syringe, Becton Dickinson and Company, Franklin Lakes, NJ) is connected through flexible plastic tubing (Polytetrafluoroethylene tubing, 1522, IDEX Corp., Oak harbor, WA) to the valve channel reservoir on the device. This outer diameter of the tubing is 1/16 inches, and the inner diameter is 0.03 inches. The self-sealing PDMS creates a water-tight connecting between the tubing and reservoir. This syringe provides the air pressure needed to operate the microfluidic valve of the device. Depressing the syringe fully was found to create sufficient pressure to close the valve.

**Procedures for conducting probe penetration and uptake into the mucin barrier**

13. Reconstituted mucin sample is loaded onto a 50 µL volume glass syringe (Model 1705, Hamilton Company, Reno, NV) and connected to the 0.35 mm diameter mucin reservoir on-chip through a 15 cm length of fused silica tubing (TSP100375, Polymicro Technologies, Phoenix, AZ) and a tubing union device (MicroTight® Union P-720, IDEX Corp., Oak Harbor, WA). The syringe is mounted on a precision syringe pump (PHD 2000, Harvard Apparatus Inc., Holliston, MA) to provide precise metering of mucin flow into the device.
14. Mucin flow is started by turning on the syringe pump, until both the mucin and probe channels are filled with mucin. Mucin filling is confirmed by the presence of fluorescently labeled microspheres added as tracers into the mucin sample.
15. Once mucin filling is complete, the mucin flow is stopped by turning off the syringe pump. The 3 mL plastic syringe is fully depressed, closing the microfluidic valve.
16. 5 µL of flush buffer is added to each of the 4 outlet probe reservoirs, and 30 µL of flush buffer is added to each of the 4 inlet probe reservoirs. This results in a gravity fed flow from each inlet to outlet reservoirs through the probe channel. The flow flushes away excess mucins in the probe channel and creates a mucin layer of fixed width in the mucin channel.
17. The 30 µL of flush buffer from each of the 4 inlet probe reservoirs are removed by pipette, and replaced with 30 µL of the probe sample containing fluorescently labeled molecular probes. These probes diffuse from the probe channel flow into the mucin layer in the mucin channel.
18. Fluorescence micrographs are taken at 10 s intervals using Micro-Manager software (Ron Vale Lab, University of California San Francisco, San Francisco, CA). The exposure time is individually experimentally determined for each molecular probe. To prevent photobleaching of the peptides, a control script developed is used to turn on the LED excitation source immediately before each exposure and turn off the LED immediately after exposure.

**Procedures for measuring the mucin loss rate using fluorescently labeled mucins**

13. Reconstituted fluorescently labeled mucin sample is loaded onto a 50 µL volume glass syringe (Model 1705, Hamilton Company, Reno, NV) and connected to the 0.35 mm diameter mucin reservoir on-chip through a 15 cm length of fused silica tubing (TSP100375, Polymicro Technologies, Phoenix, AZ) and a tubing union device (MicroTight® Union P-720, IDEX Corp., Oak Harbor, WA). The syringe is mounted on a precision syringe pump (PHD 2000, Harvard Apparatus Inc., Holliston, MA) to provide precise metering of mucin flow into the device.
14. Mucin flow is started by turning on the syringe pump, until both the mucin and probe channels are filled with mucin. Mucin filling is easily confirmed by the fluorescence of the mucins.
15. Once mucin filling is complete, the mucin flow is stopped by turning off the syringe pump. The 3 mL plastic syringe is fully depressed, closing the microfluidic valve.

16. 5 μL of flush buffer is added to each of the 4 outlet probe reservoirs, and 30 μL of flush buffer is added to each of the 4 inlet probe reservoirs. This results in a gravity fed flow from each inlet to outlet reservoirs through the probe channel. The flow flushes away excess mucins in the probe channel and creates a mucin layer of fixed width in the mucin channel.
17. Because the mucin layer is open to the flush buffer flow, mucins are gradually lost through a combination of shearing of the mucin layer interface, diffusion of the mucins, and swelling of the mucin. Fluorescence micrographs are taken at 10 s intervals using Micro-Manager software. The exposure time is experimentally determined to prevent saturation of the camera. To prevent photobleaching of the peptides, a control script developed is used to turn on the LED excitation source immediately before each exposure and turn off the LED immediately after exposure.

### 4.2.4 Peptide sample preparation

Peptides used for mucin layer penetration experiments are synthesized and labeled with FAM (6-Carboxyfluorescein) by the Koch Institute Biopolymers and Proteomics Facility (core facility of the Massachusetts Institute of Technology, Cambridge, MA).

Trifluoroacetic acid in the peptide sample as a byproduct during the peptide synthesis procedure was removed using a PD MiniTrap G-10 (GE Healthcare, Piscataway, NJ) size exclusion column with 20 mM NaCl / 20 mM Hepes at pH 7.0 as the equilibration and elution buffers. The degree of acid removal was assessed by measuring the pH of each eluted fraction using a micro pH electrode (MI-413, Microelectrodes Inc., Bedford, NH). The concentration of peptides in the eluted fractions after desalting is determined by measuring the absorption of the FAM labeled molecules at the FAM excitation wavelength of 490 nm and using the absorption of knowing concentration of free FAM molecules as a concentration standard. (Fig. 4-2) Eluted fractions with pH > 6.8 are pooled together for subsequent use, while other fractions are discarded.

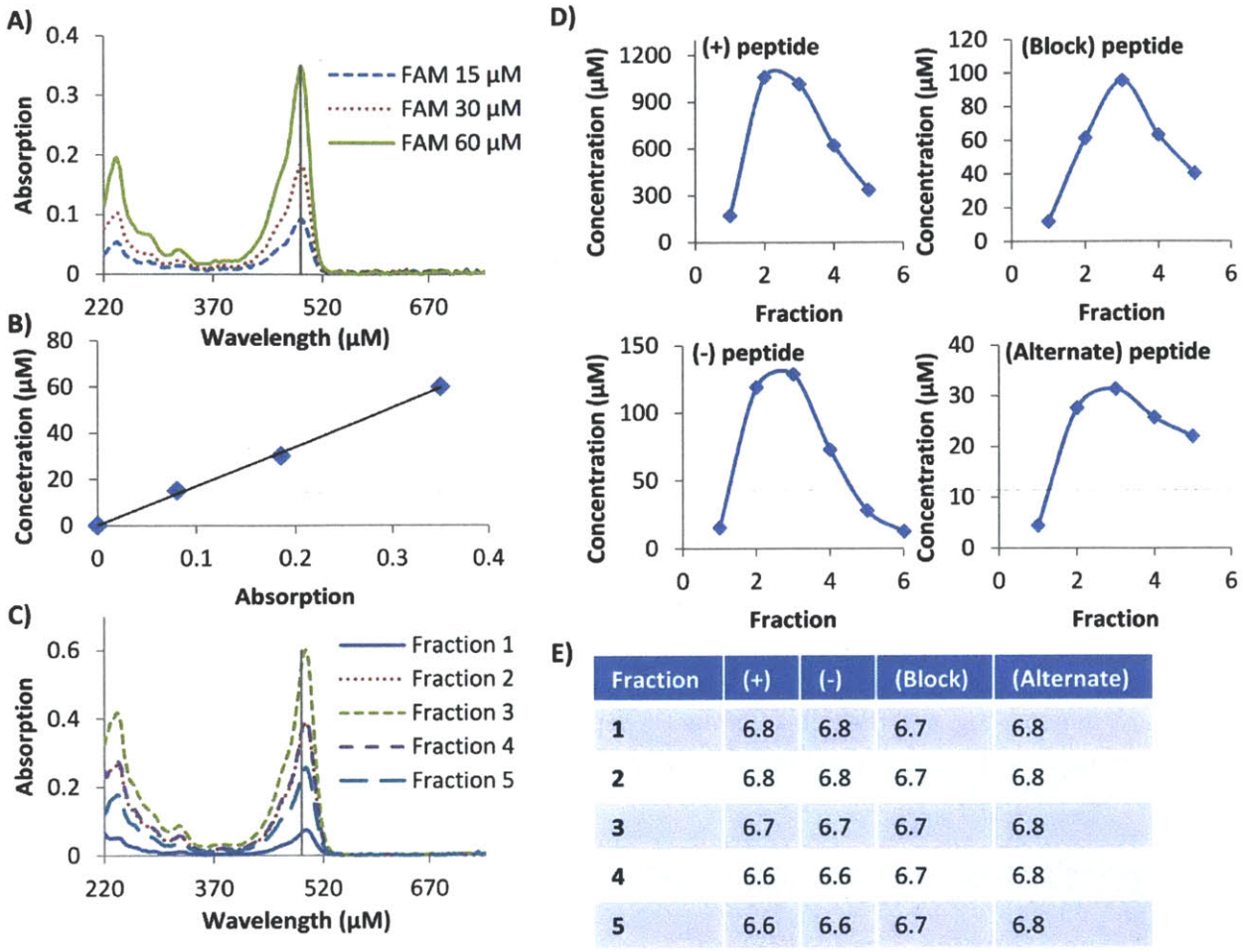


| Fraction | (+) | (-) | (Block) | (Alternate) |
|---|---|---|---|---|
| 1 | 6.8 | 6.8 | 6.7 | 6.8 |
| 2 | 6.8 | 6.8 | 6.7 | 6.8 |
| 3 | 6.7 | 6.7 | 6.7 | 6.8 |
| 4 | 6.6 | 6.6 | 6.7 | 6.8 |
| 5 | 6.6 | 6.6 | 6.7 | 6.8 |

**Fig. 4-2**: Desalting of peptides and determination of peptide concentration. A) Absorption spectrum of free fluorescein at 15, 30, and 60 μM. B) Calibration curve connecting absorption and fluorescein concentration. C) Absorption spectrum of fluorescein labeled (Block) peptides. Each peptide molecule is labeled with one fluorescein molecule. D) Fluorescence of each eluted fraction from the desalting column. E) pH of the eluted fractions.

# 4.3 Results

## 4.3.1 Microfluidic device enables stable formation of mucin layer

To confirm the stability of the mucin layer created using this method, we create a mucin layer inside the device consisting of 0.05% (w/v) fluorescently labeled purified native mucins added to 0.45% (w/v) unlabeled purified native mucins. We then track the concentration and interface location of fluorescent mucin layer over time. Fig. 4-1B confirms the formation of the mucin layer, finding that interface to the mucin layer is located at $x \approx 210$ μm. The length of the mucin layer is 250 μm. The concentration of mucins inside the concentration profile is also found to decrease gradually as a function of time. (Fig. 4-1C) The loss of mucins is likely due to shear of mucins from the mucin layer surface, mimicking the natural loss of mucus from the mucus layer *in vivo* due to enzyme action and fluid shearing. These results indicate that the mucin layer can be generated and maintained for at least 30 minutes, and the concentration of mucins is at least 50% of the initial concentration for 20 minutes.

### 4.3.2 Charge is a criterion for selective penetration of nanoscale peptides through a mucin barrier

We first compare the permeability of a layer of 0.5% (w/v) mucins in 20 mM NaCl buffer to the (+) peptide, containing positively charged lysines, to the permeability of the (-) peptide, containing negatively charged glutamic acids. (Fig. 4-3A) The concentration of both peptides in the peptide flow 4 μM, chosen because 4 μM is close to the maximum solubility at which all peptides tested here are soluble at all ionic strengths.

Fluorescent micrographs of the diffusion of the two peptides into the mucin channel in the presence and absence of mucins are shown in Fig. 4-3B. From the micrographs, concentration profiles of each biopolymer through the center cross section of the mucin channel (marked by the dotted axis $x$) are computed. Analysis of the shape of the concentration profiles yield information about the underlying interactions between mucins and the peptides. As shown in Fig. 4-3C, for the (+) peptide, the rise of the concentration profile to a peak value inside the mucin layer indicates the presence of attractive interactions between the mucins and peptides. In contrast, no evidence of attractive interactions is evident from the concentration profiles of the (-) peptide.

Analysis of the concentration profiles also show the (+) and (-) peptide transported into the mucin layer at different rates. From the concentration profile, the quantity of peptide transported into the mucin layer as function of time is estimated by computing the area under the concentration profile curve for $x >$ 210 μm. As shown in Fig. 4-3, the uptake of the (+) peptide into the mucin is significantly reduced by the presence of mucins, whereas the uptake of the (-) peptide into the mucin channel with and without mucins is approximately equal.

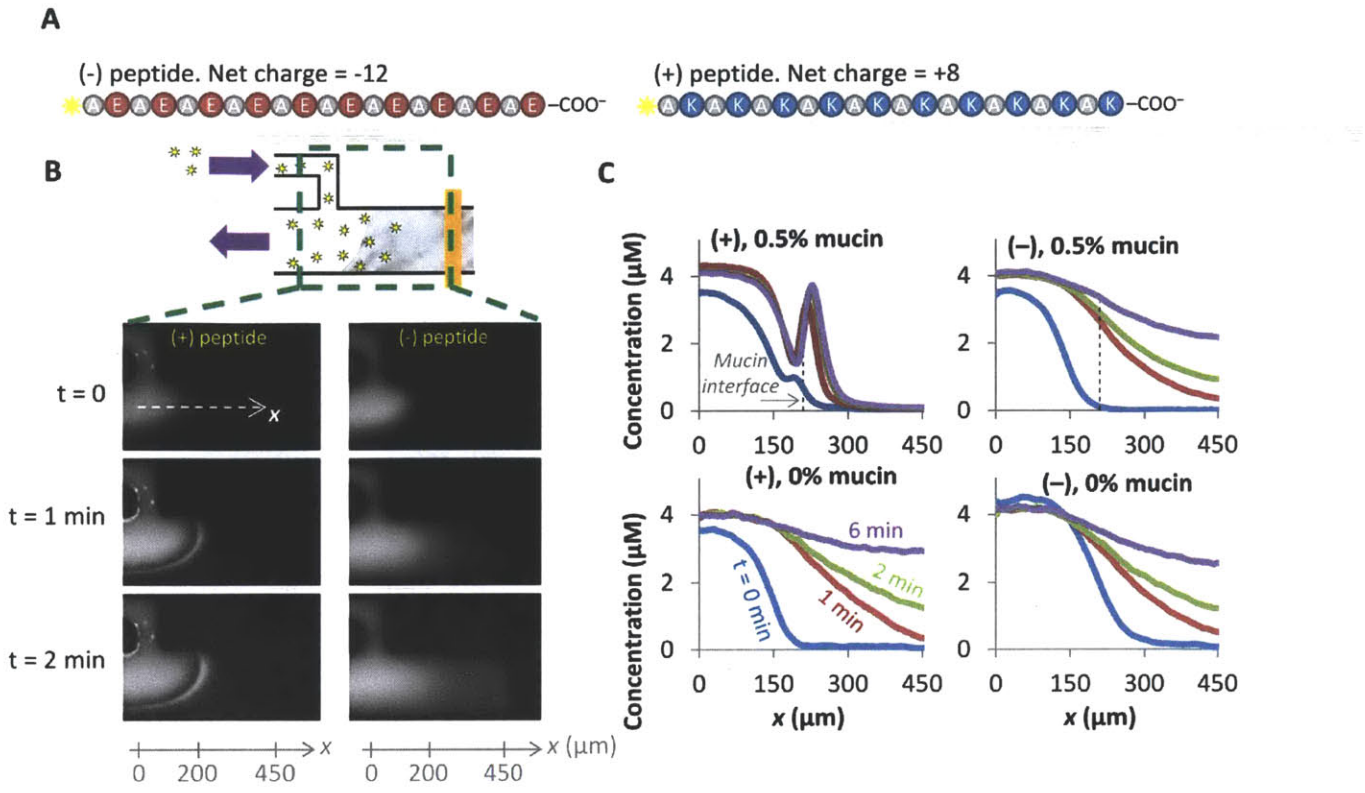


**Fig. 4-3**: Comparison of the diffusion behavior of the (+) and (–) peptides in 0.5% (w/v) mucin layer at 20 mM NaCl ionic strength. A) Sequence and net charge of the (+) and (–) peptides. B) Time elapsed fluorescence images of (+) and (-) peptide diffusion into a 0.5% (w/v) mucin layer. C) Time elapsed cross sectional concentration profiles of the diffusion and penetration of the (+) and (–) peptides into the mucin channel in the presence of 0.5% (w/v) mucins and 0% mucins at 20 mM NaCl ionic strength.

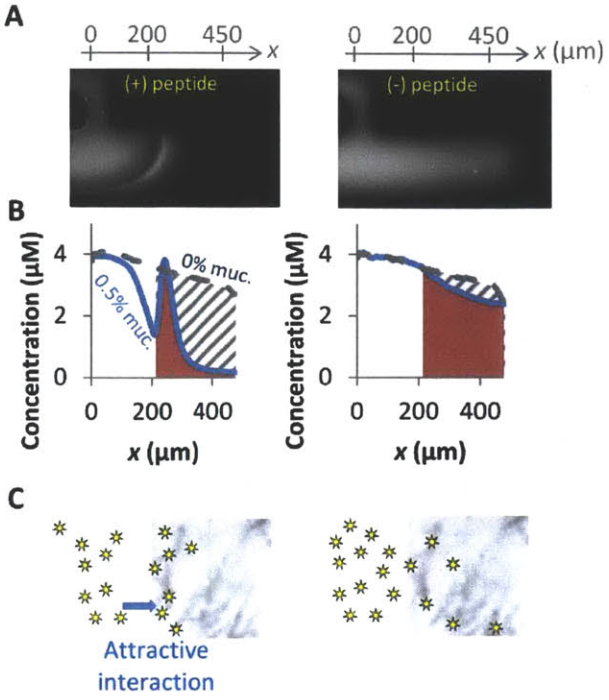


**Fig. 4-4**: Uptake rate calculation and comparison of mucin-peptide interactions for the (+) and (-) pepitdes. A) Fluorescence micrographs at t = 10 min for the transport of the (+) and (-) peptides into a 0.5% (w/v) mucin layer. B) Comparison of the (+) and (-) peptide concentration profiles in 0.5% (w/v) and 0% (buffer only) mucin layers at t = 10 min. The solid and dashed shaded areas represent the quantity of peptides transported into a mucin layer with 0.5% and 0% mucins, respectively. The (+) peptide transport rate was decreased in the presence of mucins, whereas the (-) peptide uptake is not significantly affected by the presence of mucins. C) The rise in the (+) peptide concentration profile inside the mucin layer demonstrates attractive interactions between mucins and the (+) peptide. No attractive interactions between mucins and the (-) peptides are demonstrated by the (-) peptide concentration profile.

### 4.3.3 Mucin layer ionic strength regulates mucin-peptide interactions and peptide transport

In the *in vivo* mucus layer, the ionic strength varies by anatomical location and varies with physiological states such as the menstrual cycle. (Section 1.2) To simulate these ionic strength changes, we repeat the experiment above but for several ionic strengths in the mucin layer and peptide flow.

Our results show that altered ionic strengths had different effects on the (+) and (-) peptides. As shown in Fig. 4, the (+) peptide penetrates the mucin layer much more readily at 200 mM NaCl and 200 mM $CaCl_2$ ionic strengths compared to at 5 and 20 mM NaCl ionic strengths. In addition, at the 5 and 20 mM NaCl ionic strengths, the (+) peptide is mostly distributed at the surface of the peptide, where at higher ionic strength it is distributed more evenly throughout the mucin layer by t = 10 min. In contrast to the (+) peptide, the (-) peptide concentration profile does not show peaks in the concentration profile at any ionic strength tested, and thus attractive interactions are not found between mucins and the (-) peptide. (Fig. 4)

Moreover, the relative permeability of the mucin barrier was changed by ionic strength. In Fig. 5, the uptake rate of the (+) and (-) peptides are compared. The results show that the (-) peptide uptakes into mucin layer at a higher rate than the (+) peptide for ionic strengths of 5 mM and 20 mM NaCl ionic strengths, but the (+) peptide uptake is higher than that of the (-) peptide at 200 mM NaCl. These results suggest that difference in electrostatic interaction between the (+) and (-) peptides with mucins may alter the relative permeability of the mucin layer to the peptides depending on the ionic strength of the mucus barrier, at times favoring the uptake of positively charged peptides, while at other times favoring the uptake of negatively charged peptides.

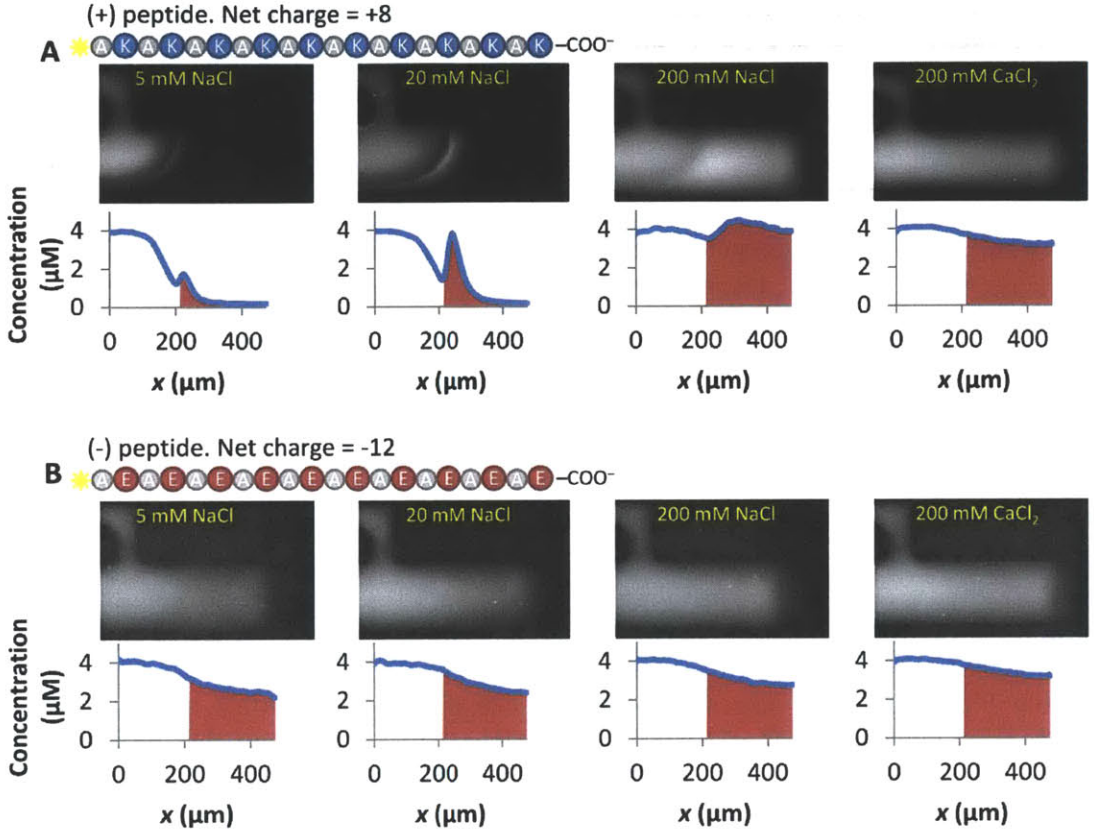


**Fig. 4-5**: Effect of ionic strength on (+) and (-) peptide transport into a mucin barrier. A) Fluorescence micrographs and cross sectional profiles for transport of the (+) peptide into a 0.5% (w/v) mucin layer at t = 10 min. The peak in the (+) peptide concentration profile varies in height and width, suggesting altered ionic strength alters the interactions between mucins and the (+) peptide. The uptake into the mucin layer (shaded area) is also altered by ionic strength. B) Fluorescence micrographs and cross sectional profiles for transport of the (-) peptide into a 0.5% (w/v) mucin layer at t = 10 min. The shape of the (-) peptide concentration profile is not significantly changed by altered ionic strength.

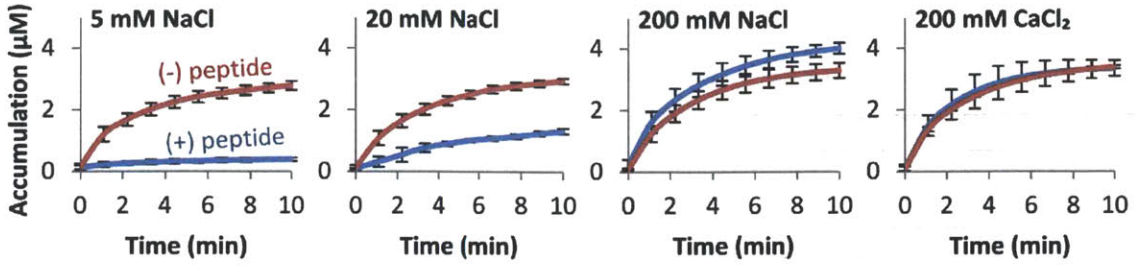


**Fig. 4-6**: Comparison of the quantity of (+) and (-) peptide accumulated inside the 0.5% (w/v) mucin layer as a function of time. The comparison demonstrates that the relative rates of uptake are ionic strength dependent.

### 4.3.4 Spatial charge distribution regulates mucin-peptide interactions and peptide transport

The comparison of (+) and (-) peptide transport into a mucin layer demonstrated that charge is a criterion for the rate of transport of a peptide into the mucin layer. However, the (+) and (-) peptides contain homogeneous positive and negative charges, respectively, whereas most native proteins and pathogens in nature exhibit heterogeneously charge surfaces containing both positive and negative charges [161]. We thus next characterize the interactions between the mucin barrier and heterogeneously charged peptides. For this purpose, we compare the transport behavior of the heterogeneously charged (Block) and (Alternate) peptides. The (Block) and (Alternate) peptides contain equal numbers of both positively and negatively residues, but at different spatial arrangements.

The results show that spatial charge distribution on the peptides affects the mucin-peptide interaction and peptide transport. Fig. 4-7 compares the concentration profiles of the (Block) and (Alternate) peptides at t = 10 min at a mucin layer ionic strength of 20 mM NaCl. The presence of a peak in the concentration profile indicates attractive interactions between the (Block) peptide and mucins, and the uptake of the (Block) peptide is increased by the presence of mucins. In contrast, the (Alternate) peptide does not show interactions with mucins and its uptake into the mucin layer on-chip is unaffected by the mucins. Since the two peptides have the same net charge and amino acid composition, such difference in their concentration profile during transport indicates that spatial charge distribution can alter mucin-peptide interaction and the peptide uptake.

As in the case of the (+) and (-) peptides, changes in the ionic strength also altered the relative permeability of the (Block) and (Alternate) peptides. As shown in Fig. 4-8 and Fig. 4-9, at 5 mM NaCl ionic strength, the (Block) peptide uptake is reduced compared to the (Alternate) peptide. The reverse is true at 20 mM NaCl ionic strength, where the (Block) peptide is increased compared to the (Alternate) peptide. Thus, the ionic environment of the mucin layer and the spatial charge distribution on the peptides jointly regulate the permeability of the peptides into a mucin barrier.

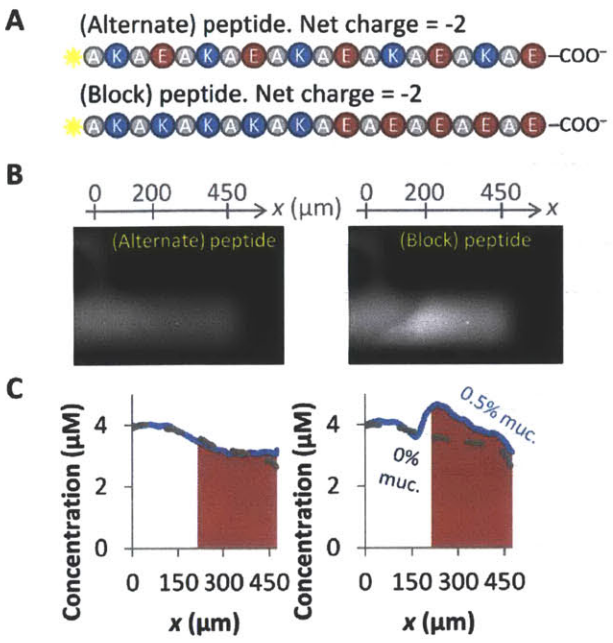


**Fig. 4-7**: Uptake rate calculation and comparison of mucin-peptide interactions for the (Alternate) and (Block) pepitdes. A) Sequence of the heterogeneously charged (Alternate) and (Block) peptides. These peptides are molecular isomers, containing equal number and type of amino acids but at different arrangements. B) Fluorescence micrographs at t = 10 min for the transport of the (Alternate) and (Block) peptides into a 0.5% (w/v) mucin layer. C) Comparison of the (Alternate) and (Block) peptide concentration profiles in 0.5% (w/v) and 0% (buffer only) mucin layers at t = 10 min. The (Block) peptide transport rate was increased in the presence of mucins, whereas the (Alternate) peptide uptake is not significantly affected by the presence of mucins.

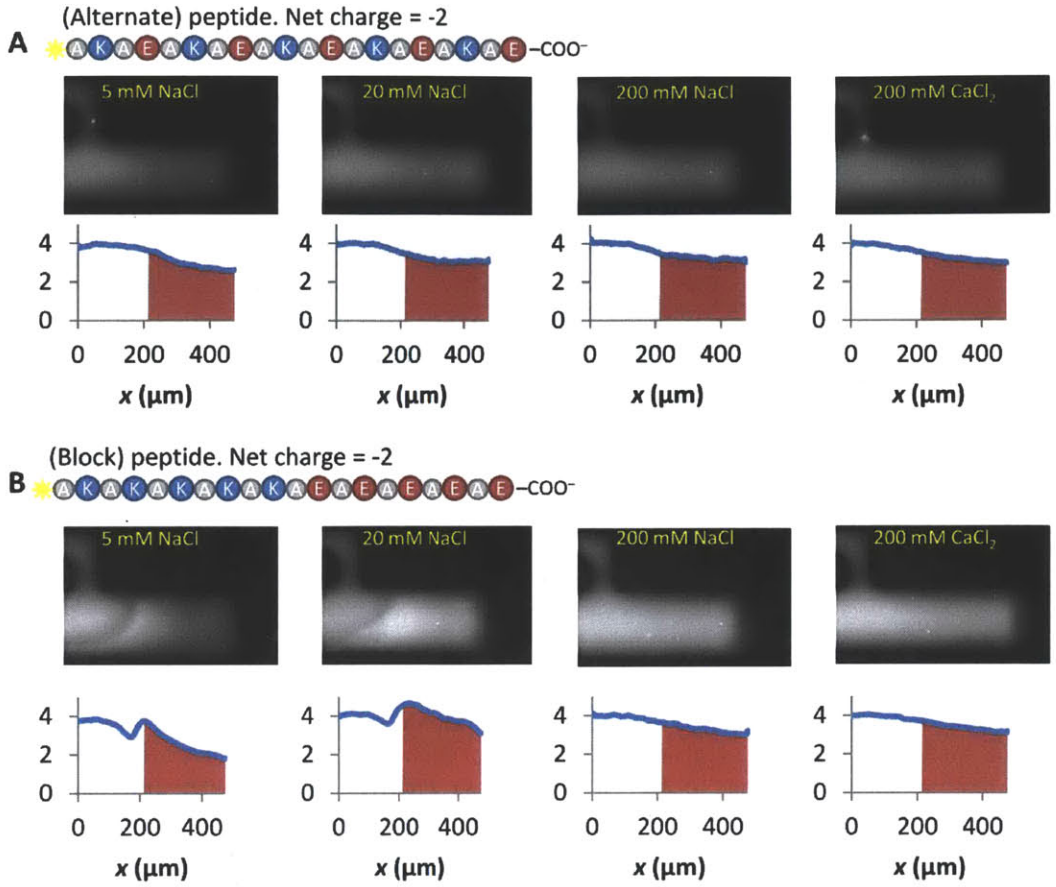


**Fig. 4-8**: Effect of ionic strength on (Alternate) and (Block) peptide transport into a mucin barrier. A) Fluorescence micrographs and cross sectional profiles for transport of the (Alternate) peptide into a 0.5% (w/v) mucin layer at t = 10 min. The shape of the (Alternate) peptide concentration profile and the rate of (Alternate) peptide transport into the mucin layer is not significantly changed by altered ionic strength. B) Fluorescence micrographs and cross sectional profiles for transport of the (Block) peptide into a 0.5% (w/v) mucin layer at t = 10 min. The peak in the concentration profile is present for 5 and 20 mM NaCl ionic strength but not present at higher ones, and the uptake of the (Block) peptide is also altered by the ionic strength changes.

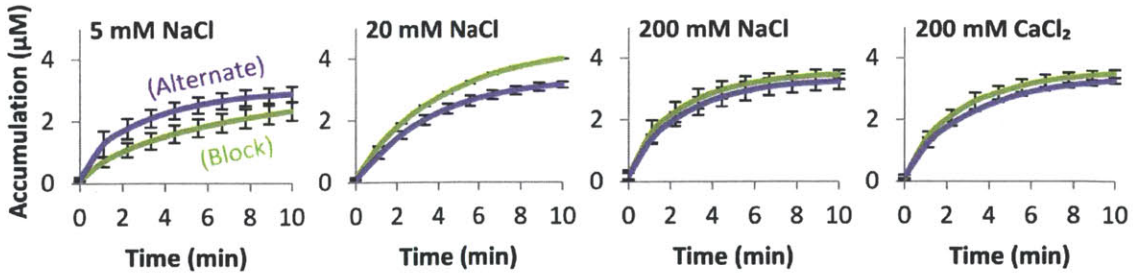


**Fig. 4-9**: Comparison of the quantity of (Alternate) and (Block) peptide accumulated inside the 0.5% (w/v) mucin layer as a function of time. This comparison demonstrates that the relative rates of uptake are ionic strength dependent.

## 4.4 Discussion

We have systematically investigated the transport of nanoscale peptides with different net charge and spatial charge configurations into the mucin layer. Fluorescently labeled, custom synthesized peptides as permeability probes can express charge and hydrophobic surface groups on the amino acid length scale. Such charge and hydrophobicity heterogeneity can be found on the same length scale on the surfaces of viruses and native proteins. [161] These charged and hydrophobic groups on the surface of peptides can also be precisely tuned using commercially available peptide synthesis methods. Our peptides are thus convenient and powerful probes to measure the selective permeability of the mucin barrier.

Our measurements of peptide transport into the mucin barrier are enabled by our novel microfluidic technique to measure molecular transport into a mucin layer. Analysis of the concentration profiles of peptides during transport elucidated the rate of peptide uptake, the distribution of peptides in the mucin layer, and whether interactions with mucin are present. Importantly, the peptide transport occurred from a peptide flow outside the mucin layer into the mucin layer initially devoid of the peptide. This setup presents a physiologically realistic experimental arrangement which models the *in vivo* transport of molecules from the lumen of the mucus lined organ tract such as the gastrointestinal or respiratory tracts into a mucus barrier. Previous technologies including FRAP [90, 91] or multiple particle tracking [92, 95, 96, 134] mix the molecules with the mucus sample and thus measure the molecular mobility once molecules mix inside the mucus barrier. These technologies are thus unable to measure the rate of transport or distribution of molecules in a physiologically realistic manner.

Using the microfluidic measurement of peptide transport, we first showed that the homogenously charged (+) and (-) peptides transported at different rates into the mucin barrier, demonstrating that the net charge of peptides is a determining criterion for the rate of transport. These findings are consistent with previous studies showing that nanoparticles uniformly coated with positive charge transported with different diffusivities inside mucus or mucin samples. [92, 95, 96, 134] Most previous findings show that positively charged molecules such as chitosan and positively charged antibiotics bind attractively to mucins, [102, 104, 114] consistent with our results that the (+) peptide but not the (-) peptide interacted attractively with mucins. These observations confirm that microfluidic measurements of peptides are able to elucidate transport differences arising from surface charge variation.

We then expanded the knowledge of the charge selectivity function of the mucin barrier to show that the (Block) and (Alternate) peptides transported into the mucin layer at different rates. These heterogeneously charged peptides are molecular isomers and differ only in charged residue arrangement. The results thus indicate net surface charge is not sufficient to determine behavior. Rather, the spatial distribution of positive and negative charges is a criterion for the peptide transport rate into a mucin layer.

We also showed that changes in ionic strength reversed the relative transport rates of the (+) and (-) peptides and that of the (Block) and (Alternate). The (-) and (Alternate) peptide uptake rates and mucin-interaction behavior were not affected significantly by changes in ionic strength, but the (+) and (Block) peptides uptake rates and mucin-interaction behavior were significantly changed. These results demonstrate that the susceptibility of peptide transport rate changes to ionic strength changes depend on the net charge and spatial charge distribution of the peptides.

Taken together, our findings demonstrate that the spatial distribution of positive and negative charge on the surfaces of drug delivery particles or molecules should be considered for each specific drug delivery application. Our systematic analysis of the transport behavior showed that functionalization of the surface of drug delivery particles with different combinations of positive and negative charges may be

used as a technique to tune transport behavior to a desired application. For example, at an ionic strength on the order of 20 mM NaCl, the use of (Block) peptide-like surface charge distribution may be used to maximize the rate of uptake. One possibility to create such particles with spatially controlled heterogeneous charges may be to functionalize such particles with our peptides. Such functionalization of particle surfaces with biopolymers to improve transport characteristics has already been demonstrated with PEG coatings. [92, 127] Spatial heterogeneity surfaces can be applied to drug delivery particles for a variety of drug and gene delivery applications to the many mucus barriers of the body.

The *in vitro* microfluidic system in this work provides a platform tool to characterize molecular transport into a mucin barrier. Its key advantage over particle tracking and FRAP techniques is the setup of molecular transport into the mucin layer from the outside. Another advantage over the particle tracking technique is the ability to test molecules with heterogeneous surface properties. In the future, this microfluidic platform may be directly used for further dissection of the mucus barrier function such as to peptides with varying hydrophobicity, the testing of drug permeation into the mucus barrier, and characterization of mucus barrier modification agents such as exogenous lipids [146] or nanoparticles. [119]

# Chapter 5

# Conclusions and outlook

## 5.1 Thesis contributions

In this thesis, we presented novel microfluidic devices to characterize the selective permeability of the mucus barrier. We showed new understanding of the criteria and mechanisms of the mucus selective permeability function.

### 5.1.1 Contributions to Microfluidics

In this thesis, we conceptualized, fabricated, and optimized microfluidic devices capable of mucin barrier function measurements, which have not been demonstrated previously.

One new technique demonstrated by this thesis is the dynamic renewal of the mucin barrier on chip. Previously, *in vitro* characterization of acid barrier function used static mucus inside a diffusion chamber. In our microfluidic device, the acid barrier function provided by stomach mucins was measured under conditions of mucus secretion as it occurs inside the body. This mimics the dynamic renewal of the mucin layer as it occurs *in vivo*, including the loss of mucins from the mucus layer on the lumen side due to convection, and the continuous replacement of mucins by secretion on the stomach wall side.

Another technique not previously available in existing *in vitro* assays is the ability to measure transport of molecules into a mucin layer from the outside. Previously, measurement techniques such as multiple particle tracking and FRAP required pre-mixing of particles/molecules with the mucus. Our microfluidic measurement technique more accurately reproduces the physiology of molecular and particle transport into a mucus barrier. This device enabled measurement of the concentration profiles of the molecules as they diffused into the mucin layer, providing much more information than previous technologies.

Very low sample volume requirement (10's of μL per chip including external reservoir, syringe, tubing, and on-chip volumes) was achieved for the devices. Minimizing sample volume requirement is significant for studies involving mucins , because native mucins are labor intensive and expensive to purify. Low sample volume requirement may prove critical in the future if the devices are to be adapted for the use of limited, precious clinical mucus samples from patients.

Overall, our microfluidic devices provide a research platform which may be developed further into devices to dissect mucus barrier function mechanisms, assess barrier function to pathogens, assess

barrier function of clinical mucus samples as a diagnostic or companion diagnostic tool, or test the transport characteristics of drugs and drug candidates.

### 5.1.2 Contributions to Biology and Bioengineering

Our microfluidic method to characterize mucus barrier function demonstrated previously unknown aspects of the barrier function.

We found that the continuous secretion of mucins contributes to a significant portion of the acid barrier function of the stomach. Mucins were found to contain $H^+$ binding groups on its glycans and protein backbone. A quantitative analysis using microfluidic experiments, acid titration, and computational modeling showed that acid binding by mucins contributes to the same order of magnitude of acid barrier function as known amounts of bicarbonate secretion by the gastric epithelium. Since the secretion rate of mucins in the stomach varies with physiological condition, our results suggest that the acid barrier arising from mucin secretion can be varied by the body based on physiological need.

We also showed that transport behavior of peptides diffusing into a mucin barrier is dependent on the charge profile on the surface of the peptides. Changes to the surface charge profile of the peptides significantly affected the penetration speeds and uptake rates of the peptides. We thus demonstrated that mucins provide a selective permeability barrier capable of distinguishing transiting peptides with amino acid length scale resolution and are therefore capable of much finer molecular discrimination than previously understood. This has significant scientific/engineering implications in drug/pathogen transport in mucus barriers.

## 5.2 Recommendations for future work

### 5.2.1 Hydrophobicity barrier of the mucin layer

The peptides used in this thesis as permeability probes varied in surface charge profile, allowing the charge selectivity of the mucin layer to be studied. We propose to employ similar peptides which vary in the distribution of hydrophobic residues to probe the hydrophobic barrier of native mucins. (Fig. 5-1)

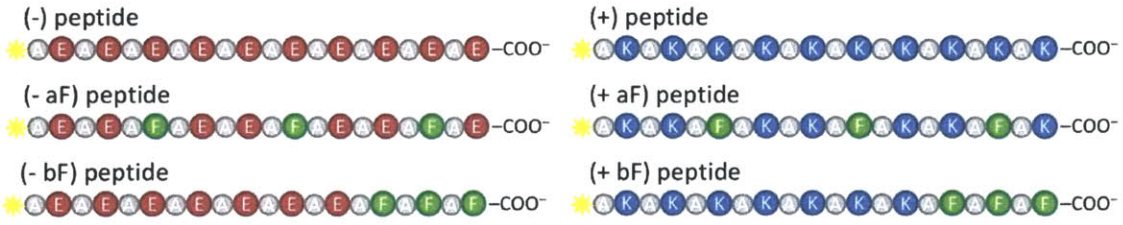


**Fig. 5-1**: Proposed peptides to probe the effect of peptide hydrophobicity on the selective penetration and uptake function of the mucin barrier.

Experimental comparison of the penetration and uptake of the (-), (- aF), and (- bF) peptides into a mucin barrier would characterize the ability of mucins to recognize hydrophobic residues on transiting peptides. First, since the (-) peptide does not interact with mucins, comparison of the (-) peptide with the (- aF) and (- bF) peptides would answer the question of whether hydrophobic residues on a peptide surface can alter penetration and uptake. Second, since the (- aF) and (- bF) peptides contain equal amino acid composition but at different arrangements, differences in the penetration or uptake behavior of the (- aF) and (- bF) peptides would provide conclusive proof that nanoscale differences in the arrangement of hydrophobic residues on a molecular surface is capable of altering transit into the mucin barrier.

We similarly propose to add hydrophobic residues to the (+) peptide to form the (+ aF) and (+ bF) peptides. Our thesis findings showed that the positive charges on a peptide bind to mucins. Thus, addition of hydrophobic groups to the (+) peptide forms peptides with two types of mucin-interacting residues. Comparison of the diffusion behavior among (+), (+ aF) and (+ bF) peptides would determine if the positively charged and hydrophobic residues interact with each other to determine peptide permeability through the mucin barrier.

### 5.2.2 Characterization of the lipid barrier of mucus layer

In the native mucus barrier, mucins are covalent linked with and reversibly bound with several types of lipids. [146] Such a lipid and mucin network may confer important barrier properties. Different concentration of lipids are found at different anatomical locations *in vivo*, [84] and the lipid concentrations of mucus can be altered with drugs such as NSAIDs [164, 165] and with diseases such as *Helicobacter pylori* infection. [166, 167] Our microfluidic platform can characterize the significance of lipids in the barrier function of the mucus layer, by measuring the transport of charged and hydrophobic peptides into a mucin layer with various lipid concentrations. The mucin purification method in our work results in mucins with significant amounts of attached lipids. [138] This lipid concentration can be reliably reduced using CsCl density ultracentrifugation during the purification process, [138] and the lipid concentration can be increased by further adding exogenous lipids.

### 5.2.3 Tunable mucus penetrating and interacting peptides for drug delivery through the mucus barrier

The findings in this thesis showed that a mucin layer enables peptides with different charge profiles to penetrate and uptake at different rates. We propose to functionalize these peptides as targeting peptides to the surface of drug delivery particles. We hypothesize the peptide interactions with mucin would drive the penetration and uptake behavior of the drug encapsulated particles into a mucus layer. This would provide a surface functionalization scheme for drug delivery particles which may be tuned to desired penetration and uptake characteristics for specific drug delivery applications.

# Bibliography


1 Rogers DF. Airway goblet cell hyperplasia in asthma: hypersecretory and anti-inflammatory? Clinical and experimental allergy : journal of the British Society for Allergy and Clinical Immunology 2002;32(8):1124-7.

2 Finkbeiner WE. Physiology and pathology of tracheobronchial glands. Respiration physiology 1999;118(2-3):77-83.

3 Fahy JV, Dickey BF. Airway Mucus Function and Dysfunction. N Engl J Med 2010;363(23):2233-47.

4 Matsui H, Randell SH, Peretti SW, Davis CW, Boucher RC. Coordinated clearance of periciliary liquid and mucus from airway surfaces. The Journal of clinical investigation 1998;102(6):1125-31.

5 Niv Y, Boltin D, Halpern M, et al. Membrane-Bound Mucins and Mucin Terminal Glycans Expression in Idiopathic or Helicobacter pylori, NSAID Associated Peptic Ulcers. Digestive diseases and sciences 2012;57(10):2535-44.

6 Atuma C, Strugala V, Allen A, Holm L. The adherent gastrointestinal mucus gel layer: thickness and physical state in vivo. American journal of physiology.Gastrointestinal and liver physiology 2001;280(5):G922-9.

7 McGuckin MA, Linden SK, Sutton P, Florin TH. Mucin dynamics and enteric pathogens. Nature reviews.Microbiology 2011;9(4):265-78.

8 Sellers LA, Carroll NJ, Allen A. Misoprostol-induced increases in adherent gastric mucus thickness and luminal mucus output. Digestive diseases and sciences 1986;31(2 Suppl):91S-5S.

9 Hafez ES, Kanagawa H. Ciliated epithelium in the uterine cervix of the macaque and rabbit. Journal of reproduction and fertility 1972;28(1):91-4.

10 Allen A, Flemstrom G, Garner A, Kivilaakso E. Gastroduodenal mucosal protection. Physiological Reviews 1993;73(4):823-57.

11 Strous GJ, Dekker J. Mucin-type glycoproteins. Critical reviews in biochemistry and molecular biology 1992;27(1-2):57-92.

12 Gum JR, Jr. Mucin genes and the proteins they encode: structure, diversity, and regulation. American journal of respiratory cell and molecular biology 1992;7(6):557-64.

13 Linden SK, Sutton P, Karlsson NG, Korolik V, McGuckin MA. Mucins in the mucosal barrier to infection. Mucosal immunology 2008;1(3):183-97.

14 Perez-Vilar J, Eckhardt AE, DeLuca A, Hill RL. Porcine Submaxillary Mucin Forms Disulfide-linked Multimers through Its Amino-terminal D-domains. Journal of Biological Chemistry 1998;273(23):14442-9.

15 Bromberg LE, Barr DP. Self-Association of Mucin. Biomacromolecules 2000;1(3):325-34.

16 Pandey P, Kharbanda S, Kufe D. Association of the DF3/MUC1 breast cancer antigen with Grb2 and the Sos/Ras exchange protein. Cancer research 1995;55(18):4000-3.

17 Li Q, Ren J, Kufe D. Interaction of human MUC1 and beta-catenin is regulated by Lck and ZAP-70 in activated Jurkat T cells. Biochemical and biophysical research communications 2004;315(2):471-6.

18 Ovesen L, Bendtsen F, Tage-Jensen U, Pedersen NT, Gram BR, Rune SJ. Intraluminal pH in the stomach, duodenum, and proximal jejunum in normal subjects and patients with exocrine pancreatic insufficiency. Gastroenterology 1986;90(4):958-62.

19 Bahari HM, Ross IN, Turnberg LA. Demonstration of a pH gradient across the mucus layer on the surface of human gastric mucosa in vitro. Gut 1982;23(6):513-6.

20 Schreiber S, Nguyen TH, Stuben M, Scheid P. Demonstration of a pH gradient in the gastric gland of the acid-secreting guinea pig mucosa. American journal of physiology.Gastrointestinal and liver physiology 2000;279(3):G597-604.

21 Boskey ER, Cone RA, Whaley KJ, Moench TR. Origins of vaginal acidity: high d/l lactate ratio is consistent with bacteria being the primary source. Human Reproduction 2001;16(9):1809-13.
22 McCloy RF, Greenberg GR, Baron JH. Duodenal pH in health and duodenal ulcer disease: effect of a meal, Coca-Cola, smoking, and cimetidine. Gut 1984;25(4):386-92.
23 Washington N, Steele RJ, Jackson SJ, et al. Determination of baseline human nasal pH and the effect of intranasally administered buffers. International journal of pharmaceutics 2000;198(2):139-46.
24 Karnad DR, Mhaisekar DG, Moralwar KV. Respiratory mucus pH in tracheostomized intensive care unit patients: Effects of colonization and pneumonia. Critical Care Medicine 1990;18(7):699-701.
25 Fallingborg J. Intraluminal pH of the human gastrointestinal tract. Danish medical bulletin 1999;46(3):183-96.
26 Suarez SS, Pacey AA. Sperm transport in the female reproductive tract. Human reproduction update 2006;12(1):23-37.
27 Jenkins JM, Brook PF, Sargeant S, Cooke ID. Endocervical mucus pH is inversely related to serum androgen levels and waist to hip ratio. Fertility and sterility 1995;63(5):1005-8.
28 Eggert-Kruse W, Kohler A, Rohr G, Runnebaum B. The pH as an important determinant of sperm-mucus interaction. Fertility and sterility 1993;59(3):617-28.
29 Celli JP, Turner BS, Afdhal NH, et al. Rheology of gastric mucin exhibits a pH-dependent sol-gel transition. Biomacromolecules 2007;8(5):1580-6.
30 Chace KV, Naziruddin B, Desai VC, Flux M, Sachdev GP. Physical properties of purified human respiratory mucus glycoproteins: effects of sodium chloride concentration on the aggregation properties and shape. Experimental lung research 1989;15(5):721-37.
31 Smith JJ, Travis SM, Greenberg EP, Welsh MJ. Cystic fibrosis airway epithelia fail to kill bacteria because of abnormal airway surface fluid. Cell 1996;85(2):229-36.
32 Riddell MJ, Strong JA, Cameron D. THE ELECTROLYTE CONCENTRATION OF HUMAN GASTRIC SECRETION. Experimental physiology 1960;45(1):1-11.
33 Gupta KA, Purohit GN. Use of vaginal electrical resistance (VER) to predict estrus and ovarian activity, its relationship with plasma progesterone and its use for insemination in buffaloes. Theriogenology 2001;56(2):235-45.
34 Chrétien FC, Berthou J. A new crystallographic approach to fern-like microstructures in human ovulatory cervical mucus. Human Reproduction 1989;4(4):359-68.
35 Kopito LE, Kosasky HJ, Sturgis SH, Lieberman BL, Shwachman H. Water and electrolytes in human cervical mucus. Fertility and sterility 1973;24(7):499-506.
36 Gould KG, Ansari AH. Electrolyte interactions in cervical mucus and their relationship to circulating hormone levels. Contraception 1981;23(5):507-16.
37 Wagner G, Levin RJ. Electrolytes in vaginal fluid during the menstrual cycle of coitally active and inactive women. Journal of reproduction and fertility 1980;60(1):17-27.
38 Joris L, Dab I, Quinton PM. Elemental composition of human airway surface fluid in healthy and diseased airways. The American Review of Respiratory Disease 1993;148(6 Pt 1):1633-7.
39 Kozlova I, Vanthanouvong V, Johannesson M, Roomans GM. Composition of airway surface liquid determined by X-ray microanalysis. Upsala journal of medical sciences 2006;111(1):137-53.
40 Knowles MR, Robinson JM, Wood RE, et al. Ion composition of airway surface liquid of patients with cystic fibrosis as compared with normal and disease-control subjects. The Journal of clinical investigation 1997;100(10):2588-95.
41 Lieleg O, Lieleg C, Bloom J, Buck CB, Ribbeck K. Mucin biopolymers as broad-spectrum antiviral agents. Biomacromolecules 2012;13(6):1724-32.
42 Chen CC, Baylor M, Bass DM. Murine intestinal mucins inhibit rotavirus infection. Gastroenterology 1993;105(1):84-92.

43 McAuley JL, Linden SK, Png CW, et al. MUC1 cell surface mucin is a critical element of the mucosal barrier to infection. The Journal of clinical investigation 2007;117(8):2313-24.
44 McGuckin MA, Every AL, Skene CD, et al. Muc1 mucin limits both Helicobacter pylori colonization of the murine gastric mucosa and associated gastritis. Gastroenterology 2007;133(4):1210-8.
45 Blalock TD, Spurr-Michaud SJ, Tisdale AS, et al. Functions of MUC16 in corneal epithelial cells. Investigative ophthalmology & visual science 2007;48(10):4509-18.
46 Lu W, Hisatsune A, Koga T, et al. Cutting edge: enhanced pulmonary clearance of Pseudomonas aeruginosa by Muc1 knockout mice. Journal of immunology (Baltimore, Md.: 1950) 2006;176(7):3890-4.
47 Lillehoj EP, Kim BT, Kim KC. Identification of Pseudomonas aeruginosa flagellin as an adhesin for Muc1 mucin. American journal of physiology.Lung cellular and molecular physiology 2002;282(4):L751-6.
48 Kato K, Lu W, Kai H, Kim KC. Phosphoinositide 3-kinase is activated by MUC1 but not responsible for MUC1-induced suppression of Toll-like receptor 5 signaling. American Journal of Physiology - Lung Cellular and Molecular Physiology 2007;293(3):L686-L92.
49 Linden SK, Wickstrom C, Lindell G, Gilshenan K, Carlstedt I. Four modes of adhesion are used during Helicobacter pylori binding to human mucins in the oral and gastric niches. Helicobacter 2008;13(2):81-93.
50 Iontcheva I, Oppenheim FG, Offner GD, Troxler RF. Molecular mapping of statherin- and histatin-binding domains in human salivary mucin MG1 (MUC5B) by the yeast two-hybrid system. Journal of dental research 2000;79(2):732-9.
51 Phalipon A, Cardona A, Kraehenbuhl JP, Edelman L, Sansonetti PJ, Corthesy B. Secretory component: a new role in secretory IgA-mediated immune exclusion in vivo. Immunity 2002;17(1):107-15.
52 Mochon AB, Liu H. The antimicrobial peptide histatin-5 causes a spatially restricted disruption on the Candida albicans surface, allowing rapid entry of the peptide into the cytoplasm. PLoS pathogens 2008;4(10):e1000190.
53 Katz DF, Slade DA, Nakajima ST. Analysis of pre-ovulatory changes in cervical mucus hydration and sperm penetrability. Advances in Contraception : The Official Journal of the Society for the Advancement of Contraception 1997;13(2-3):143-51.
54 Fleetwood L, Landgren BM, Eneroth P. Quantitation of human cervical mucin during consecutive days and hourly during one day at midcycle. Gynecologic and obstetric investigation 1986;22(3):145-52.
55 Morales P, Roco M, Vigil P. Human cervical mucus: relationship between biochemical characteristics and ability to allow migration of spermatozoa. Human Reproduction 1993;8(1):78-83.
56 Bigelow JL, Dunson DB, Stanford JB, Ecochard R, Gnoth C, Colombo B. Mucus observations in the fertile window: a better predictor of conception than timing of intercourse. Human Reproduction 2004;19(4):889-92.
57 Katz DF, Morales P, Samuels SJ, Overstreet JW. Mechanisms of filtration of morphologically abnormal human sperm by cervical mucus. Fertility and sterility 1990;54(3):513-6.
58 Barros C, Vigil P, Herrera E, Arguello B, Walker R. Selection of morphologically abnormal sperm by human cervical mucus. Archives of Andrology 1984;12 Suppl:95-107.
59 Parkhurst MR, Saltzman WM. Leukocytes migrate through three-dimensional gels of midcycle cervical mucus. Cellular immunology 1994;156(1):77-94.
60 Mathur S, Rosenlund C, Carlton M, et al. Studies on sperm survival and motility in the presence of cytotoxic sperm antibodies. American Journal of Reproductive Immunology and Microbiology : AJRIM 1988;17(2):41-7.
61 Kutteh WH, Prince SJ, Hammond KR, Kutteh CC, Mestecky J. Variations in immunoglobulins and IgA subclasses of human uterine cervical secretions around the time of ovulation. Clinical and experimental immunology 1996;104(3):538-42.

62 Mullins KJ, Saacke RG. Study of the functional anatomy of bovine cervical mucosa with special reference to mucus secretion and sperm transport. The Anatomical Record 1989;225(2):106-17.
63 Mattner PE. THE DISTRIBUTION OF SPERMATOZOA AND LEUCOCYTES IN THE FEMALE GENITAL TRACT IN GOATS AND CATTLE. Journal of reproduction and fertility 1968;17(2):253-61.
64 Suarez SS. Chapter 3 - Gamete and Zygote Transport. In: Jimmy DNAPDATMPAPDADWPAPDAJRG, Paul M. Wassarman PD, eds. *Knobil and Neill's Physiology of Reproduction (Third Edition)*. St Louis: Academic Press; 2006:113-45.
65 Fawcett DW, Bloom W, Raviola E. *A textbook of histology*. New York: Chapman & Hall; 1994.
66 Katz DF, Mills RN, Pritchett TR. The movement of human spermatozoa in cervical mucus. Journal of reproduction and fertility 1978;53(2):259-65.
67 Chretien FC. Involvement of the glycoproteic meshwork of cervical mucus in the mechanism of sperm orientation. Acta Obstetricia et Gynecologica Scandinavica 2003;82(5):449-61.
68 Tampion D, Gibbons RA. Orientation of spermatozoa in mucus of the cervix uteri. Nature 1962;194:381.
69 Alexander NJ. Evaluation of male infertility with an in vitro cervical mucus penetration test. Fertility and sterility 1981;36(2):201-8.
70 Gervais R, Dumur V, Letombe B, et al. Hypofertility with thick cervical mucus: another mild form of cystic fibrosis? JAMA : the journal of the American Medical Association 1996;276(20):1638.
71 Chamley LW, Clarke GN. Antisperm antibodies and conception. Seminars in immunopathology 2007;29(2):169-84.
72 Alexander NJ, Schmidt SS. Incidence of antisperm antibody levels and granulomas in men. Fertility and sterility 1977;28(6):655-7.
73 Kutteh WH, Byrd W, Blankenship L, Kutteh CC, Carr BR. Cervical mucus anti-sperm antibodies: treatment with intrauterine insemination. American journal of reproductive immunology (New York, N.Y.: 1989) 1996;35(4):429-33.
74 Kremer J, Jager S. The sperm-cervical mucus contact test: a preliminary report. Fertility and sterility 1976;27(3):335-40.
75 Kremer J, Jager S. The significance of antisperm antibodies for sperm-cervical mucus interaction. Human reproduction (Oxford, England) 1992;7(6):781-4.
76 Jager S, Kremer J, Kuiken J, Mulder I. The significance of the Fc part of antispermatozoal antibodies for the shaking phenomenon in the sperm-cervical mucus contact test. Fertility and sterility 1981;36(6):792-7.
77 Allen A, Flemstrom G. Gastroduodenal mucus bicarbonate barrier: protection against acid and pepsin. American journal of physiology.Cell physiology 2005;288(1):C1-19.
78 Flemstrom G, Garner A. Gastroduodenal HCO3(-) transport: characteristics and proposed role in acidity regulation and mucosal protection. The American Journal of Physiology 1982;242(3):G183-93.
79 Flemstrom G, Sachs TG. Ion transport by amphibian antrum in vitro. I. General characteristics. The American Journal of Physiology 1975;228(4):1188-98.
80 Flemstrom G. Active alkalinization by amphibian gastric fundic mucosa in vitro. The American Journal of Physiology 1977;233(1):E1-12.
81 Werther JL, Hollander F, Altamirano M. Effect of Acetazolamide on Gastric Mucosa in Canine Vivo-Vitro Preparations. The American Journal of Physiology 1965;209:127-33.
82 Engel E, Peskoff A, Kauffman GL, Jr., Grossman MI. Analysis of hydrogen ion concentration in the gastric gel mucus layer. The American Journal of Physiology 1984;247(4 Pt 1):G321-38.
83 Lichtenberger LM. The hydrophobic barrier properties of gastrointestinal mucus. Annual Review of Physiology 1995;57:565-83.
84 Hills BA, Butler BD, Lichtenberger LM. Gastric mucosal barrier: hydrophobic lining to the lumen of the stomach. The American Journal of Physiology 1983;244(5):G561-8.

85 Sarosiek J, Slomiany A, Takagi A, Slomiany BL. Hydrogen ion diffusion in dog gastric mucus glycoprotein: effect of associated lipids and covalently bound fatty acids. Biochemical and biophysical research communications 1984;118(2):523-31.
86 Yao X, Forte JG. Cell biology of acid secretion by the parietal cell. Annual Review of Physiology 2003;65:103-31.
87 Schreiber S, Scheid P. Gastric mucus of the guinea pig: proton carrier and diffusion barrier. AJP - Gastrointestinal and Liver Physiology 1997;272(1):G63-70.
88 Bhaskar KR, Garik P, Turner BS, et al. Viscous fingering of HCl through gastric mucin. Nature 1992;360(6403):458-61.
89 Nittmann J, Daccord G, Stanley HE. Fractal growth viscous fingers: quantitative characterization of a fluid instability phenomenon. Nature 1985;314(6007):141-4.
90 Olmsted SS, Padgett JL, Yudin AI, Whaley KJ, Moench TR, Cone RA. Diffusion of macromolecules and virus-like particles in human cervical mucus. Biophysical journal 2001;81(4):1930-7.
91 Saltzman WM, Radomsky ML, Whaley KJ, Cone RA. Antibody diffusion in human cervical mucus. Biophysical journal 1994;66(2, Part 1):508-15.
92 Lai SK, O'Hanlon DE, Harrold S, et al. Rapid transport of large polymeric nanoparticles in fresh undiluted human mucus. Proceedings of the National Academy of Sciences of the United States of America 2007;104(5):1482-7.
93 Lai SK, Wang YY, Hida K, Cone R, Hanes J. Nanoparticles reveal that human cervicovaginal mucus is riddled with pores larger than viruses. Proceedings of the National Academy of Sciences of the United States of America 2010;107(2):598-603.
94 Lieleg O, Vladescu I, Ribbeck K. Characterization of particle translocation through mucin hydrogels. Biophysical journal 2010;98(9):1782-9.
95 Crater JS, Carrier RL. Barrier Properties of Gastrointestinal Mucus to Nanoparticle Transport. Macromolecular bioscience 2010.
96 Dawson M, Wirtz D, Hanes J. Enhanced viscoelasticity of human cystic fibrotic sputum correlates with increasing microheterogeneity in particle transport. The Journal of biological chemistry 2003;278(50):50393-401.
97 Bergogne-Berezin E, Berthelot G, Kafe HP, Dournovo P. Influence of a fluidifying agent (bromhexine) on the penetration of antibiotics into respiratory secretions. International journal of clinical pharmacology research 1985;5(5):341-4.
98 Ricevuti G, Pasotti D, Mazzone A, Gazzani G, Fregnan GB. Serum, sputum and bronchial concentrations of erythromycin in chronic bronchitis after single and multiple treatments with either propionate-N-acetylcysteinate or stearate erythromycin. Chemotherapy 1988;34(5):374-9.
99 Iiboshi Y, Nezu R, Cui L, et al. Adhesive mucous gel layer and mucus release as intestinal barrier in rats. JPEN.Journal of parenteral and enteral nutrition 1996;20(2):98-104.
100 Suk JS, Boylan NJ, Trehan K, et al. N-acetylcysteine enhances cystic fibrosis sputum penetration and airway gene transfer by highly compacted DNA nanoparticles. Molecular therapy : the journal of the American Society of Gene Therapy 2011;19(11):1981-9.
101 Achterrath-Tuckermann U, Saano V, Minker E, et al. Influence of azelastine and some selected drugs on mucociliary clearance. Lung 1992;170(4):201-9.
102 Niibuchi J-J, Aramaki Y, Tsuchiya S. Binding of antibiotics to rat intestinal mucin. International journal of pharmaceutics 1986;30(2–3):181-7.
103 Bhat PG, Flanagan DR, Donovan MD. The limiting role of mucus in drug absorption: Drug permeation through mucus solution. International journal of pharmaceutics 1995;126(1–2):179-87.
104 Bataillon V, Lhermitte M, Lafitte JJ, Pommery J, Roussel P. The binding of amikacin to macromolecules from the sputum of patients suffering from respiratory diseases. The Journal of antimicrobial chemotherapy 1992;29(5):499-508.

105 Cheema MS, Groth S, Marriott C. Binding and diffusion characteristics of 14C EDTA and 99mTc DTPA in respiratory tract mucus glycoprotein from patients with chronic bronchitis. Thorax 1988;43(9):669-73.
106 Kearney P, Marriott C. The effects of mucus glycoproteins on the bioavailability of tetracycline. II. Binding. International journal of pharmaceutics 1987;35(3):211-7.
107 Ozdemir N, Ordu S, Ozkan Y. Studies of floating dosage forms of furosemide: in vitro and in vivo evaluations of bilayer tablet formulations. Drug development and industrial pharmacy 2000;26(8):857-66.
108 Hoffman A, Stepensky D, Lavy E, Eyal S, Klausner E, Friedman M. Pharmacokinetic and pharmacodynamic aspects of gastroretentive dosage forms. International journal of pharmaceutics 2004;277(1-2):141-53.
109 Weitschies W, Cardini D, Karaus M, Trahms L, Semmler W. Magnetic marker monitoring of esophageal, gastric and duodenal transit of non-disintegrating capsules. Die Pharmazie 1999;54(6):426-30.
110 Quon MG, Mena I, Valenzuela JE. Abnormalities in the duodenal transit and motility in duodenal ulcer patients: studies with a new isotopic technique. Gut 1989;30(5):579-85.
111 Boddupalli BM, Mohammed ZN, Nath RA, Banji D. Mucoadhesive drug delivery system: An overview. Journal of advanced pharmaceutical technology & research 2010;1(4):381-7.
112 Akiyama Y, Nagahara N, Kashihara T, Hirai S, Toguchi H. In vitro and in vivo evaluation of mucoadhesive microspheres prepared for the gastrointestinal tract using polyglycerol esters of fatty acids and a poly(acrylic acid) derivative. Pharmaceutical research 1995;12(3):397-405.
113 Nagahara N, Akiyama Y, Nakao M, Tada M, Kitano M, Ogawa Y. Mucoadhesive microspheres containing amoxicillin for clearance of Helicobacter pylori. Antimicrobial Agents and Chemotherapy 1998;42(10):2492-4.
114 Bowman K, Leong KW. Chitosan nanoparticles for oral drug and gene delivery. International journal of nanomedicine 2006;1(2):117-28.
115 Fernandez-Urrusuno R, Calvo P, Remunan-Lopez C, Vila-Jato JL, Alonso MJ. Enhancement of nasal absorption of insulin using chitosan nanoparticles. Pharmaceutical research 1999;16(10):1576-81.
116 El-Shabouri MH. Positively charged nanoparticles for improving the oral bioavailability of cyclosporin-A. International journal of pharmaceutics 2002;249(1-2):101-8.
117 Prego C, Garcia M, Torres D, Alonso MJ. Transmucosal macromolecular drug delivery. Journal of controlled release : official journal of the Controlled Release Society 2005;101(1-3):151-62.
118 Luessen HL, de Leeuw BJ, Langemeyer MW, de Boer AB, Verhoef JC, Junginger HE. Mucoadhesive polymers in peroral peptide drug delivery. VI. Carbomer and chitosan improve the intestinal absorption of the peptide drug buserelin in vivo. Pharmaceutical research 1996;13(11):1668-72.
119 Wang YY, Lai SK, So C, Schneider C, Cone R, Hanes J. Mucoadhesive nanoparticles may disrupt the protective human mucus barrier by altering its microstructure. PloS one 2011;6(6):e21547.
120 Artursson P, Lindmark T, Davis SS, Illum L. Effect of chitosan on the permeability of monolayers of intestinal epithelial cells (Caco-2). Pharmaceutical research 1994;11(9):1358-61.
121 Hombach J, Bernkop-Schnurch A. Mucoadhesive drug delivery systems. Handbook of Experimental Pharmacology 2010;(197)(197):251-66.
122 Smart JD. The basics and underlying mechanisms of mucoadhesion. Advanced Drug Delivery Reviews 2005;57(11):1556-68.
123 Bernkop-Schnurch A, Scholler S, Biebel RG. Development of controlled drug release systems based on thiolated polymers. Journal of controlled release : official journal of the Controlled Release Society 2000;66(1):39-48.

124 Lehr C-M. Lectin-mediated drug delivery:: The second generation of bioadhesives. Journal of Controlled Release 2000;65(1–2):19-29.
125 Tang BC, Dawson M, Lai SK, et al. Biodegradable polymer nanoparticles that rapidly penetrate the human mucus barrier. Proceedings of the National Academy of Sciences of the United States of America 2009;106(46):19268-73.
126 Forier K, Messiaen AS, Raemdonck K, et al. Transport of nanoparticles in cystic fibrosis sputum and bacterial biofilms by single-particle tracking microscopy. Nanomedicine (London, England) 2012.
127 Ensign LM, Tang BC, Wang YY, et al. Mucus-penetrating nanoparticles for vaginal drug delivery protect against herpes simplex virus. Science translational medicine 2012;4(138):138ra79.
128 Wang YY, Lai SK, Suk JS, Pace A, Cone R, Hanes J. Addressing the PEG mucoadhesivity paradox to engineer nanoparticles that "slip" through the human mucus barrier. Angewandte Chemie (International ed.in English) 2008;47(50):9726-9.
129 Pfeiffer CJ. Experimental analysis of hydrogen ion diffusion in gastrointestinal mucus glycoprotein. AJP - Gastrointestinal and Liver Physiology 1981;240(2):G176-82.
130 Bhakta NR, Garcia AM, Frank EH, Grodzinsky AJ, Morales TI. The Insulin-like Growth Factors (IGFs) I and II Bind to Articular Cartilage via the IGF-binding Proteins. Journal of Biological Chemistry 2000;275(8):5860-6.
131 Garcia AM, Szasz N, Trippel SB, Morales TI, Grodzinsky AJ, Frank EH. Transport and binding of insulin-like growth factor I through articular cartilage. Archives of Biochemistry and Biophysics 2003;415(1):69-79.
132 Alcaraz J, Buscemi L, Grabulosa M, et al. Microrheology of human lung epithelial cells measured by atomic force microscopy. Biophysical journal 2003;84(3):2071-9.
133 Lai SK, Wang Y-Y, Wirtz D, Hanes J. Micro- and macrorheology of mucus. Advanced Drug Delivery Reviews 2009;61(2):86-100.
134 Dawson M, Krauland E, Wirtz D, Hanes J. Transport of polymeric nanoparticle gene carriers in gastric mucus. Biotechnology progress 2004;20(3):851-7.
135 Avdeef A. Liposome-Water Partitioning. In. *Absorption and Drug Development*: John Wiley & Sons, Inc.; 2012:220-50.
136 Axelrod D, Koppel DE, Schlessinger J, Elson E, Webb WW. Mobility measurement by analysis of fluorescence photobleaching recovery kinetics. Biophysical journal 1976;16(9):1055-69.
137 Perez-Vilar J. Mucin granule intraluminal organization. American journal of respiratory cell and molecular biology 2007;36(2):183-90.
138 Gong DH, Turner B, Bhaskar KR, Lamont JT. Lipid binding to gastric mucin: protective effect against oxygen radicals. The American Journal of Physiology 1990;259(4 Pt 1):G681-6.
139 Celli JP, Turner BS, Afdhal NH, et al. Helicobacter pylori moves through mucus by reducing mucin viscoelasticity. Proceedings of the National Academy of Sciences of the United States of America 2009;106(34):14321-6.
140 Meeroff JC, Rofrano JA, Meeroff M. Electrolytes of the gastric juice in health and gastroduodenal diseases. The American Journal of Digestive Diseases 1973;18(10):865-72.
141 Gerken TA, Gupta R, Jentoft N. A novel approach for chemically deglycosylating O-linked glycoproteins. The deglycosylation of submaxillary and respiratory mucins. Biochemistry 1992;31(3):639-48.
142 Duffy DC, McDonald JC, Schueller OJA, Whitesides GM. Rapid Prototyping of Microfluidic Systems in Poly(dimethylsiloxane). Analytical Chemistry 1998;70(23):4974-84.
143 Desai SP, Freeman DM, Voldman J. Plastic masters-rigid templates for soft lithography. Lab on a chip 2009;9(11):1631-7.
144 Nussbaum JH, Grodzinsky AJ. Proton diffusion reaction in a protein polyelectrolyte membrane and the kinetics of electromechanical forces. Journal of Membrane Science 1981;8(2):193-219.

145 Turner BS, Bhaskar KR, Hadzopoulou-Cladaras M, Specian RD, LaMont JT. Isolation and characterization of cDNA clones encoding pig gastric mucin. The Biochemical journal 1995;308 ( Pt 1)(Pt 1):89-96.
146 Gwozdzinski K, Slomiany A, Nishikawa H, Okazaki K, Slomiany BL. Gastric mucin hydrophobicity: effects of associated and covalently bound lipids, proteolysis, and reduction. Biochemistry international 1988;17(5):907-17.
147 Saparov SM, Antonenko YN, Pohl P. A new model of weak acid permeation through membranes revisited: does Overton still rule? Biophysical journal 2006;90(11):L86-8.
148 Kauffman GL, Jr., Reeve JJ, Jr., Grossman MI. Gastric bicarbonate secretion: effect of topical and intravenous 16,16-dimethyl prostaglandin E2. The American Journal of Physiology 1980;239(1):G44-8.
149 Rees WD, Botham D, Turnberg LA. A demonstration of bicarbonate production by the normal human stomach in vivo. Digestive diseases and sciences 1982;27(11):961-6.
150 Forssell H, Olbe L. Continuous computerized determination of gastric bicarbonate secretion in man. Scandinavian Journal of Gastroenterology 1985;20(6):767-74.
151 Cox AJ. Variations in size of human stomach. California and western medicine 1945;63:267.
152 Flemstrom G. Gastric and Duodenal Mucosal Bicarbonate Secretion. In: Johnson LR, ed. *Physiology of the Gastrointestinal Tract*. New York: Raven Press; 1987:1011-29.
153 Tanaka S, Podolsky DK, Engel E, Guth PH, Kaunitz JD. Human spasmolytic polypeptide decreases proton permeation through gastric mucus in vivo and in vitro. The American Journal of Physiology 1997;272(6 Pt 1):G1473-80.
154 Tanaka S, Meiselman HH, Engel E, et al. Regional differences of H+, HCO3-, and CO2 diffusion through native porcine gastroduodenal mucus. Digestive diseases and sciences 2002;47(5):967-73.
155 Bickel M, Kauffman GL, Jr. Gastric gel mucus thickness: effect of distention, 16,16-dimethyl prostaglandin e2, and carbenoxolone. Gastroenterology 1981;80(4):770-5.
156 Lee SP, Nicholls JF. Diffusion of charged ions in mucus gel: effect of net charge. Biorheology 1987;24(6):565-9.
157 Bilski J, Sarosiek J, Murty VL, et al. Enhancement of the lipid content and physical properties of gastric mucus by geranylgeranylacetone. Biochemical pharmacology 1987;36(23):4059-65.
158 Nardone G, Laccetti P, Civiletti C, Budillon G. Phospholipid composition of human gastric mucosa: a study of endoscopic biopsy specimens. Gut 1993;34(4):456-60.
159 Johansson ME, Phillipson M, Petersson J, Velcich A, Holm L, Hansson GC. The inner of the two Muc2 mucin-dependent mucus layers in colon is devoid of bacteria. Proceedings of the National Academy of Sciences of the United States of America 2008;105(39):15064-9.
160 Knowles MR, Boucher RC. Mucus clearance as a primary innate defense mechanism for mammalian airways. The Journal of clinical investigation 2002;109(5):571-7.
161 Wada A, Nakamura H. Nature of the charge distribution in proteins. Nature 1981;293(5835):757-8.
162 Li L, Lieleg O, Jang S, Ribbeck K, Han J. A microfluidic in vitro system for the quantitative study of the stomach mucus barrier function. Lab on a chip 2012;12(20):4071-9.
163 Unger MA, Chou H-P, Thorsen T, Scherer A, Quake SR. Monolithic Microfabricated Valves and Pumps by Multilayer Soft Lithography. Science 2000;288(5463):113-6.
164 Lichtenberger LM, Wang ZM, Romero JJ, et al. Non-steroidal anti-inflammatory drugs (NSAIDs) associate with zwitterionic phospholipids: insight into the mechanism and reversal of NSAID-induced gastrointestinal injury. Nature medicine 1995;1(2):154-8.
165 Goddard PJ, Hills BA, Lichtenberger LM. Does aspirin damage canine gastric mucosa by reducing its surface hydrophobicity? The American Journal of Physiology 1987;252(3 Pt 1):G421-30.

166 Spychal RT, Goggin PM, Marrero JM, et al. Surface hydrophobicity of gastric mucosa in peptic ulcer disease. Relationship to gastritis and Campylobacter pylori infection. Gastroenterology 1990;98(5 Pt 1):1250-4.
167 Goggin PM, Marrero JM, Spychal RT, Jackson PA, Corbishley CM, Northfield TC. Surface hydrophobicity of gastric mucosa in Helicobacter pylori infection: effect of clearance and eradication. Gastroenterology 1992;103(5):1486-90.